Permeation of small molecules across a polymer membrane

Sok, Robert Martin

Permeation of Small Molecules across a Polymer Membrane:

a Computer Simulation Study

RuG

Dit onderzoek is mede tot stand gekomen door financiële ondersteuning door het KSLA (Koninklijke/Shell-Laboratorium, Amsterdam) in het kader van een donatie aan de RUG.

RIJKSUNIVERSITEIT GRONINGEN

Permeation of Small Molecules across a Polymer Membrane:

a Computer Simulation Study

Proefschrift
ter verkrijging van het doctoraat in de
WISKUNDE en NATUURWETENSCHAPPEN
aan de Rijksuniversiteit Groningen
op gezag van de
Rector Magnificus Dr. F. van der Woude
in het openbaar te verdedigen op
18 november 1994
des namiddags te 2.45 uur precies

door

Robert Martin Sok

geboren op 1 februari 1964
te Zuidwolde (Dr.)

Promotor : Prof. Dr. H.J.C. Berendsen

Voor mezelf,
aan iedereen.

Preface

Ryokan once said:

"Who says my poems are poems?
My poems are not poems
After you know my poems are not poems
Then we can begin to discuss poetry!"

Ryokan was a Bhuddist monk, living two hundred years ago in the mountain areas of Japan. His life was characterized by purity and joy; apart from meditation he spent the days by playing with children, picking flowers or reciting his poems.

Now you might wonder what this has got to do with this thesis. Nothing, actually. That's the main reason for putting it here. After all, in Zen-Buddhism everything is connected to everything, at least for those who are enlightened. But for those who are not, there are still some remarkable analogues between Ryokan's and Rob's worlds.

First we have the resemblance in personal character. Rob also leads a very pure and joyful life. Instead of picking flowers or playing with children he chooses the more up to date leisures as picking girls or playing with weights. Times are changing, of course.

Then we should notice the remarkable similarity in appearance between the two of them. Like Ryokan, Rob also shaved of all his hair, or actually he just lost it. Boldness as prerequisite on the way to enlightment...

Most noticeable is the similarity in their written output. Like Ryokan's poems, also this thesis breathes a profound Zen spririt in all of its chapters. Instead of poems, however, Rob expresses his ideas through simulations, and instead of themes derived from peasant life he uses polymer matrices. But the essence of both Ryokan's poems and Rob's simulations boils down to the same question: what is reality and what not? Reading through Rob's thesis you will notice that you are constantly hovering between utter surprise, true admiration and honest disbelief. Facts that seemed sure for long suddenly are shown to be very, very wrong indeed. When reading this thesis with full attention, it offers a modern way of experiencing Zen. But beware,

Rob would say:

"Who says my simulations are simulations?
My simulations are not simulations
After you know my simulations are not simulations
Then you may start reading my thesis!"

Siewert-Jan Marrink.

Contents

1 General introduction **1**

2 Transport through polymer membranes **5**
2.1 The polymer matrix . . . 5
2.2 Solution-diffusion mechanism . . . 7
2.3 Experimental measurement of permeabilities. . . . 9
2.4 Industrial applications . . . 11

3 Molecular dynamics simulations **13**
3.1 Algorithm . . . 13
3.2 Atomic interaction potentials . . . 14
3.2.1 Two-body interactions. . . . 15
3.2.2 Many-body interactions. . . . 15
3.3 Temperature and pressure . . . 16
3.4 Practical tricks . . . 17

4 MD simulation of PDMS **19**
4.1 Introduction . . . 19
4.2 Polydimethylsiloxane . . . 19
4.3 Generation of starting structure . . . 22
4.4 Computational details . . . 23
4.5 Analysis of the results . . . 24
4.5.1 Structural properties . . . 24
4.5.2 Radius of gyration, end-to-end distance . . . 25
4.5.3 Diffusion . . . 25
4.6 Results . . . 26
4.6.1 Structural properties . . . 27
4.6.2 Dynamical properties . . . 30
4.7 Discussion . . . 32

5 MD simulation of gas transport through PDMS **35**
5.1 Introduction . . . 35
5.2 Analysis of the results . . . 37
5.2.1 Solubility / Chemical potential . . . 37

5.2.2 Diffusion . . . 39
5.2.3 Estimation of errors . . . 40
5.3 Small system . . . 40
5.4 Large system . . . 41
5.5 Results . . . 42
5.5.1 Radial distribution functions . . . 42
5.5.2 Diffusion . . . 46
5.5.3 Solubility / Chemical potential . . . 54
5.5.4 Permeability . . . 58
5.6 Discussion . . . 60

6 Free volume **67**
6.1 Introduction . . . 67
6.2 Percolation theory . . . 69
6.2.1 General . . . 69
6.2.2 Percolation threshold . . . 69
6.2.3 Fractal dimension . . . 70
6.2.4 Correlation length . . . 71
6.2.5 Universal constants and power laws . . . 71
6.2.6 Cluster size distribution . . . 72
6.3 Percolation principles in real systems . . . 74
6.4 Computer experiments . . . 74
6.4.1 Percolation models . . . 75
6.4.2 Extended percolation descriptions for PDMS . . . 76
6.4.3 Analysis of the results . . . 77
6.5 Results . . . 79
6.5.1 Percolation thresholds . . . 79
6.5.2 Cluster / Hole size - distribution at p_c . . . 82
6.5.3 Cluster / Hole size - distribution in the polymer system away from p_c . . . 86
6.5.4 Free / Accessible volume in the polymer system . . . 86
6.5.5 Extended percolation models . . . 88
6.5.6 Diffusion of accessible volume holes . . . 88
6.6 Discussion . . . 89

7 Permeation and free volume **93**
7.1 Introduction . . . 93
7.2 Solubility and accessible volume . . . 93
7.3 Diffusion in a static percolation system . . . 96
7.3.1 The polymer as a percolating system . . . 98
7.4 Diffusion models . . . 98
7.4.1 Free volume models . . . 99

7.4.2 Fit of the calculated data to free volume models 100
7.5 Diffusion, accessible volume and hole size distributions 101
7.6 Diffusion and percolation energy 103
7.7 Permeation, Diffusion and Solubility ; Current views 104

A Reprint **109**

B The error in the diffusion coefficient **117**

C Deriviation of enthalpy expression **119**

References **123**

Samenvatting **129**

Dankwoord **133**

Chapter 1

General introduction

There is a considerable interest in the study of the transport of small molecules across polymer membranes, mainly because of the large number of applications in which this transport process plays a major role. These applications include protective coatings (paints, varnishes), electronic devices, cable materials and biomedical devices (biosensors). In industry, polymeric membranes are mainly used as barrier plastics, or as separation membranes. These two applications require membranes with completely different properties. In the first application the membrane should have high resistance to gas and*e.g.* flavor-aroma molecules while in the second application it is important that the polymeric material is highly selective and sufficiently permeable.

The industrial interest has stimulated the development of theoretical models to describe the transport process. There are a large number of models, all of which however lack a correct microscopic description of the permeation process. Computer simulation methods and in particular molecular dynamics simulations are an essential tool to obtain a more detailed picture. A qualitative description of the underlying processes and eventually quantitative predictions of permeability and selectivity open the prospect for the design of membranes with predefined properties. At present we are not yet at the stage of predictions. Most studies at this moment are concerned with describing the diffusion and permeation process and are restricted to comparison with existing membranes. This thesis describes one study in this fast moving field of research.

Aim of the research

The aim of this research is to study the permeation process of small molecules through rubbery polymers in detail using computer simulation methods. From these simulations I want to be able to predict permeation transport properties for various penetrants. Specifically the *penetrant size* dependency of the transport properties, permeability, diffusion and solubility.

As computer simulations give concrete numbers they can be compared to experiment.

This is a neccessary step in order to validate the model and the method, but computer simulations have the ability to go beyond reality. Therefore, in the study of the penetrant size effect I will not restrict myself to "real" penetrants. Although the results for these nonphysical particles can not be compared to experiment one can observe trends more clearly than in reality.

I will also look in detail at the diffusion process and give a microscopic description of the nature of this complex transport process.

Choice of method

For the determination of the permeability I have to calculate both the diffusion constant and the solubility constant (See also chapter 2). For the evaluation of the dynamic process of diffusion I use the technique of *molecular dynamics*.

Molecular dynamics (MD) simulation provides in principle the direct evaluation of the time evolution of a system of interacting particles and can thus be very useful for the determination of the diffusion coefficients. Relevant physical quantities can be calculated using statistical mechanics. Molecular dynamics also provides detailed information about the diffusional process which enables us to study the key factors influencing the diffusion. The major drawback of the method is the limited time scale and sample size which we can simulate. Computer power now available enables us to simulate samples up to 1000 nm^3 into the nanosecond region. Thus the range of properties that can be studied directly is limited to those evolving over this time scale and sample size.

For the determination of the solubility constant there are a number of options. One of these is through use of the above mentioned MD method[1, 2], but in our special case of the solvation of small penetrants in a macromolecular system this is not the most efficient method. Even though the process of solvation is a dynamic process, the solubility constant can be evaluated very efficiently by use of a static method: the*particle insertion method* of Widom[3].

Choice of polymer

The polymer model I use is a simplified model of polydimethylsiloxane (PDMS), the simplest silicone rubber. I chose this model for a number of reasons. First it is simple, the repeating unit has only four atoms (I model the CH_3 group as one united atom). Second, it has industrial interest, PDMS is used as a selective membrane [4, 5] and in biomedical applications [6, 7]. Third, the rate of diffusion of small penetrants is very high, so it is possible to determine the diffusion constants within the average simulation time.

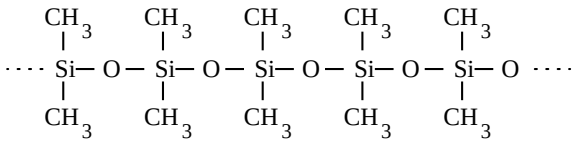

Polydimethylsiloxane

Outline of this thesis

Chapter 2 gives a brief overview of the theoretical models used in the description and prediction of the gas transport through polymer membranes, the experimental methods to determine the permeability, and several industrial applications. In chapter 3 I describe the basic principles of the technique of molecular dynamics and give the foundations for the analysis of the results. Chapter 4 is concerned with the simulation of the polymer itself, the generation of a starting structure and some results. The next chapter gives the results of the simulation of the polymer including penetrants, giving the diffusion and solubility constants. From these quantities the permeability constant will be calculated and compared to experiment. Chapter 6 gives the description of an important quantity in the description of the diffusion process, the free volume. It is explained how this free volume and the free volume distribution is measured, and how these results can be compared to results from percolation theory.

In the last chapter (chapter 7) I will try to combine the results of the two previous chapters. We will see how the permeation process is connected to the free volume properties of the polymer. The chapter ends with some final remarks and conclusions.

Chapter 2

Transport through polymer membranes

In this chapter I will give a short introduction in the process of transport through membranes, concentrating on the gas phase/rubbery polymer system. The transport from the gas phase through rubbery polymers can be described by the solution-diffusion model, which will be outlined in this chapter. Also a brief look at the experimental measurement of the permeability by means of the time-lag method and some interesting industrial applications are given.

2.1 The polymer matrix

Before looking at the mechanism of gas transport through membranes it is necessary to consider some features of the two principal microstructural conditions of polymeric material, the *glassy* and *rubbery* state.

It has been known for a long time that the mechanism of diffusion is very different in rubbery and glassy polymers. This is mainly due to the fact that glassy polymers are not in a true state of equilibrium. The difference in mechanism is reflected in the significant differences observed in the dependence of the diffusion coefficient, as well as the permeability and solubility coefficients, on the penetrant gas pressure or concentration in polymers and on the temperature [8]. For example, the diffusion coefficients for light gases in rubbery polymers are often independent of concentration. By contrast, in glassy polymers the diffusion coefficients are highly nonlinear functions of concentration and reach a constant value at sufficiently high concentration.

At temperatures below the glass transition temperature T_g the polymer is in its glassy state and is hard and may be brittle, which is directly related to the restricted chain mobility. The intermolecular forces between the chains do not allow other movement

than vibrations. All structural properties as the distribution of cavities in the polymer have effectively become static quantities. Depending on the conditions during the formation of the glassy state (for example, the temperature gradient) the polymer is more or less trapped in a non-equilibrium state. In glassy polymers the penetrant diffusion is low but size selectivity is very good.

Above the glass transition temperature the polymer is in its rubbery state. In this state the polymers are generally tough and flexible, which is associated with freer chain motion. Rubbery polymers have very short relaxation times (compared to glassy polymers) and respond very rapidly to external stresses. Thus a change in temperature causes an "immediate" adjustment to the new equilibrium state. A similar immediate adjustment occurs when small penetrants are absorbed in a rubbery polymer. Larger segments of the polymer are thought to participate in the penetrant diffusion process due to internal chain motions such as chain rotations, translations and stronger vibrational motions. The penetrant diffusion is much faster than in a glassy polymer but size selectivity is lower.

In both the glassy and rubbery state the polymer properties can be further modified by the presence of crystalline phases, by stress induced orientations or as a function of cross-link density. They tend to place additional constraints on the mobility of the amorphous phase through which diffusion takes place. (It is partly because of these possible variations in polymer properties that there is such a wide range in experimental values of permeability coefficients)

Gas versus liquid permeation

Permeation through polymer membranes can occur from both the gas and the liquid phase. In gas permeation diffusion coefficients are independent of penetrant concentration in the membrane in contrast to vapor or liquid permeation. There the membrane may be highly swollen by a penetrating liquid. This opens up the structures with the result that the absolute flux rates through the membrane can be 2 or 3 orders of magnitude larger than for a (noncondensible) gas. Thus in vapor or liquid permeation the diffusion coefficients are strong (typically exponential) functions of concentration.

For vapor and liquid separation different theories have been used, for example: irreversible thermodynamics, preferential sorption-capillary flow theory or the solution-diffusion mechanism. But in permeation from the gas phase the picture is simpler and only the solution-diffusion mechanism is used.

As the process of permeation from vapor or liquid phases involves many extra difficulties I will limit myself to the permeation of small molecules from a gaseous phase. And even though polymers are used for various permeation processes in both their rubbery and glassy state, we shall concentrate on the permeation process in polymers in their rubbery state only. Thus in this thesis I shall express the transport properties in the cast

of the solution-diffusion picture.

2.2 Solution-diffusion mechanism

The first to use the term "solution-diffusion mechanism" was Graham [9] in 1866. He postulated that the penetrant leaves the external phase by dissolving in the membrane. It then undergoes molecular diffusion in the membrane, driven towards the downstream face by for example a concentration or pressure gradient, after which it evaporates again in the external phase. Thus the permeability coefficient P, defined by the ratio between the flux J of the permeant species and its concentration gradient Δc over the membrane of thickness d

$$J = P\frac{\Delta c}{d} \tag{2.1}$$

is given by the product of the diffusion coefficient D and a solubility factor S

$$P = DS \tag{2.2}$$

A postulate of which the theoretical foundation will be shown next.

In the solution-diffusion model we consider an isothermal homogeneous stationary membrane in which particles at a position $\boldsymbol{r}$ are dissolved with a local concentration $c(\boldsymbol{r})$. The particle flux $\boldsymbol{J}$ is assumed to behave in the regime of a linear irreversible process with the gradient of the chemical potential as the driving force. The flux is given by

$$\boldsymbol{J}(\boldsymbol{r}) = c(\boldsymbol{r})\boldsymbol{v}(\boldsymbol{r}) \tag{2.3}$$

where $\boldsymbol{v}(\boldsymbol{r})$ is the average velocity of the dissolved particles. In the linear regime $\boldsymbol{v}(\boldsymbol{r})$ can be written as

$$\begin{aligned} \boldsymbol{v}(\boldsymbol{r}) &= \tfrac{1}{\zeta}\boldsymbol{F}_{th} \\ &= -\tfrac{1}{\zeta}\nabla\mu(\boldsymbol{r}) \end{aligned} \tag{2.4}$$

where $\boldsymbol{F}_{th}$ is the thermodynamic force, ζ a friction coefficient and μ the chemical potential of the dissolved particles. The latter can be written as

$$\mu(\boldsymbol{r}) = \mu^0 + RT\ln c(\boldsymbol{r}) + \mu_{ex}(\boldsymbol{r}) \tag{2.5}$$

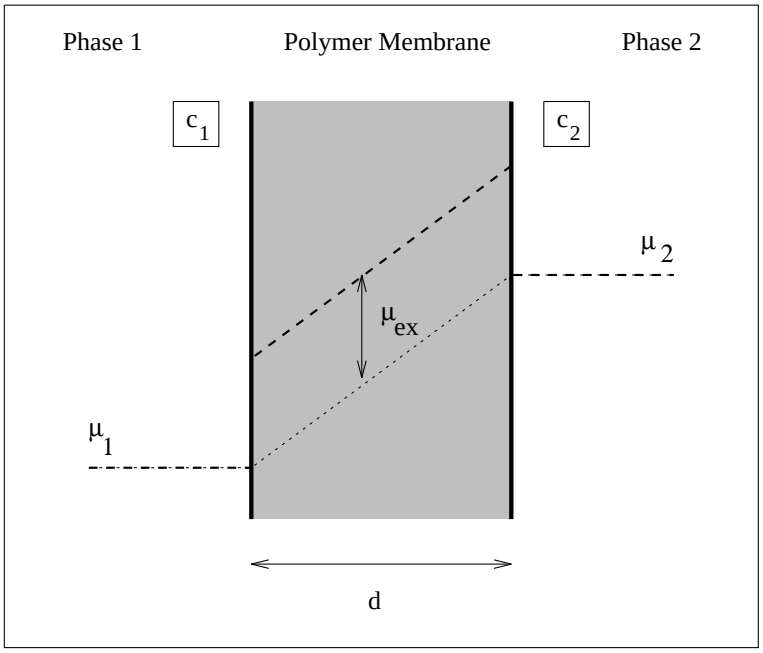

Figure 2.1: The schematic polymer membrane. The membrane separates two phases with concentrations c_1 and c_2 and chemical potential μ_1 and μ_2. We assume that μ is continuous at the interface and that μ_{ex} (the excess chemical potential) is constant throughout the homogeneous membrane.

in which μ^0 is the standard chemical potential of the ideal gas phase based on unit molar concentration, c is the local concentration and $\mu_{ex}(\boldsymbol{r})$ is the excess chemical potential of the dissolved species with respect to the ideal gas state. Equations 2.3, 2.4 and 2.5 give

$$\boldsymbol{J}(\boldsymbol{r}) = \frac{-RT}{\zeta}\nabla c(\boldsymbol{r}) - \frac{c(\boldsymbol{r})}{\zeta}\nabla\mu_{ex}(\boldsymbol{r}). \tag{2.6}$$

Equating RT/ζ with the diffusion coefficient D, eq. 2.6 can be written as

$$\boldsymbol{J}(\boldsymbol{r}) = -D\ \exp(-\mu_{ex}(\boldsymbol{r})/RT) \cdot \nabla\left\{c(\boldsymbol{r})\ \exp(\mu_{ex}(\boldsymbol{r})/RT\right\}. \tag{2.7}$$

Equation 2.7 is still general. We now consider a membrane with thickness d in the x-direction and infinite dimensions in the yz-plane. The interfaces at $x = 0$ and $x = d$ are in contact with concentrations c_1 and c_2 ($\Delta c = c_2 - c_1$) and we assume that an ideal gas phase is in equilibrium across both interfaces. Hence μ is continuous at the interfaces. Furthermore μ_{ex} is assumed to be constant throughout the homogeneous membrane. This implies that any concentration dependence of μ_{ex} is neglected. Thus

$$\mu^0 + RT \ln c_1 = \mu^0 + RT \ln c(0) + \mu_{ex} \tag{2.8}$$

or

$$c(0) = c_1 \ \exp(-\mu_{ex}/RT) \tag{2.9}$$

similarly

$$c(d) = c_2 \ \exp(-\mu_{ex}/RT). \tag{2.10}$$

If μ_{ex} is constant then $\nabla\mu_{ex}$ is zero. Then, for a stationary flux $\boldsymbol{J}(\boldsymbol{r})$ we find that according to equation 2.6, $c(x)$ is a linear function of x and the gradient in equation 2.7 is equal to $(c(d) - c(0))/d$. Equation 2.7 now reduces to

$$J = -DS\frac{\Delta c}{d}, \tag{2.11}$$

with

$$S = \exp(-\mu_{ex}/RT). \tag{2.12}$$

Equation 2.11 expresses the solution-diffusion mechanism. [1]

2.3 Experimental measurement of permeabilities.

The simplest method to experimentally measure both the permeability coefficient P and the diffusion coefficient D is the **time-lag method**. This method was first proposed by Daynes [10] and refined by Barrer[11]. In this technique the membrane is initially evacuated from any residual gas by applying vacuum to both sides of the membrane for several hours. A schematic set-up of the experiment is show in fig. 2.2. Then at time $t = 0$ the upstream side of the membrane is exposed to the desired gas at the desired pressure $\mathcal{P}_{feed}$. From that moment on the pressure on the downstream side is measured and plotted. A typical plot of the pressure vs. time is also shown in fig. 2.2. From the

[1] Note that it is not necessary to explicitly simulate a membrane with actual interfaces. This would place high constraints on the MD simulations. All the information needed from the simulations is the diffusion constant D in the bulk polymer and the excess chemical potential μ_{ex} of the particles in the bulk polymer compared to the ideal gas phase.

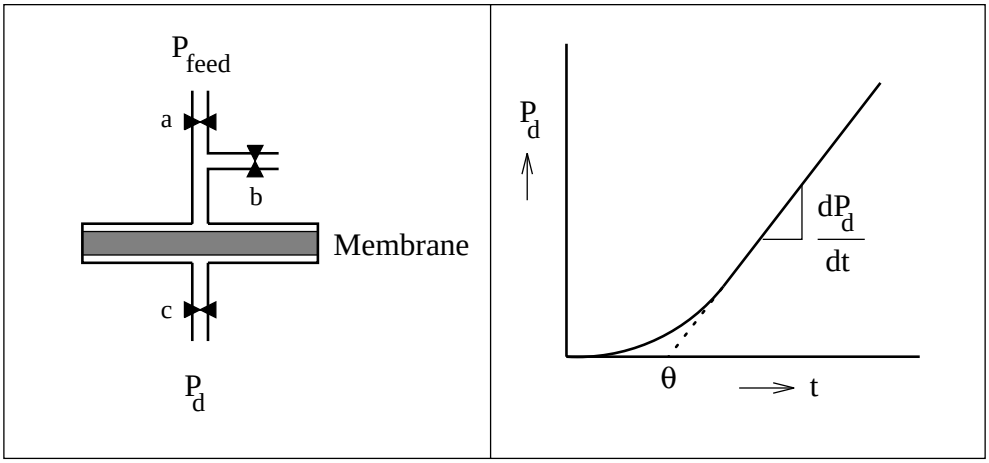

Figure 2.2: Left: Schematic representation of the set-up of a time-lag measurement. Before the experiment the valve (a) is closed and vacuum is applied to valves (b) and (c). Then (b) is closed and at time $t = 0$ valve (a) is opened and $\mathcal{P}_d$ is recorded. Right: A typical time-lag plot. From the time-lag θ the diffusion constant can be calculated directly and from the slope $d\mathcal{P}_d/dt$ the permeability coefficient can be calculated.

extrapolation of the steady-state part of the curve, the time-lag θ can be obtained and the diffusivity can be calculated with:

$$D \;=\; \frac{d^2}{6\,\theta}, \tag{2.13}$$

where d is the membrane thickness. The permeation coefficient P can be calculated from the slope of the straight steady-state part directly, using:

$$P \;=\; \frac{1}{\mathcal{P}_{feed}} \cdot \frac{V_d\; M_{gas}\; d}{\rho\; RT\; A} \cdot \frac{d\mathcal{P}_d}{dt}, \tag{2.14}$$

in which $\mathcal{P}_{feed}$ is the applied upstream pressure, V_d the downstream compartment volume, M_{gas} the molecular weight of the penetrant gas at density ρ and A the membrane area.

The solubility coefficient S is usually calculated from the diffusion and the permeability coefficients, using the relation $P = DS$. But if the permeation rate is too fast it is not possible to determine the diffusion coefficient with the desired accuracy. Then S has to be measured separately.

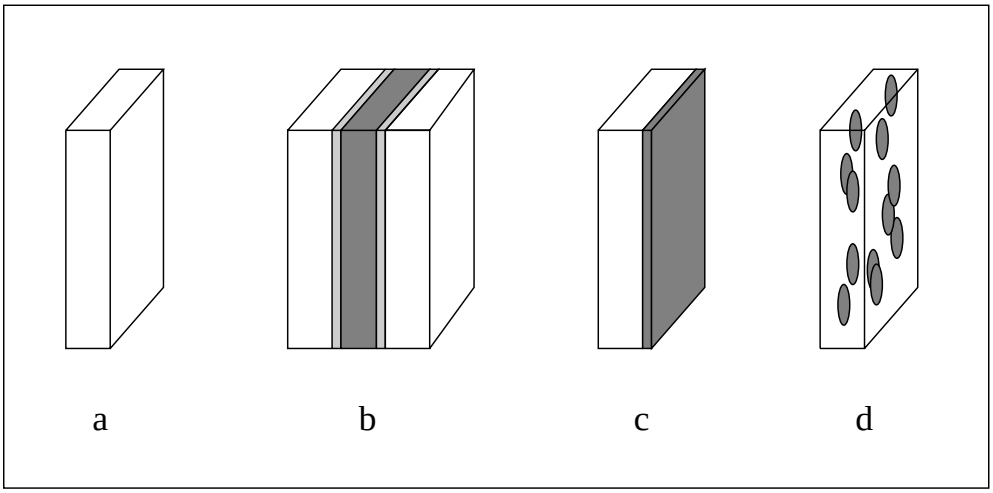

Figure 2.3: Primary types of barrier structures. a) Monolithic, single polymer. b) Laminate of two or more polymers. Middle high barrier layer e.g. EvOH, covered with surface layers. These interact with the environment which could damage the middle layer. c) Reactively formed, or coated laminate. d) Polymer filled with inorganic platelet's or higher barrier polymer lamellae to enhance the turtuosity of the path of the penetrants.

2.4 Industrial applications

The type and structure of polymer film used depends on the application on hand. One major application is the packaging industry. In this industry there usually is a demand for high barrier properties. For example, for the packaging of carbonated soft drinks the package should not allow the permeation of carbon dioxide, oxygen or water. For this purpose one normally uses poly(ethylene tetraphtalate) (PET)[12]. In the packaging of products containing fats and oils like fried snacks and meat, protection against the effects of oxygen and light is required.

An interesting exception to the simple barrier demands is the storage of blood platelets [13]. Blood platelets are living cells that both consume oxygen to live and generate carbon dioxide as a metabolic byproduct. This generation of carbon dioxide presents a large problem, since it tends to cause undesirable changes in the pH unless the carbon dioxide can escape. An added requirement enters because the aqueous solution containing the platelets should not lose significant amounts of water by permeation. This case, therefore, illustrates the need for an advanced controlled atmosphere package that is able to allow relatively free exchange of oxygen and carbon dioxide while essentially preventing outward permeation losses of water.

But not only the type of polymer can be adjusted to the needs, also the macroscopic structure of the membrane can be altered. As shown in figure 2.3 one can use a variety of barrier structures besides that of a simple film to control the exchange between the

internal and external environment.

For example, in an application where there is a need for a barrier to oxygen an often used polymer is ethylene-vinyl alcohol(EvOH). EvOH has a very low permeability to oxygen in the dry state. The problem however is that it loses its barrier properties at high relative humidities, so in those cases an interface layer is placed on the EvOH membrane such that it is shielded from the humid environment.

Another application which has large industrial interest is the selective separation of gases by use of membranes. In these cases there is a need for both high selectivity and high permeability. Silicone polymers have been used as selective membranes mainly because of the latter requirement. Even though for example the selectivity of the membranes of $\alpha(O_2/CO_2)$ is only 2.0 thus allowing only an oxygen enrichment of 30% [14], the rate of permeation is so large that it is still usefull in certain applications. The enhancement of the selectivity usually has a negative influence on the rate of permeation, so for every application a new tradeoff has to be made. An interesting example of the enhancement of the selectivity is the use of polymer films containing metal complexes. The incorporation of cobalt-porphorine complexes in a copolymer of poly(alkyl methacrylate) produced an increase of the selectivity $\alpha(O_2/CO_2)$ from 3.4 to 12.8. The complex selectively absorbs (according to a Langmuir isotherm) and transports oxygen in the membrane [15, 16].

Another class of applications are the bio(medical) applications, for example the usage of polymers as contact lenses. Contact lenses are classified based on their mechanical strength and physical behavior as “hard”, to denote glassy polymers, or “soft” for amorphous or semicrystalline polymers [17]. Important properties for polymers used as contact lenses are surface wettability and flexure and high oxygen permeability. Silicone films have been used as a material for the past three decades[18]. Presently the polymer used in hard lenses is usually PMMA (polymethylmethacrylaat). Most of the present soft contact lenses are prepared from poly(2-hydroxyethyl methacrylate) (PHEMA), but also polypeptide films are used as contact lenses (as well as in other biomedical applications) [19].

Controlled drug release is another biomedical application. The therapeutic efficacy of drugs can be greatly enhanced and their toxicities reduced by delivering the drugs at a controlled rate. Controlled release drug administration not only means prolongation in the duration of drug delivery, but also implies predictability and reproducibility. A number of therapeutic transdermal (*through-skin*) products employing silicone rubbers (including PDMS) are commercially available. For example for the controlled release of anesthetic vapors [20] or steroids [21].

In all these and other applications computer modeling of the permeation transport could be of crucial importance to either a better understanding of the process or even the design of new polymers.

Chapter 3

Molecular dynamics simulations

This chapter describes the computational methods used to model the transport process in atomic detail. The algorithm by which the classical equations of motion of the atoms are evaluated and the interatomic interaction potential are described in the first two sections. It also deals with some important physical properties and the way they can be evaluated from the simulations.

3.1 Algorithm

The method of molecular dynamics[1] solves the classical equations of motion of N-particles interacting through a known potential V. In practice the equations of motion cannot be solved exactly and have to be evaluated by use of finite difference methods. The simplest and most frequently used method, first used by Verlet [23] [24], is obtained from the Taylor expansions of the coordinates $\boldsymbol{r}_i$ at times $t + \Delta t$ and $t - \Delta t$ about $\boldsymbol{r}_i(t)$.

$$\begin{aligned} \boldsymbol{r}_i(t \pm \Delta t) &= \boldsymbol{r}_i(t) \pm \Delta t \frac{d}{dt} \boldsymbol{r}_i(t) + \frac{(\Delta t^2)}{2!} \frac{d^2}{dt^2} \boldsymbol{r}_i(t) \\ &\quad \pm \frac{(\Delta t)^3}{3!} \frac{d^3}{dt^3} \boldsymbol{r}_i(t) + O(\Delta t^4) \end{aligned} \tag{3.1}$$

Adding the two expansions leads to the prediction of the position at time $t + \Delta t$.

$$\boldsymbol{r}_i(t + \Delta t) \simeq -\boldsymbol{r}_i(t - \Delta t) + 2\boldsymbol{r}_i(t) + \frac{(\Delta t)^2}{m_i} \boldsymbol{F}_i(t), \tag{3.2}$$

[1] In this thesis not all details of the method will be explained. For a detailed description of the background of the method I refer to the book of Allen and Tildesley [22] and references therein.

where $\boldsymbol{F}_i$ is the force acting on particle i with mass m_i. Note that the velocities do not enter the equation; they can however easily be evaluated from the positions. Another integration algorithm in which the velocity is incorporated, is the Leap-Frog algorithm[25]. This is essentially equal to the Verlet algorithm and is given by two steps:

$$\boldsymbol{v}_i(t + \tfrac{1}{2}\Delta t) = \boldsymbol{v}_i(t - \tfrac{1}{2}\Delta t) + \frac{\Delta t}{m_i}\ \boldsymbol{F}_i. \tag{3.3}$$

$$\boldsymbol{r}_i(t + \Delta t) = \boldsymbol{r}_i(t) + \Delta t\ v_i(t + \tfrac{1}{2}\Delta t), \tag{3.4}$$

3.2 Atomic interaction potentials

The forces acting on particles are obtained from the derivative of the interatomic potential V

$$\boldsymbol{F} = \frac{-\,dV}{d\boldsymbol{r}}. \tag{3.5}$$

This interatomic potential V for a system of N particles is a function of the positions of all the particles:

$$V = V(\boldsymbol{r}_1 ... \boldsymbol{r}_N), \tag{3.6}$$

which can in principle be broken down into a series of summations

$$V = \sum_{ij} V(\boldsymbol{r}_i, \boldsymbol{r}_j) + \sum_{ijk} V(\boldsymbol{r}_i, \boldsymbol{r}_j, \boldsymbol{r}_k) + \sum_{ijkl} V(\boldsymbol{r}_i, \boldsymbol{r}_j, \boldsymbol{r}_k, \boldsymbol{r}_l) + ... \tag{3.7}$$

where the first term refers to the 2-body interactions, the second to 3-body interactions, etc. In principle this could be continued up to the N-body interaction term. But because of limited computer power we have to restrict ourselves to the most significant terms. This means that the series is truncated and that the significant terms represent effective interactions that incorporate higher terms in an averaged way. In the simulation package that has been used (GROMOS [26]), V is written as a limited sum of additive effective potentials:

$$V(r, \theta, \phi) = \sum V_{bond}(r) + \sum V_{nonbonded}(r) + \sum V_{angle}(\theta) + \sum V_{dihedral}(\phi). \tag{3.8}$$

depending only on the interatomic distance r, the bond angle θ and the dihedral angle ϕ.

3.2.1 Two-body interactions.

The first two terms in equation 3.8 describe the two-body bonded and nonbonded interactions and depend only on distance r between the two atoms. The most widely used function to describe the covalent bond interaction between two atoms is a harmonic potential:

$$V_{bond}(r) = \tfrac{1}{2}\, k_{bond}\,(r - r_{bond})^2 \tag{3.9}$$

where k_{bond} is the force constant. This function is adequate for distances close to the average bond length r_{bond}. Alternatively it can be replaced by a bond length constraint[27], which reduces the needed computation time considerably. Two atoms that are not chemically bonded interact with each other through so called *nonbonded* potentials. These usually consist of a Lennard-Jones potential and if the atoms are charged also an electrostatic potential. The Lennard-Jones term takes the form of:

$$V(r) = 4\varepsilon \left[\left(\frac{\sigma}{r}\right)^{12} - \left(\frac{\sigma}{r}\right)^{6} \right] \tag{3.10}$$

with a steep r^{-12} term describing the interatomic repulsion and an attractive r^{-6} term modeling the dispersive interaction. ε is the minimum energy of the function and σ can be interpreted as the approximate radius of the atom.

The electrostatic interactions for a pair of atoms with charges q_i and q_j at distance r are given by the Coulomb potential:

$$V(r) = \frac{q_i q_j}{4\pi\varepsilon_0 r} \tag{3.11}$$

3.2.2 Many-body interactions.

The third and fourth term in equation 3.8 refer to interactions ranging over more than two atoms. The angle vibrations between three atoms that are covalently bonded are also treated by a harmonic potential:

$$V(\theta) = \tfrac{1}{2} k_\theta\, (\theta - \theta_0)^2 \tag{3.12}$$

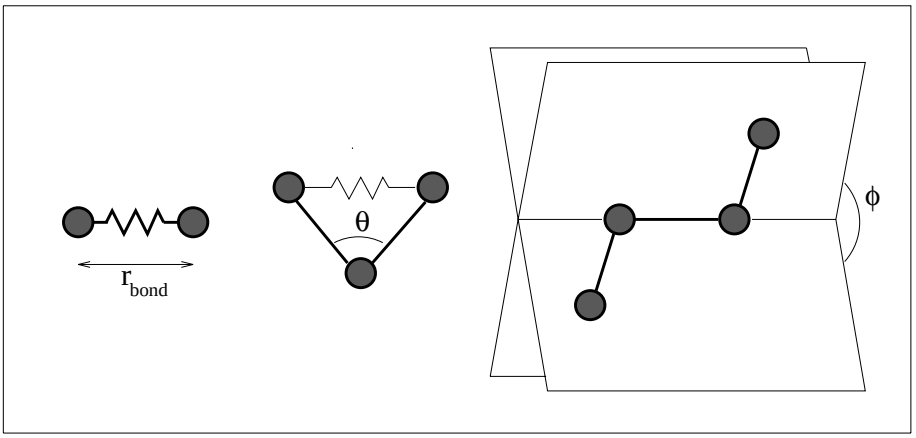

Figure 3.1: Illustration of bond, angle and dihedral definitions.

and the four-body dihedral rotations are described by a potential function of the form :

$$V(\varphi) = k_\varphi \, [1 + \cos(n\varphi - \delta)] \tag{3.13}$$

where θ_0 is the equilibrium angle, k_θ and k_φ are the force constants, δ a phase shift and n the multiplicity factor.

3.3 Temperature and pressure

The temperature of a system is calculated using the average kinetic energy of the N particles with N_f degrees of freedom:

$$\frac{1}{2} k_b N_f T = \sum_{i=1}^{N} \frac{1}{2} m_i {\boldsymbol{v}_i}^2 \tag{3.14}$$

Where v_i the velocity of particle i with mass m_i.

The expression for the pressure of the system is based on the virial theorem[22]. The pressure P is expressed as the sum of an ideal part $PV = NkT$ and the summed product of all forces $\boldsymbol{F}_{ij}$ acting on, and distances $\boldsymbol{r}_{ij}$ between, the centers of mass of the molecules.

$$PV = NkT + \frac{1}{3} \sum_{i<j}^{N} \langle \boldsymbol{r}_{ij} \cdot \boldsymbol{F}_{ij} \rangle \tag{3.15}$$

In order to control the temperature of the simulated system, its pressure or both I make use of a *weak temperature and/or pressure coupling* to an external bath. In GROMOS this means [28] that at each integration step the velocities $\boldsymbol{v}$ are scaled to $\lambda\boldsymbol{v}$ with:

$$\lambda = \left[1 + \frac{\Delta t}{\tau_T} \left(\frac{T^{ref}}{T(t - \frac{1}{2}\Delta t)} - 1 \right) \right]^{\frac{1}{2}} \tag{3.16}$$

to bring the temperature of the system $T(t - \frac{1}{2}\Delta t)$ towards the reference temperature T_{ref}. The time constant τ_T describes how "tight" the coupling is. A tight coupling, $(\Delta t/\tau_T) \gtrsim 1$, means that there is little fluctuation around the T^{ref}. The coupling to the desired pressure P^{ref} is done by scaling the coordinates $\boldsymbol{r}$ to $\eta\boldsymbol{r}$ as well as the simulation box with

$$\eta = \left[1 \; + \; \frac{\gamma \Delta t}{\tau_P} \left(P(t) - P^{ref} \right) \right]^{\frac{1}{2}} . \tag{3.17}$$

where $P(t)$ is the pressure of the system at time t and γ the compressibility of the system. Again τ_P describes the strength of the coupling.

3.4 Practical tricks

In order to reduce the simulation time GROMOS [26] uses the concept of *united atoms*. This means that two or more atoms are modeled by only one *united* atom. The reason for this is twofold. First it reduces the number of atoms to be simulated. Second, it enables the use of a larger time step in the integration scheme[2]. If for example we model a CH_3 group as one united atom we don't have to explicitely simulate the fast motions of the H-atom, but only in an averaged way. I have employed this concept on the CH_3 side group and for the CH_4 (that is used as penetrant). The use of united atoms induces one artifact. For the nonbonded interaction of united atoms with atoms separated by three covalent bonds (third neighbors) the repulsions are too large. In order to avoid this effect the van der Waals parameters used in the calculation of the third neighbor interactions are smaller than normal.

The simulation of finite samples calls for a correct treatment of the sample boundaries. The classical way to do this is by use of *periodic boundary conditions*. The atoms of the sample are put into a cubic, or more general any periodic space filling box, which is surrounded by 26 identical translated images of itself. The emposed periodicity is an

[2]The time-step should be small enough to sample the fastest motion in the system sufficiently. As a rule of thumb, the smallest harmonic should be sampled in at least 30 integration steps

artefact of the computation. We are simulating a "quasi infinite" system with an artifical periodicity.

The effects of this periodicity should be kept at a minimum. In principle we do not wish the include the interaction of a particle with its own periodic image. This implies that we have to use some kind of cut-off on the interaction potential and this cut-off distance should not be larger than half the box size. In our simulation we used the spherical twin-range [29] cut-off procedure. This means that all interactions within a sphere of size r_1 are calculated. For $r_1 < r < r_2$ only the Coulomb forces are calculated. If the mobility of atoms in the outer shell is small enough one can calculate the Coulomb forces every n (ususally $n = 10$) steps.

As was discussed above the nonbonded interaction between two atoms is modeled by the Lennard-Jones potential. In this potential there are two parameter: ε - the minimum energy of the interaction and σ - the distance at which the interaction is zero. In practice these parameters for the potential between two particles a and b are calculated from the single particle parameters $\varepsilon_a, \varepsilon_b, \sigma_a$ and σ_b by the use of simple combination rules. A combination rule that is used often is:

$$\sigma_{ab} = \frac{\sigma_a + \sigma_b}{2}, \quad \varepsilon_{ab} = \sqrt{\varepsilon_a \varepsilon_b}. \tag{3.18}$$

In GROMOS a different approach is used, which is not entirely equivalent. The Lennard-Jones potential is rewriten as:

$$V(r) = \frac{C_{12}}{r^{12}} - \frac{C_6}{r^6}, \tag{3.19}$$

in which $C_{12} = 4\varepsilon\sigma^{12}$, $C_6 = 4\varepsilon\sigma^6$. For two particles i and j these parameters are calculated as:

$$C_{12}(i,j) = \sqrt{C_{12}(i,i)}\sqrt{C_{12}(j,j)}, \tag{3.20}$$

and

$$C_6(i,j) = \sqrt{C_6(i,i)}\sqrt{C_6(j,j)}. \tag{3.21}$$

Chapter 4

MD simulation of PDMS

This chapter deals with the molecular dynamics simulation of a polymer without penetrants, which was performed to evaluate the polymer model. Results are given for the structural properties as inter- and intra- chain radial distribution functions, order parameters and accessible volume distributions. Also some dynamical properties are presented, as polymer chain diffusion, the autocorrelation function of end-to-end distance and radius of gyration, as well as a description of the dynamics of the accessible volume.

4.1 Introduction

Before we are able to simulate the transport of gas molecules through a polymer matrix, we first have to be able to simulate the polymer itself. The structural and dynamical properties of the polymer are important for the transport of penetrants through the polymer. The physics of polymers is a fascinating and challenging area of research of its own and simulation of polymer systems is a nontrivial problem. The difficulty, of course, lies in the molecular connectivity. While there is a strong energetic drive to fill the entire volume uniformly in order to archieve a maximum overlap of the van der Waals attractive wells, the connectivity within the polymer chains does not allow this.

4.2 Polydimethylsiloxane

As was previously mentioned the polymer we used in our simulation models polydimethylsiloxane (PDMS). It has several advantages above, for example, the often used

polyethelene (PE)[30–34].

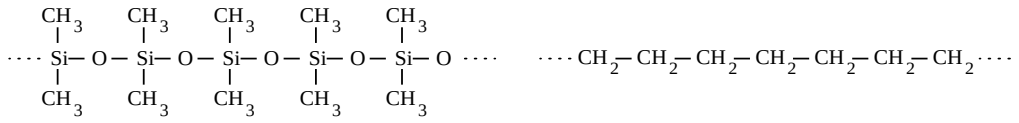

Polydimethylsiloxane Polyethylene

Because of the presence of the side groups and the difference in the equilibrium value and flexibility of adjacent bond angles Si-O-Si and O-Si-O (see table 4.2), PDMS is almost always amorphous. Therefore simulations of PDMS are expected to be easier compared to experiment than those for PE, since due to the presence of crystallites in PE one has to make certain assumptions in the interpretation of experimental data. Some physical properties of PDMS are listed in table 4.1.

Most parameters used in the simulation were taken from the GROMOS force field. The σ and ϵ parameters for Si, O and CH_3, were set to standard GROMOS values. The partial charges on the polymer structure however had to be generated. For this we used the CINDO routine, as embedded in the QUANTA package, for a series of PDMS chains of 4,8,10 and 16 monomers. As the charges converged we used the charges on the 16 monomer chain for our simulation. To increase computational speed we wanted to use a united atom model for the CH_3 group. (A factor of 2.5 in number of atoms per monomer unit and a larger time step for the integration scheme, see section 3.4) The sum of charges on the three hydrogen atoms attached to the carbon atom almost matched that of the carbon atom so that we could set the overall charge on the united atom to zero.

The values for the equilibrium angle Si-O-Si and its force constant (which are not present in the GROMOS force field) have been fitted to literature data [36]. The equilibrium angle and its force constants were given for zeolite structures based on *ab-initio* quantum mechanical calculations. The complete data set used a coupling between bond distances and the bond angle. At increasing Si-O-Si angle the bond length decreases and *vice-*

repeating unit	$-Si(CH_3)_2$-O–
mw repeating unit	74.15
glass transition temperature	-128 ^{0}C
melting temperature	-40 ^{o}C
average density (T=300K)	0.95 cm^{-3}

Table 4.1: Some characteristic properties of short chain polydimethylsiloxane(PDMS) (from [35]). Note, the properties depend slightly on the polymer chain length.

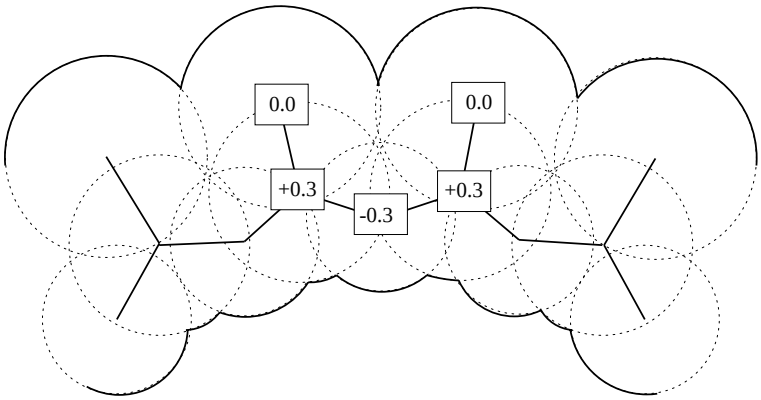

Figure 4.1: Schematic picture of part of a PDMS chain. Indicated are the van der Waals spheres, the partial charges and the bonds. Note that only one of the CH_3 groups is shown.

versa. In GROMOS there is no such coupling however, so care has to be taken to extract the correct data. The complete parameter set is shown in table 4.2.

Bonds	l(nm)			
Si–O	0.160			
Si–CH_3	0.188			
Angles	k_θ (kJ/mol)	θ_0		
Si–O–Si	118.4	144.0		
O–Si–O	791.2	109.5		
O–Si–CH_3	418.4	109.5		
CH_3–Si–CH_3	418.4	109.5		
Dihedrals	k_φ (kJ/mol)	n	δ	
CH_3–Si–O–Si	3.77	3	0	
Si–O–Si–CH_3	3.77	3	0	
O–Si–O–Si	3.77	3	0	
Non-bonded	ϵ (kJ/mol)	σ (nm)	q (e)	m (a.m.u.)
Si	2.4480	0.3385	0.3	28.080
O	0.8493	0.2955	-0.3	15.999
CH_3	0.7532	0.3786	0.0	15.035
CH_4	1.2466	0.3733	0.0	16.043
He	0.0850	0.2580	0.0	4.0026

Table 4.2: Force field parameters.

4.3 Generation of starting structure

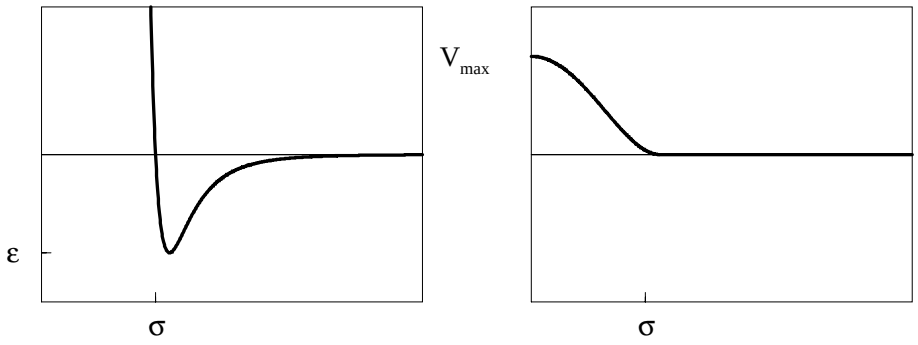

Figure 4.2: Left: normal 'Lennard Jones' potential. Right: soft-core potential

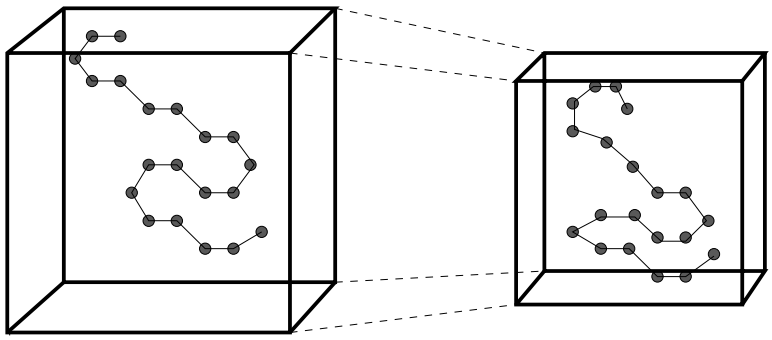

Figure 4.3: During the generation of the starting structure the boxsize is constantly decreased while using a soft-core interaction so polymer chains can move through eachother.

The specific properties of (amorphous) polymers prevent the usual way of preparing a starting configuration. In liquid simulations one can simply start from an idealized, randomly perturbed (crystal) structure and during the first few picoseconds of the simulation the system will equilibrate. The relaxation times of polymers, even of moderate lengths however, are some orders of magnitude larger than the average simulation time. (Of the order of 10^{-3} s instead of 10^{-9} s.) Because of these longer relaxation times, we need some other way of preparing a starting sample. A commonly used method is based on a self-avoiding random walk [37]. In this method a chain is built up site by site. The position of the next site is chosen on the basis of the position of the previous site, using a given bond length and angle and a randomly chosen dihedral angle. This site is then either accepted or rejected with a Monte Carlo-like criterion based on its interaction energy. The disadvantage of this method is that at higher densities the acceptance rate of adding another site is practically zero.

The method we have employed to avoid this problem is based on MD rather than MC and uses *soft-core potentials*. The procedure is as follows. One starts with a very

dilute system of several chains subject to the normal periodic boundary conditions and interacting through the normal *bonded* forces. But if we also used the normal van-der-Waals like potentials, then chains never could get entangled. They would simply be pressed together as blobs of soft matter. So instead of using the van-der-Waals like potentials we model the non-bonded interactions between atoms by a soft core repulsive potential (see figure 4.2):

$$\begin{aligned} V(r) &= V_{max}\left(1-\left[\tfrac{r}{r_{sc}}\right]^2\right)^2 && r < r_{sc} \\ &= 0 && r \geq r_{sc} \end{aligned} \tag{4.1}$$

In the preparation phase V_{max} is set such that molecules are able to move through each other and thus can form entanglements. Even though the process is unphysical it does prevent the chains from getting trapped in unphysical conformations. Every MD step the size of the simulation box is decreased by a small amount until the correct density is reached. (One can even go to a slightly higher density to allow for pressure relaxation in the first normal MD steps.)

At this time an energy minimization is performed with the normal Lennard-Jones like non-bonded interaction to relieve the excess stress in the system, after which normal constant pressure molecular dynamics steps can be done.

4.4 Computational details

In this chapter we will give the results of a 500 ps simulation of a PDMS sample of 12 chains of 60 monomer units each. This simulation has been performed using the GROMACS[1] simulation package on the 32 processor intel i860 machine developed at the university of Groningen. The simulations were carried out under NVT conditions (at that time GROMACS was not able to perform NPT simulations.) The temperature was kept on average at 300 K, by use of a weak coupling to a temperature bath (equation 3.16), with a coupling constant of 0.1 ps. Lennard Jones-forces were considered for $r <$ 1.0 nm and Coulomb forces for $r <$ 1.2 nm. The latter were computed every time step for $r <$ 1.0 nm and once every 10 time steps for 1.0 nm $< r <$ 1.2 nm. The time step in the leap-frog integration scheme was 5 fs. The energies, coordinates and velocities were written to disk every 0.5 ps.

[1] GROningen MAchine for Chemical Simulations

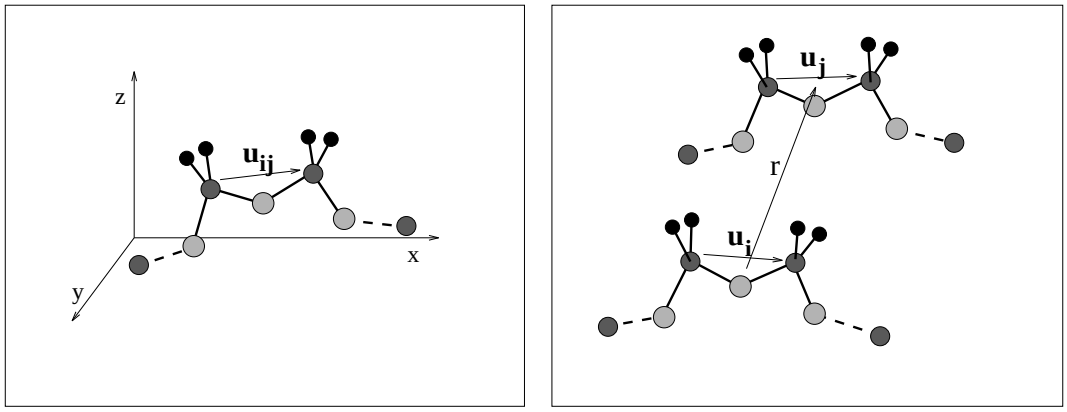

Figure 4.4: Definition of the two order parameters. Left: The order parameter $S(|i-j|)$ is a function of the angle θ_{ij} between the vector $\mathbf{u}_{ij}$ and one axis in a laboratory frame. The vector $\mathbf{u}_{ij}$ is defined between the Si-atom belonging to monomer i to the Si-atom belonging to monomer j. (The picture showing the case j=i+1). Right: In the alternative definition of the order parameter $S(r_{ij})$, θ_{ij} is the angle between two vectors $\mathbf{u}_i$ and $\mathbf{u}_j$. These describe the direction of two monomer units i and j, either belonging to the same or different polymer chains.

4.5 Analysis of the results

4.5.1 Structural properties

The local structure of the system can be described by the pair-correlation or radial distribution function $g(r)$. This is the probability of finding a particle center at distance r from another particle center. This property can be evaluated *intra*-chain and *inter*-chain.

The order parameter S provides a check on the amorphous character of the polymer sample. In general, overall segmental orientation may be expressed in terms of a Legendre polynomial

$$S(\mid i-j \mid) = \left\langle \frac{3\ \cos^2(\theta_{ij}) - 1}{2} \right\rangle \tag{4.2}$$

where θ_{ij} is the angle between the directional vector $\boldsymbol{u}_{ij}$ characteristic of a given segment (between monomer i and j) and an axis in a given laboratory frame, as shown in figure 4.4. The angular brackets denote an ensemble average. This order parameter S can vary between -0.5 and 1.0. A value of 0.0 indicates random ordering of segments. This way to define the order parameter shows the average order of the polymer chains with respect to the laboratoy frame. The order parameter is in fact a tensor defined by the products of direction cosines; I shall only use the diagonal elements given by eq. 4.2

A similar formulation can be used to investigate the intrinsic order of the total polymer matrix as the $\cos^2$ of the angle between vectors defined by two different monomer segments, as a function of their cartesian distance:

$$S(r_{ij}) = \left\langle \frac{3\ \cos^2(\theta(r_{ij})) - 1}{2} \right\rangle \tag{4.3}$$

but now $\theta(r_{ij})$ is the angle between two vectors $\boldsymbol{u}_i$ and $\boldsymbol{u}_j$ with cartesian distance r. These vectors are now defined between the two adjacent monomer units each. This property can be evaluated intra-chain as well as inter-chain.

4.5.2 Radius of gyration, end-to-end distance

The size of a polymer chain is usually given as radius of gyration R_{gyr} or as the end-to-end distance R_{ee} of the polymer chain. The radius of gyration is defined as

$$R_{gyr} = \sum_{i=1}^{N} (\boldsymbol{r}_i - \boldsymbol{R}_{CG})^2 \tag{4.4}$$

where $\boldsymbol{R}_{CG}$ is the center of geometry of the polymer chain fo N monomer units. The autocorrelation function of R_{gyr} and R_{ee} give an indication of the relaxation times in the polymer.

4.5.3 Diffusion

The diffusion coefficients are directly calculated from the motion of the particles, in particular from the mean square displacement of the particles.

$$D = \lim_{t\to\infty} \frac{1}{6t} \left\langle [\boldsymbol{r}_t - \boldsymbol{r}_0]^2 \right\rangle \tag{4.5}$$

To increase statistics the squared displacement is evaluated using all possible time origins. This equation holds only in the case that the observation time (i.e. the simulation time) is large enough to allow the particles to show uncorrelated motion. This means that the mean squared displacement is linear with time. There are cases however, in which the mean squared displacement $\left\langle [\boldsymbol{r}_t - \boldsymbol{r}_0]^2 \right\rangle$ or $\left\langle r^2(t) \right\rangle$ is not linear in time but displays a different power law :

$$\left\langle r^2(t) \right\rangle \propto t^n \tag{4.6}$$

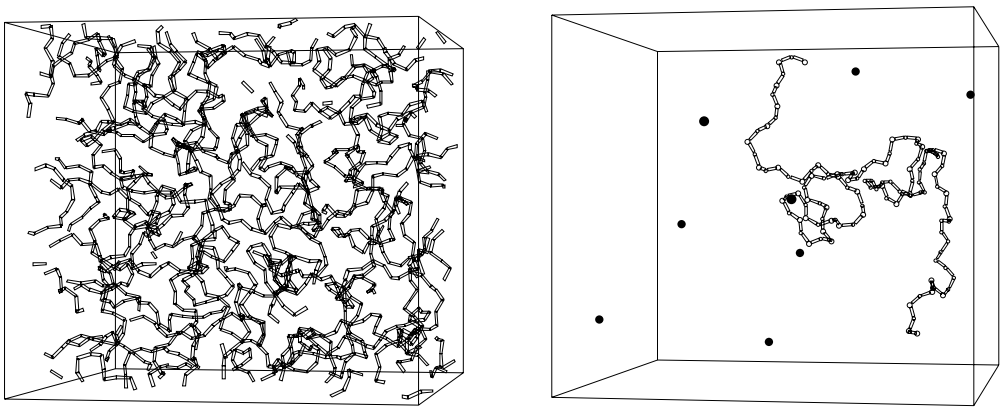

Figure 4.5: **Left:** *Snapshot of polymer system after equilibration. Only the backbones are shown.* **Right***: Only one chain and the inserted penetrants (see next chapter) are shown.*

where n has a fractal value different from 1 (denoting normal diffusion) or 2 (denoting linear motion). If $1 < n < 2$ it is called superdiffusive motion and it can occur if besides diffusive motion also *e.g.* convective motion is present. If $n < 1$ we are talking about subdiffusion or anomalous diffusion. Diffusion of a particle in a fractal medium exhibits this behavior. A medium is fractal if a quantity (*e.g.* the for diffusion available volume V_d) does not scale with sample size L with the Euclidean dimension, but with some non-integer value,

$$V_d \propto L^D \tag{4.7}$$

An example of this behavoir is the *"ant in the labyrinth"*, a term coined by de Gennes in 1976 [38], where a particle (the ant) performs a random walk on a grid on which sites are randomly blocked for diffusion (the labyrinth). At certain concentrations of blocked sites the medium displays fractal behavior. Due to the presence of large and small holes, bottlenecks, and dangling ends, the motion of the ant is slowed down. In those circumstances Fick's diffusion laws are not longer valid and the diffusion is anomalous.

4.6 Results

Starting structure

Using the above described shrinking procedure for a box containing 12 chains of 60 monomer units we started at a density of 0.1 g/cm^3. We then shrunk the box (employing the soft-core potential) to 1.0 g/cm^3 and performed an energy minimization. Following the energy minimization we simulated the system under constant NPT conditions during

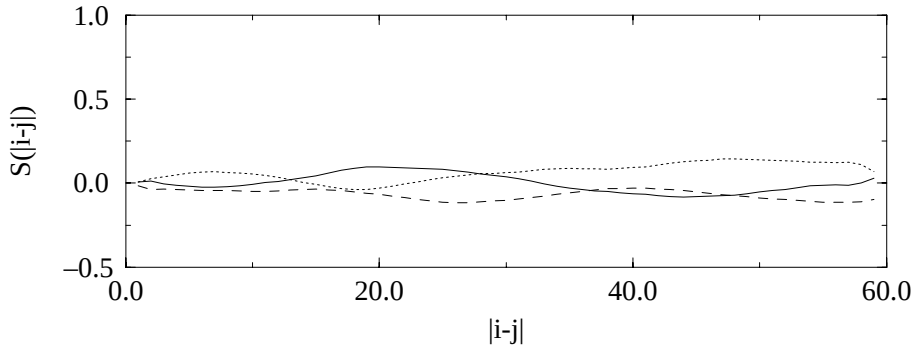

Figure 4.6: Order parameter $S(|i-j|)$ with respect to a reference frame. The three curves show the ordering with respect to the x- y- and z- axes of the laboratory frame.

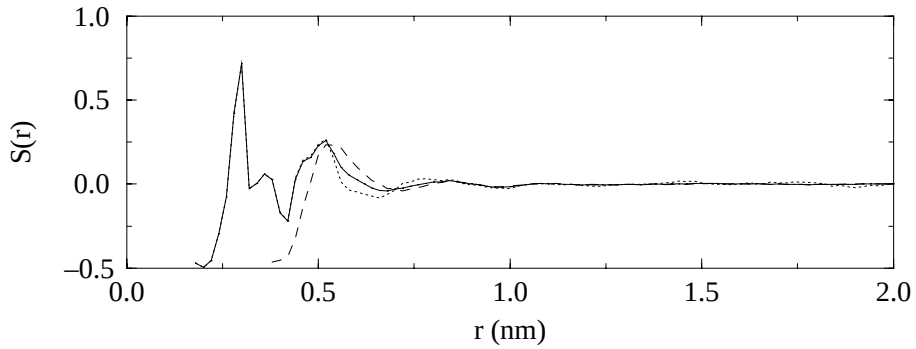

Figure 4.7: Order parameter as function of cartesian distance S(r). The solid line displays the total order parameter, the dotted curve the intra-chain contibution and the dashed curve the inter-chain contribution.

200ps by use of the GROMOS simulation package [26]. In the first 20 ps of the constant pressure molecular dynamics run (with normal Lennard-Jones potential) the system shrunk from the density of 1.00 g/cm^3 to 1.02 g/cm^3, which is close to the experimental density of PDMS with chain lengths of 60 units. After these 20 ps the volume of the system remained constant as well as the total, potential and kinetic energies. The resulting configuration after the equilibration of 200 ps was used as the starting point for the 500 ps production run under NVT-conditions.

4.6.1 Structural properties

Order parameter

The order parameter as defined in equation 4.2 gives information about specific ordering of parts of the chains with respect to a reference frame. Figure 4.6 shows this order parameter $S(|i-j|)$ which is calculated over the complete 500 ps simulation (sampled

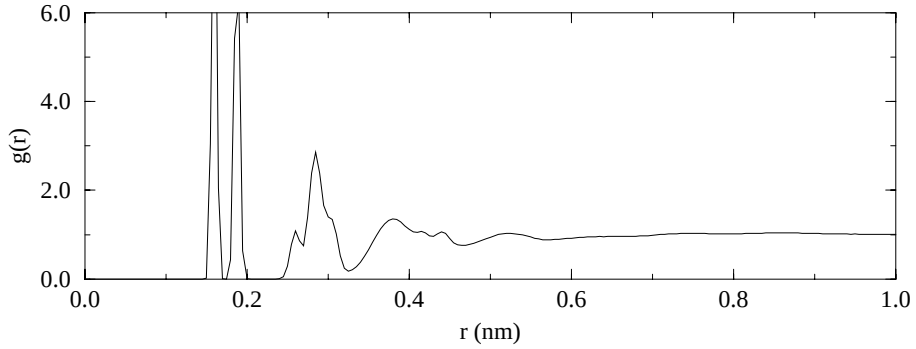

Figure 4.8: Total radial distribution function g(r) of PDMS.

every 0.5 ps). It can be seen from this figure that there is no ordering of the chains with respect to either of the three axes of the laboratory frame. The values are in the range of +0.2 to -0.2. The fluctuations are probably a result of the limited simulation time and sample size. (Note that for the first point ($|i-j|=1$) there are $12 \times 59 = 708$ samples, but for the last($|i-j|=59$) only 12.) Figure 4.7 shows the order parameter as defined in equation 4.3 calculated from the same simulation. In the range from 0 to 0.16 nm the order parameter can not be calculated because of the van der Waals interactions of the atoms. It is clear that there is a certain order at close distances, but this effect vanishes at distances beyond 1.0 nm. The order parameter can be split into an inter-chain and an intra-chain contribution. They are also displayed in figure 4.3 and it shows that the ordering in the range from 0 to 0.75 nm is largely due to the intra-chain part. The inter-chain order parameter is not defined until 0.36 nm. In the range of 0.36 to 0.48 nm S(r) is negative, denoting a perpendicular ordering. This is a result of the fact that chains can come closer to each other if they are perpendicular. In this configuration the bulky methyl side groups have the least interference, like two dumbells placed perpendicular on top of each other. From the results of both $S(r)$ and $S(|i-j|)$ it is clear that the PDMS sample is effectively amorphous.

Radial distribution function

Figure 4.8 shows the total radial distribution function or pair-correlation function $g(r)$ between all the atoms of PDMS. This reflects the complex internal structure of the polymer matrix. In order to understand the multitude of peaks it is useful to split this up in an intra- and inter-chain part. The intra-chain contribution, broken up in the individual atom pair correlation functions is shown in figure 4.9. The origin of the designated peaks in this figure is explained in the accompanying scheme (figure 4.10).

The inter-chain rdf's, shown in figure 4.11, are more interesting from the viewpoint of permeation. They show the environment which a penetrant would "feel". There is very little structure in the total interchain rdf.

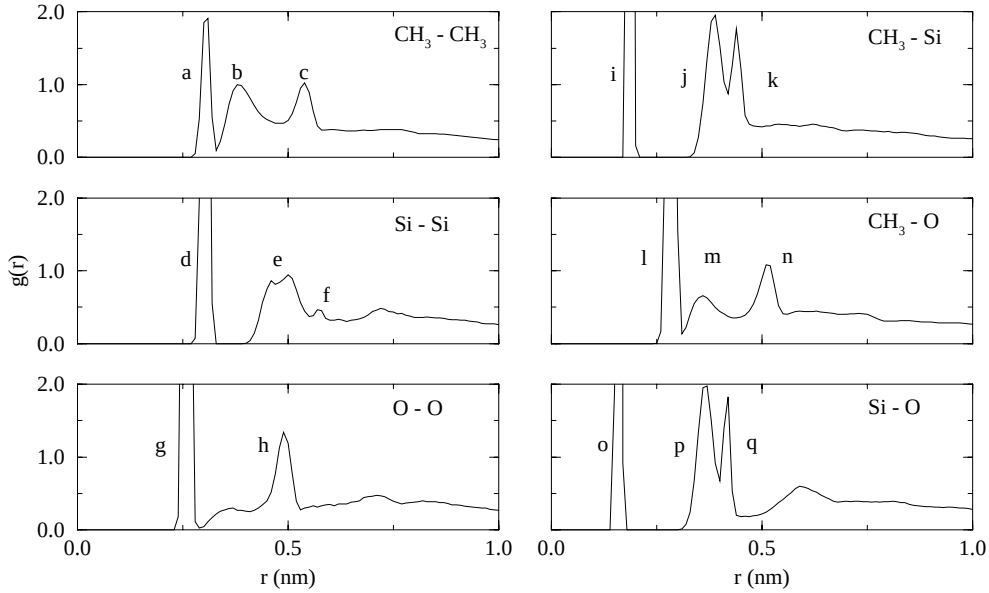

Figure 4.9: Intra-chain radial distribution functions g(r).

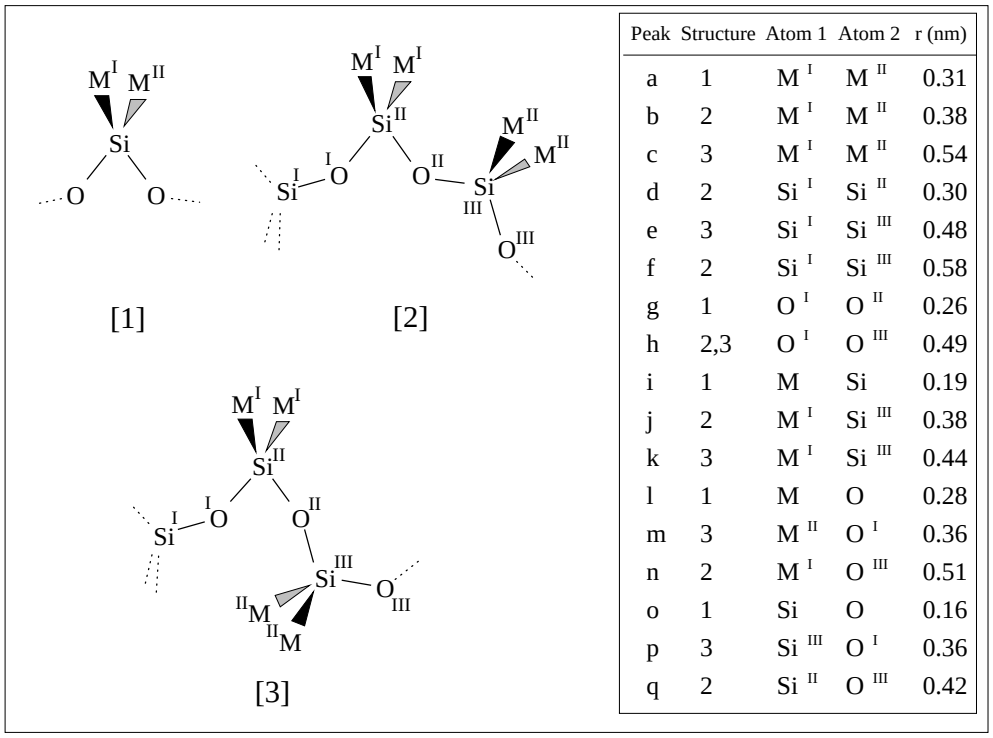

Peak	Structure	Atom 1	Atom 2	r (nm)
a	1	M^{I}	M^{II}	0.31
b	2	M^{I}	M^{II}	0.38
c	3	M^{I}	M^{II}	0.54
d	2	Si^{I}	Si^{II}	0.30
e	3	Si^{I}	Si^{III}	0.48
f	2	Si^{I}	Si^{III}	0.58
g	1	O^{I}	O^{II}	0.26
h	2,3	O^{I}	O^{III}	0.49
i	1	M	Si	0.19
j	2	M^{I}	Si^{III}	0.38
k	3	M^{I}	Si^{III}	0.44
l	1	M	O	0.28
m	3	M^{II}	O^{I}	0.36
n	2	M^{I}	O^{III}	0.51
o	1	Si	O	0.16
p	3	Si^{III}	O^{I}	0.36
q	2	Si^{II}	O^{III}	0.42

Figure 4.10: Schematic picture of different conformations of a PDMS chain. The table illustrates the origin of the rdf-peaks in the previous figure. (M is the code for the methyl side group).

From this figure it is clear to see that the exterior of the chain, that is the part of the chain that comes into contact with a penetrant, consists mainly of methyl side chain groups and backbone oxygen atoms. The silicon atoms are more or less shielded by the other atoms. It only comes into play after ≈ 0.5 nm, after the first contacts of the CH_3 and O groups. This shielding of the silicon atoms might become important if we were to look at the diffusion of charged particles.

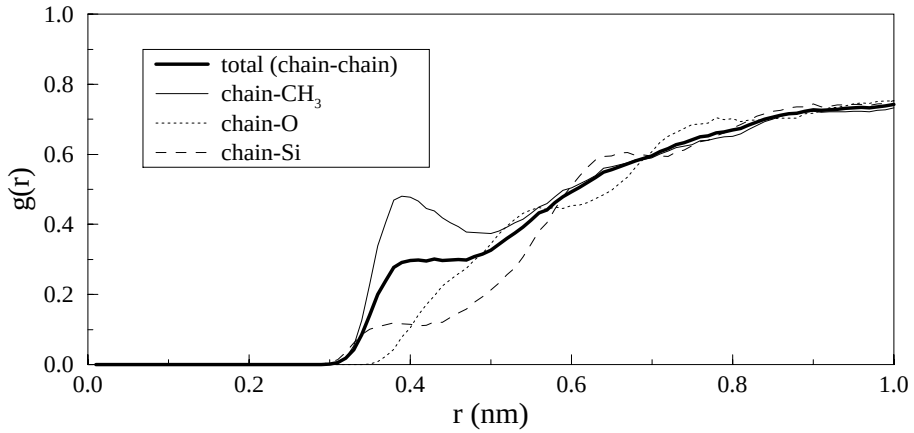

Figure 4.11: Inter-chain radial distribution functions g(r). The total chain-chain radial distribution function is shown by the solid line, while the seperate chain-atom contributions are shown by the thin solid, the dashed and the dotted lines.

4.6.2 Dynamical properties

Diffusion of the polymer chains

The motion of the polymer chains themselves can contribute substantially to the diffusion of penetrant particles trapped in the polymer. We have calculated the diffusion coefficients of the polymer segments during the simulation, where we have taken the first segment together with the last and averaged over 8 segments (so segment 1-4 and 57-60 are represented by one point). Figure 4.12 shows a typical mean squared displacement curve through which the diffusion coefficients are calculated (top figure). The same curve is also shown on log-log scale (bottom figure). The slope of this curve gives the exponent of the time dependence of motion n ($\left\langle r^2(t) \right\rangle \propto t^n$). At first it is approximately 0.20 and slowly increases to 0.66. It is clear that the motion of these chains shows no real diffusive motion yet, which would require a slope of unity.

According to Kremer [30] the system size is too small to see reptative motion[2]. In this mode of motion the slope of the curve would decrease to 0.25 at longer times after which

[2]predominant motion along the diameter of the reptation tube

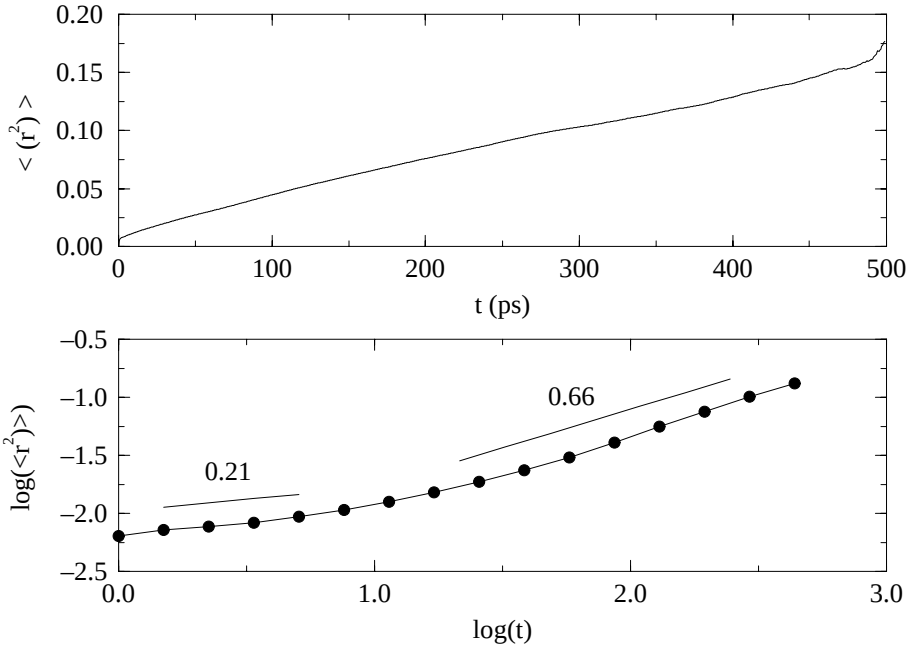

Figure 4.12: Mean squared displacement curve of segments 5 to 8 (and 53 to 60) (top) and the same curve on log-log scale (bottom) (also indicated is the slope at two different points of the curve).

it would finally reach the real diffusive regime. The estimated chain length at which Kremer[30] first sees this reptation regime corresponds to $\approx$ 175 monomer units and the estimated reptation diameter for PDMS is 6 nm. So in both aspects our system is too small to see this reptation motion. At longer simulation times the exponent would gradually increase to a value of unity. The crossover time to normal diffusion is also estimated by Kremer and it is of the order of 10 ns[30].

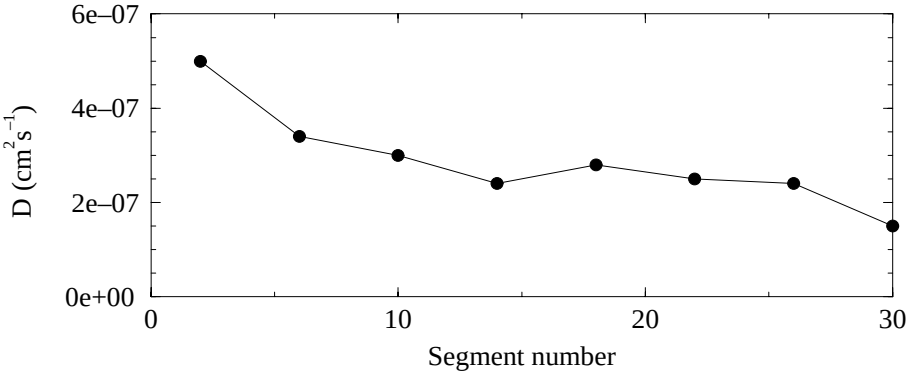

Figure 4.13: Esimates of the diffusion coefficients of the chain segments along the polymer chain. Several monomers are taken together in the calculation.

The resulting *estimates of the* diffusion coefficients are presented in figure 4.13. As can be seen in this figure the end-groups of the chains are more mobile by a factor of ≈ 2.5. This is an important fact, because this shows that the chain length of the polymer chains has an influence on the dynamic properties of the polymer matrix. A system of longer chains has a smaller end-group density and will thus be less mobile.

The diffusion coefficient of the centers of mass of the twelve seperate chains is estimated at $3.10^{-8}\mathrm{cm}^2\mathrm{s}^{-1}$. But here also the real diffusive regime has not been reached yet. And this number should be seen as an upper limit of D.

Radius of gyration, end-to-end distances

To get an idea of the relaxation times in the polymer matrix I have calculated the auto correlation function of the chain radius of gyration and the end-to-end distances of the chain (see figure 4.14). If we define the relaxation time as that time where the auto correlation function has dropped to $1/e$, we find values of 25 ps for the radius of gyration and 75 ps for the end-to-end distances.

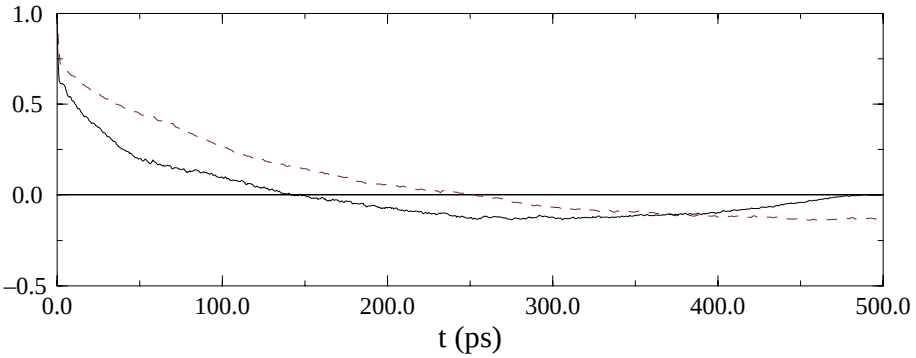

Figure 4.14: Auto correlation function of the radius of gyration of the 12 seperate PDMS chains (solid line) and the auto correlation function of the end-to-end distance of the chains (dotted line). (Before calculating the autocorrelation function the average value was substracted first.

4.7 Discussion

From the results presented above we can conclude that the polymer sample is effectively amorphous. Also the density of the system is comparable to experiment, and together this shows that, within the limits of the classical model, the simulation model is a good representation of a polydimethylsiloxane polymer. However there is always a need for further verification using other experimental methods (for example spectroscopic methods).

The complex nature of the radial distribution functions directly shows the need for atomistic molecular dynamic simulations instead of coarse grained lattice methods. A detailed representation of the environment of the penetrant is a requirement for the simulation of the motion of the penetrants.

The neccessary time scale of simulation is not yet clear from these results; for a good description of *polymer* diffusion we would have to simulate up to 10 ns! But we are not directly interested in the long time diffusion behavior of polymer chains, but in penetrant diffusion through polymers. At first instance we only need a good description of the penetrants environment. For this the relaxation times of the radius of gyration and the end-to-end distance are a better indication.

Chapter 5

MD simulation of gas transport through PDMS

In this chapter results will be presented of the simulation of the actual penetrant diffusion process in the polymer matrix. Eight penetrants are inserted in the polymer sample and followed over a simulation period of 500 ps. This is done for seven sets of different penetrant sizes. For all of these penetrants (and more) the chemical potential is calculated as well. Using the diffusion coefficients and the chemical potential the permeability coefficients are calculated as function of penetrant size. All results will be discussed and compared to other simulations and experimental data.

5.1 Introduction

In recent history there have been a number of reports about simulations concerned with the process of diffusion of penetrants in polymers. Most early polymer-penetrant simulations were carried out using largely simplified but tested models, picking the fruits of the first polymer simulations. The first study was performed by Trohalaki *et al.* [39] in 1989. He simulated 25 chains of 20 (united atom) CH_2 units for 200 ps with 4 penetrants modeling CO_2. The diffusion coefficients obtained were too large, which he attributed to the presence of crystallytes in the real polymer, an argument frequently used afterwards by several other researchers. An even more idealized polymer model was used by Sonnenburg *et al.* [40]. They simulated a freely jointed chain (no angle or dihedral potential) where the end-groups of the 16 chains (of 20 monomer units each) were fixed to lattice sites of a diamond lattice. The (single) penetrant and the polymer beads interacted through a potential which consisted of the repulsive part of the Lennard-Jones potential (see eq. 3.10) only. As a result of the highly idealized

nature of the model it was not possible to compare the resulting diffusion coefficients quantitatively, but qualitatively the effect of penetrant size on diffusion was comparable to experimental data.

Takeuchi *et al.* reported an elaborate study of the diffusion characteristics of penetrants in rubbery as well as glassy polymers [41–44]. They used a united atom polyethylene (PE) polymer model, first a system consisting of 30 chains of 20 segments each, later an *infinite* chain model[1]. Calculating the free volume and the diffusion coefficients of the 20 penetrants[2] at different temperatures above the glass transition temperature they found that the diffusion coefficients obeyed the simple free volume model of Fujita[46]. The values of the diffusion coefficients they obtained are similar to those of Trohalaki *et al.*, thus too large by two orders of magnitude. Takeuchi also simulated a system of freely rotating chains (same PE model without dihedral potential) and found that it had a clear effect on the diffusion. The rotational relaxation time was about 30 times shorter than in the PE model and D was twice as large [41]. The use of an infinite chain model in his earlier simulations [43] reduced the rotational relaxation time by only 50%, but also resulted in a factor of 2 difference in D. This led Takeuchi to conclude that other effects, *i.e.* coupled motions of the chains and penetrants and difference in structure of the infinite and finite model, influence the diffusion as well.

Other simulations of penetrant diffusion in polyethylene also show the discrepancy of experiment and simulations [47] but this was largely corrected by including either an all-atom description of the polymer [48, 49] or an anisotropic united atom (AUA) description [50–52][3]. This resulted in satisfactory agreement with experimental data for diffusion in polyethylene, polyisobutylene and polypropylene.

The details of diffusion in glassy polymers was also studied by Takeuchi [42]. In glassy polymers the diffusion is slower than in rubbery polymers and meaningful diffusion coefficients could not be obtained. He did find, however, that the diffusive motion could clearly be identified as a *jump motion*. The jump occurs when the cage which traps the penetrant connects to another cage by fluctuative motion of the polymer chains. This happens without a significant change in energy barrier. Boyd and Pant [50–52] also found jump diffusive behavior and found that the average jump length increases with increasing temperature, while the distribution of jump lengths broadens significantly.

By changing the bond-angles of the polymer Takeuchi *et al.* [44] changed the free volume distribution while keeping the total free volume content equal. The diffusion constant *did* depend on the free volume distribution so that the free volume model of

[1]The infinite chain model makes use of the periodic boundary conditions usually applied in MD simulations. A new periodic condition is imposed so that the "beginning" of the chain connects to the L'th (usually 3rd) periodic image of the "end" of the chain [45]

[2]this large number of penetrant was reduced to 10 in latter studies to achieve a more realistic penetrant concentration.

[3]In the AUA description the center of the Lennard Jones is placed outward from the carbon center on the valence angle bisector. This model was first used by Toxvaerd [53].

Fujita was not obeyed.

Anomalous diffusion of oxygen penetrants in polymers (polyisobutylene) was reported by Müller-Plathe [54].[4] Helium also displayed anomalous diffusion up to 10 ps, and between 10 to 100 ps there was a gradual crossover to normal diffusion. Müller-Plathe also used nonequilibrium MD techniques to study penetrant diffusion [55], but concluded that although the method is useful, there is no significant gain in computational speed.

Gusev and Suter [56] used a short equilibrium MD simulation to study the fast (elastic) thermal motion of the polymer and used this information for a stochastic simulation of solute dynamics up to ca. 1 ms! Although all-long time motions of the polymer were left out, the resulting diffusion coefficients are surprisingly close to experiment.

I have simulated two different PDMS samples. As a preliminary study I simulated a small system of five chains of 30 monomer units each. In this sample I introduced one penetrant, either He or CH_4 making a total of 606 (united) atoms and performed two MD runs of 250 ps with CH_4 and one of 150 ps with He as a penetrant. This particular choice of penetrants shows the interesting feature that experimentally He has a larger diffusion coefficient than CH_4, but because of its lower solubility He permeates slower than CH_4.

After that I simulated a larger system (12 chains of 60 monomer units). In the larger system I introduced 8 penetrants, in total 2900 (united) atoms. As there have been a number of simulations which focus on different temperatures, in these simulations I concentrated on the effect of penetrant size. This means that I used seven sets of penetrants with different size, but equal interaction parameter.

5.2 Analysis of the results

5.2.1 Solubility / Chemical potential

The solubility is given by equation 2.12 as :

$$S = \exp(-\mu_{ex}/RT). \tag{5.1}$$

This chemical potential μ_{ex} is calculated using the particle insertion method based on an idea of Widom in 1963 [3]. In this method one inserts a virtual particle i at a random position in the sample and calculates its interaction energy E_{0i} it would experience if it would really be at that position. The thermodynamic potential is then calculated using :

[4] The mean squared displacement curve of oxygen was fitted to a function $\langle r^2(t) \rangle = a + bt^n$ and n was found to be ≈ 0.8.

$$\mu_{ex} = -RT \ln \langle \exp(-E_{0i}/kT) \rangle \tag{5.2}$$

where the angular brackets denote an ensemble average, which in practice means that the insertion is repeated many times and for many polymer configurations and the energy is averaged according to its Boltzmann weight. This expression for the chemical potential is derived in the canonical (NVT) ensemble. (In the constant NPT-ensemble one finds an analogue relation[22] :

$$\mu_{ex} = -RT \ln \left[\langle V \rangle^{-1} \langle V \exp(-E_{0i}/kT) \rangle \right]. \tag{5.3}$$

The results obtained by both formulations usually do not differ significantly [55].) The angular brackets in both eq. 5.2 and eq. 5.3 denote an ensemble average. Since we are limited to a finite numbers of insertions there is a possibility that we do not sample phase space sufficiently. A good measure on exactly how many insertions are necessary is given by the distribution of states [57]. This is given by the product of the the probability $\rho(E)dE$ that the penetrant upon insertion experiences an energy between E and $E + dE$ and its Boltzmann weight. The function $f(E)d(E)$ (eq. 5.4) should be sampled well across its maximum value, so it should include the low energy region.

$$f(E)dE = \exp(-E/kT)\rho(E)dE. \tag{5.4}$$

This will fail when the density of the sample is too high (or equivalently if the particle to be inserted is too large) resulting in a low ratio of insertions with a non-negligible Boltzmann-weight.

The excess partial molar enthalpy h_{ex} associated with the process of solvation can also be calculated in a way similar to that of the chemical potential (See appendix C for details) :

$$h_{ex} = \frac{\left\langle E_{0i} e^{-\beta E_{0i}} \right\rangle}{\left\langle e^{-\beta E_{0i}} \right\rangle} + \frac{\left\langle E_{ij} e^{-\beta E_{0i}} \right\rangle}{\left\langle e^{-\beta E_{0i}} \right\rangle} - \langle E_{ij} \rangle, \tag{5.5}$$

where E_{0i} is the energy of the inserted penetrant, and E_{ij} the internal energy of the host (=polymer) system. The $<>$ brackets again denote an ensemble average.

Using both μ_{ex} (eq. 5.2) and h_{ex} (eq. 5.5) the excess partial molar entropy s_{ex} associated with the process can also be evaluated using the equation:

$$\mu_{ex} = h_{ex} - T s_{ex}. \tag{5.6}$$

5.2.2 Diffusion

For the determination of the diffusion coefficient I use the mean squared displacement

$$D = \lim_{t\to\infty} \frac{1}{6t} \left\langle [\boldsymbol{r}_t - \boldsymbol{r}_0]^2 \right\rangle \tag{5.7}$$

as described in the previous chapter (section 4.5.3) and the reader is referred to that chapter for details.

Van Hove self-correlation function

Next to the determination of D we also want to visualize the diffusion process. One way to do this is by use of the van Hove function $G(\boldsymbol{r}, t)$. This van Hove function is related to neutron scattering data [58] and can be split up in a *self* (G_s) and a *distinct* (G_d) part:

$$G(\boldsymbol{r}, t) = G_s(\boldsymbol{r}, t) + G_d(\boldsymbol{r}, t) \tag{5.8}$$

$$G_s(\boldsymbol{r}, t) = \frac{1}{N} \left\langle \sum_{i=1}^{N} \delta \left[\boldsymbol{r} + \boldsymbol{r}_i(0) - \boldsymbol{r}_i(t)\right] \right\rangle \tag{5.9}$$

$$G_d(\boldsymbol{r}, t) = \frac{1}{N} \left\langle \sum_{i\neq j=1}^{N} \delta \left[\boldsymbol{r} + \boldsymbol{r}_i(0) - \boldsymbol{r}_j(t)\right] \right\rangle \tag{5.10}$$

So the self part of $G(\boldsymbol{r}, t)$ is the probability that at time t a penetrant will be in a volume $d\boldsymbol{r}$ at $\boldsymbol{r}$ from its original position. The distinct part shows the cross-correlation effects (which will not be discussed in this thesis). The limiting values for $t = 0$ are $G_s(\boldsymbol{r}, t) = \delta(\boldsymbol{r})$ and $G_d(\boldsymbol{r}, t) = g(\boldsymbol{r})$. In this thesis I will use the scalar version of the self part of the van Hove function $G_s(r, t)$. That is the probability that a penetrant has traveled a distance r in time t. Note that in the van Hove correlation function all possible time origins are used just as is normal practice in the calculation of the mean squared displacement.

Residence time

The van Hove self correlation functions show the difference in diffusion properties very nicely, but to get some additional feeling for the difference between the different penetrants I have defined a quantity $f_r(t)$:

$$f_r(t) = \int_0^r G(r', t)dr'. \tag{5.11}$$

This is the average fraction of penetrants that is within a distance of r from its origin (at time $t = 0$) at time t. If I choose a distance r equal to an average hole size, then $f_1(t)$ is a measure for the fraction of penetrants to stay within a hole. I now define a time $t_{0.50}$, the time at which $f_r(t)$ drops to 0.50, as a measure for a "residence time". (This fraction of 0.5 is an arbitrary measure of course but will serve its purpose.).

5.2.3 Estimation of errors

The error in the diffusion constant is calculated by use of equations presented in appendix B :

$$\left\langle r^2 \right\rangle = 6Dt \left(1 \pm \frac{\sqrt{\frac{2}{3}\sqrt{\pi}}}{\sqrt{n}} \right), \tag{5.12}$$

where the number of independent samples n is taken as the total simulation time divided by the "residence time", $t_{0.50}$ described above. Note that only that part of the mean square displacement curve can be used for which real diffusive behavior is observed (see previous chapter).

The statistical errors in the values for the chemical potential and excess molar enthalpies are simply calculated by taking several independent samples. The time between independent samples is taken to be 50 ps. This is roughly the relaxation time of the end-to-end distance and the radius of gyration of the polymer chains (see previous chapter).

5.3 Small system

In this section we will only give some of the results of the simulation of the small system. A full description, including computational details can be found in appendix A.

A starting structure was generated of a system consisting of five chains of 30 monomer units each using the aforementioned method. The density of this system was 0.95 g/cm^3. The simulations were performed using the GROMOS [26] simulation package under constant NPT conditions.

The diffusion constants calculated with the mean squared displacements (eq. 4.5) from the one-particle trajectories are fairly close to the experimental data ($2.1 \cdot 10^{-5}$ cm^{2}s^{-1} for CH_4 and $18 \cdot 10^{-5}$ cm^{2}s^{-1} for He). The diffusion constant for CH_4 has been

calculated from two separate runs of 250 ps to get the desired accuracy. For He, one run of 150 ps was sufficient.

The chemical potential calculated with the particle insertion method (eq. 5.2) is -6.3 kJ mol^{-1} for CH_4 and +3.8 for He. All data on the small system is accumulated in table 5.1, and compared to experimental data.

The diffusion constants are in good agreement with experiment and although the absolute values of the solubilities are too high, the simulation is able to show the relative difference between He and CH_4. The diffusion constant of helium is larger that that of methane, but because of it's lower solubility the total permeation coefficient is smaller.

5.4 Large system

I have done a series of simulations of penetrant diffusion in the larger PDMS sample (12 chains of 60 monomer units). The starting configurations for all simulations was the same as for the simulation without penetrant (see previous chapter). Eight penetrants (with the parameters of helium) were inserted in the polymer at random positions where their interaction energy with the polymer was favorable. This sample was equilibrated for 50 ps under NPT conditions and no appreciable change in volume was observed.

In order to check the effect of penetrant size on diffusion I have chosen a series of penetrant sizes based on the Lennard-Jones parameters of He (penetrant diameter σ = 0.258 nm and interaction energy parameter ε = 0.085 kJ mol^{-1}). Seven different penetrant diameters ranging from σ = 0.150 to 0.450 nm have been used in the simulations. The penetrants of the equilibrated sample were changed in size and additional equilibration simulations of 20 ps were performed before starting the actual production simulations (under NVT conditions)[5].

Next to these standard molecular dynamics simulations I have performed several *position*

[5] At that moment the simulation package GROMACS was not able to perform constant pressure simulations

	$D \cdot 10^5$ (cm^2s^{-1})		μ_{ex} (kJ mol^{-1})		S	$P \cdot 10^5$ (cm^2s^{-1})	
CH_4 (simulation)	2.1	(0.8)	-6.3	(0.2)	12.5	26	(7)
He (simulation)	18	(2)	+3.8	(0.2)	0.22	3.9	(0.6)
CH_4 (exp.)	2.0		+1.9		0.56	1.11	
He (exp.)	10		+7.4		0.05	0.5	

Table 5.1: Summary of simulation results and comparison with experimental data ([59, 60]) of the small system. Errors are given in parentheses.

restrained simulations of 250 ps each. This is done to investigate the effect of the polymer dynamics on the diffusional process. In position restrained simulations a part of the system is restrained to its starting position. This is done by applying an extra harmonic potential with a very high force constant[6] k, $V = \frac{1}{2}k(r_t - r_0)$ where r_t and r_0 are the positions of the restrained atoms at time t and time 0 respectively. Thus effectively this part of the system is taken to be fixed.

Two different sets of position restrained simulations have been performed, one with the complete polymer fixed and an intermediate system where only the polymer backbone is fixed, and the CH_3 side chain groups are allowed to move freely (this will be refered to as "restrained backbone"). But the motion of the methyl groups is highly restricted; they can only undergo very limited vibrational motion as the angle potential by which they are bound to silicon does not allow a large range of motion. (see table 4.2).

The starting configurations for these simulations were equal to those of the normal simulations with penetrants after the equilibration process.

5.5 Results

5.5.1 Radial distribution functions

The environment the penetrants feel is shown by the radial distribution functions of the penetrants with the polymer atoms. Figure 5.1 shows these distribution functions for the penetrants upto 0.4 nm.

There is very little structure in the total rdf's. Only one clear peak can be seen, although there is a hint for a very broad second peak in the curves for large σ at $r \approx 0.7$ nm.

The increasing penetrant size is directly reflected by the shifting of the peak to the right. The peak does not only shift however, but it becomes smaller as well. At $\sigma > 0.300$ nm the "peak" even drops below unity. This means that the density in the first "shell" around the penetrant atom is lower for larger penetrants. This probably is an effect of the inefficient packing around the penetrant atom.

The oxygen contribution for the smallest penetrant size clearly consists of two peaks, the first at $r \approx 0.23$ nm and the second at $r \approx 0.5$ nm. With increasing penetrant size we not only see the two peaks shift to the right, but the first peak also gradually decreases to a small plateau. So holes which have oxygen atoms at their surface can be occupied more easily by the smallest penetrants than by the larger penetrants. This could be explained by the fact that holes with an oxygen surrounding are relatively smaller than those surrounded by methyl groups, which could be a result of the difference in bond angle in the oxygen and silicon.

[6] in the simulations k = 9000 kJ mol^{-1}

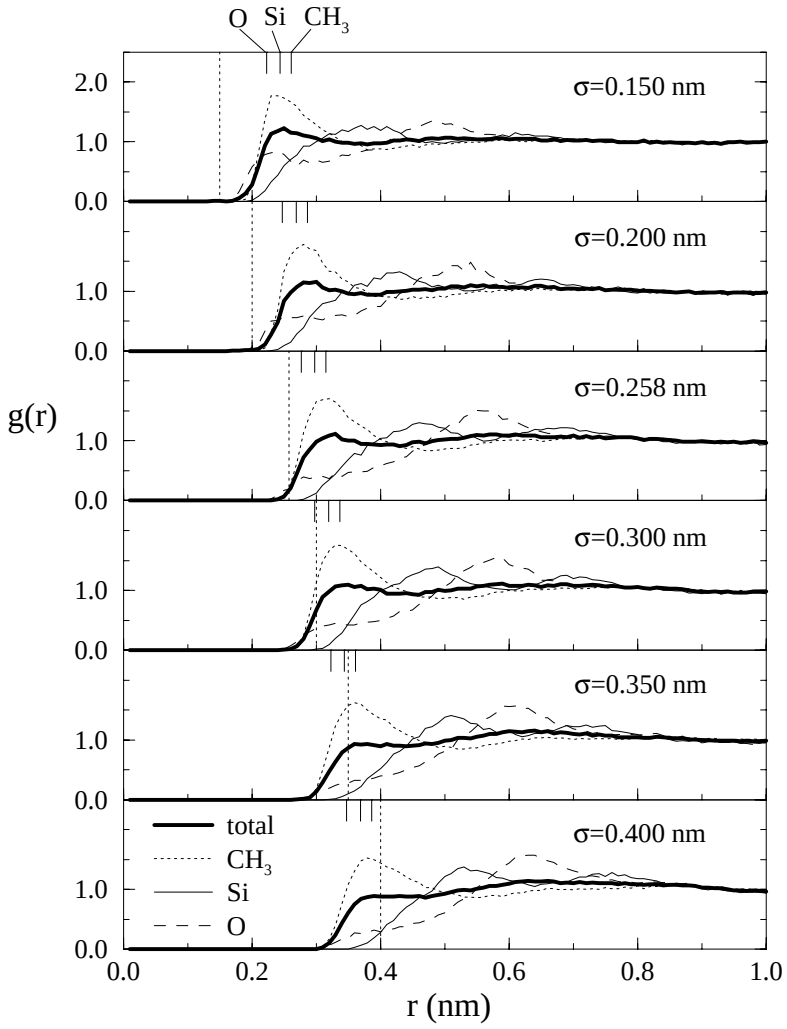

Figure 5.1: Radial distribution function $g(r)$ of the penetrants with the polymer chains. Not only the total curve is shown but also the seperate atom contibutions. The vertical dotted line is the penetrant diameter σ. Also indicated, by the small solid lines at the top of each graph, are the effective σ's (see text).

The product of the radial distribution function with the Lennard-Jones pair potential gives further insight into the energetic nature of the contacts of the penetrant in the polymer. This effective pair interaction is given in figure 5.2. From this figure one can clearly see that most positive (unfavorable) interactions of the penetrants are with the methyl groups. Showing the same picture as was shown by the inter-chain radial distribution function (fig. 4.11), *i.e.*, the surface of the chain mainly consist of methyl groups. The interactions of the penetrants with the other polymer atoms are mainly favorable.

The peak for the CH_3 contribution is highly unfavorable for all penetrants. Thus even

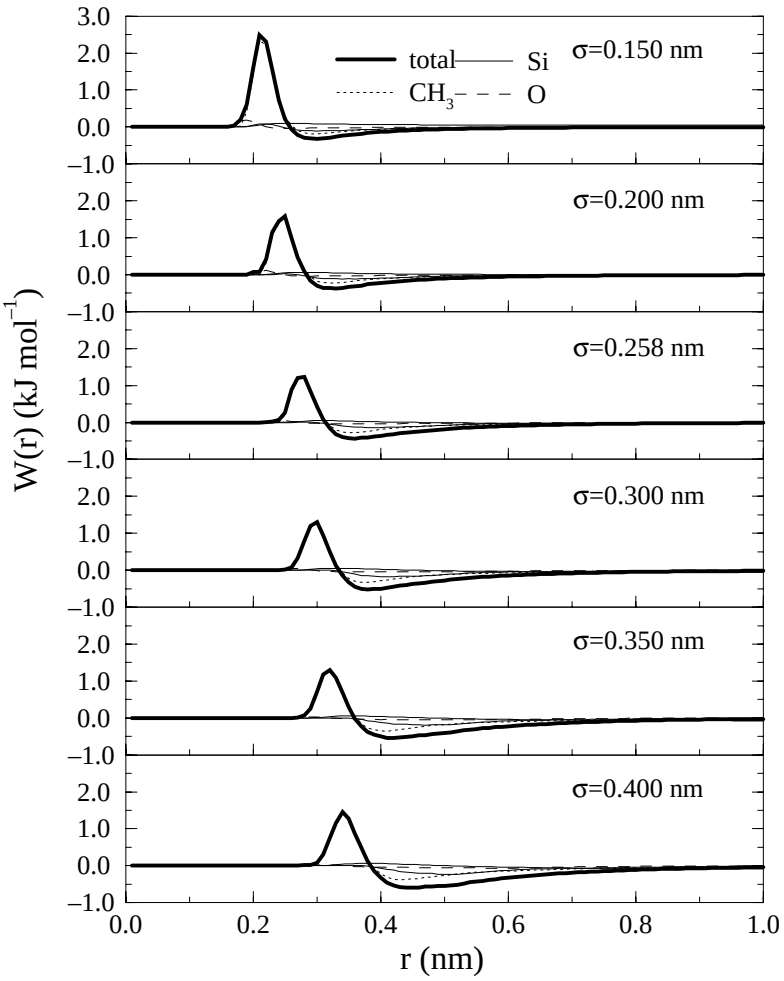

Figure 5.2: Effective pair interactions $W(r)$ of the penetrants withs the polymer environment. The effective pair interaction is calculted from the radial distribution function $g(r)$ and the interaction potential $V(r)$. The curve of the CH_3 contribution is almost completely covered by the total curve.

though there are no atoms within σ for the smallest penetrant the effective interaction is largely unfavorable (at its maximum in the order of kT ($\approx$ 2.5 kJ mol^{-1}).) The reason for this is that, although the Lennard Jones σ parameter of the smallest particle is 0.150 nm, the real σ's of interaction with the polymer atoms are larger. [7] There are polymer atoms within these effective σ's. The same rule holds for the largest penetrant, but as all the σ-values for the polymer are smaller than 0.4 nm, the effective σ's are smaller! So eventhough there is a substantial number of polymer atoms within σ, the effective interaction never surpasses kT. The attractive part of the potential increases for larger penetrants, a direct result of the larger penetrant surface resulting in a larger number of

[7]

neighbors.

The sum of integrals $W_{total} = \sum_i W_i$, with

$$W_i = \int_0^{r_{cut}} g(r)_i \; 4\pi r^2 \; \rho_i V(r) dr, \tag{5.13}$$

where i is the polymer atom species (CH_3, O, Si), gives the total effective interaction. In table 5.2 these are given, and we see that this W_{total} decreases with penetrant size. So, within this range of σ, the largest penetrant has the most favorable interaction with the polymer.

σ (nm)	W_{total} (kJ mol^{-1})
0.150	0.046
0.200	-0.005
0.258	-0.039
0.300	-0.060
0.350	-0.080
0.400	-0.102

Table 5.2: Total effective interactions W_{total} as function of penetrant size.

The penetrant diameter σ is not the appropriate parameter to look at at this moment. In the radial distribution functions we are looking at the distance between the **centers** of the atoms. This distance, which is used in the pairwise additive Lennard-Jones potential, is calculated from the particle diameters, by use of *e.g.* the simple combination rule: $\sigma = (\sigma_1 + \sigma_2)/2$. For example, the separation parameter for the smallest penetrant (σ_{pen} = 0.150 nm) with the methyl group is 0.26 nm.
These σ's are also indicated in figure 5.1.

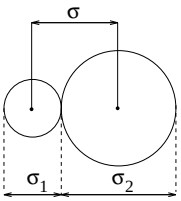

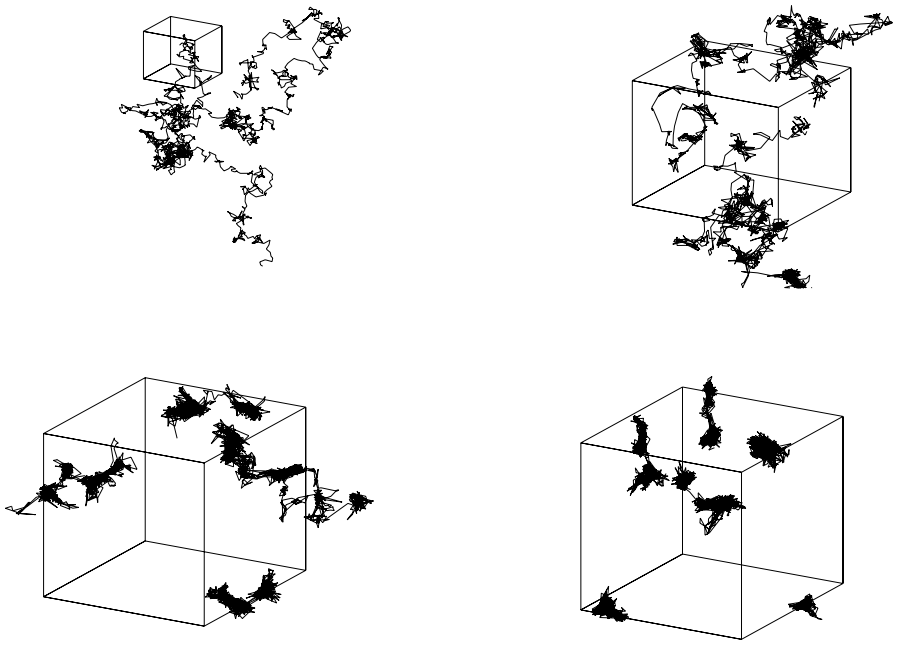

Figure 5.3: Trajectories of penetrants during 500 ps (for clearity not all 8 penetrants are shown). The simulation box (length approx. 4.2 nm) is shown to indicate scale and periodicity is removed. Top left: 2 penetrants with σ = 0.150 nm, top right: 2 penetrants with σ = 0.258 nm (helium), bottom left: 4 penetrants with σ = 0.350 nm, bottom right: 6 penetrants with σ = 0.450 nm.

5.5.2 Diffusion

In figure 5.3 the trajectories of some of the penetrants during the 500 ps simulations are shown. Looking at the trajectories, one sees that there is a clear difference, and not only in scale, but also in the nature of the diffusive paths for the different penetrant sizes. The smallest penetrant shows normal diffusive motion, like a particle in a liquid. For the penetrants with parameters like helium (σ = 0.258 nm) one can already see the "hopping" mechanism appear in the trajectories. A penetrant is situated in one hole for a while after which it "hops" to another hole. This *jump diffusion* mechanism becomes even more pronounced for the larger penetrants and for the largest penetrant in these simulations (σ = 0.450 nm) the time it spends in one hole is in the order of the simulation time.

Another view on the penetrant motion is presented in figures 5.4 and 5.5 where the scalar van Hove self-correlation function $G_s(r,t)$ is shown for the various simulations.

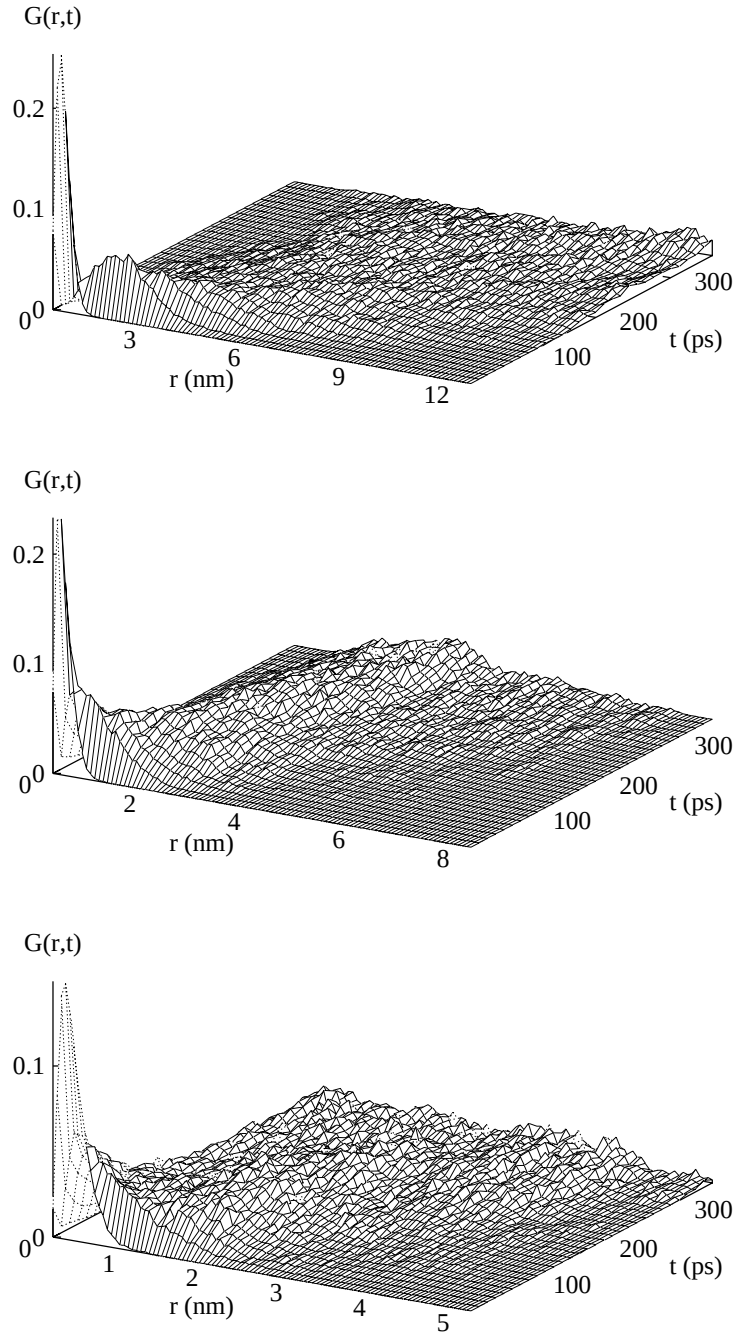

Figure 5.4: Scalar van Hove self correlation functions $G_s(r,t)$ for the penetrants of size σ = 0.150 nm (top), σ = 0.258 nm (middle) σ = 0.300 nm (bottom). Note the difference in length scale. ($G_s(r,0)$ is not shown.)

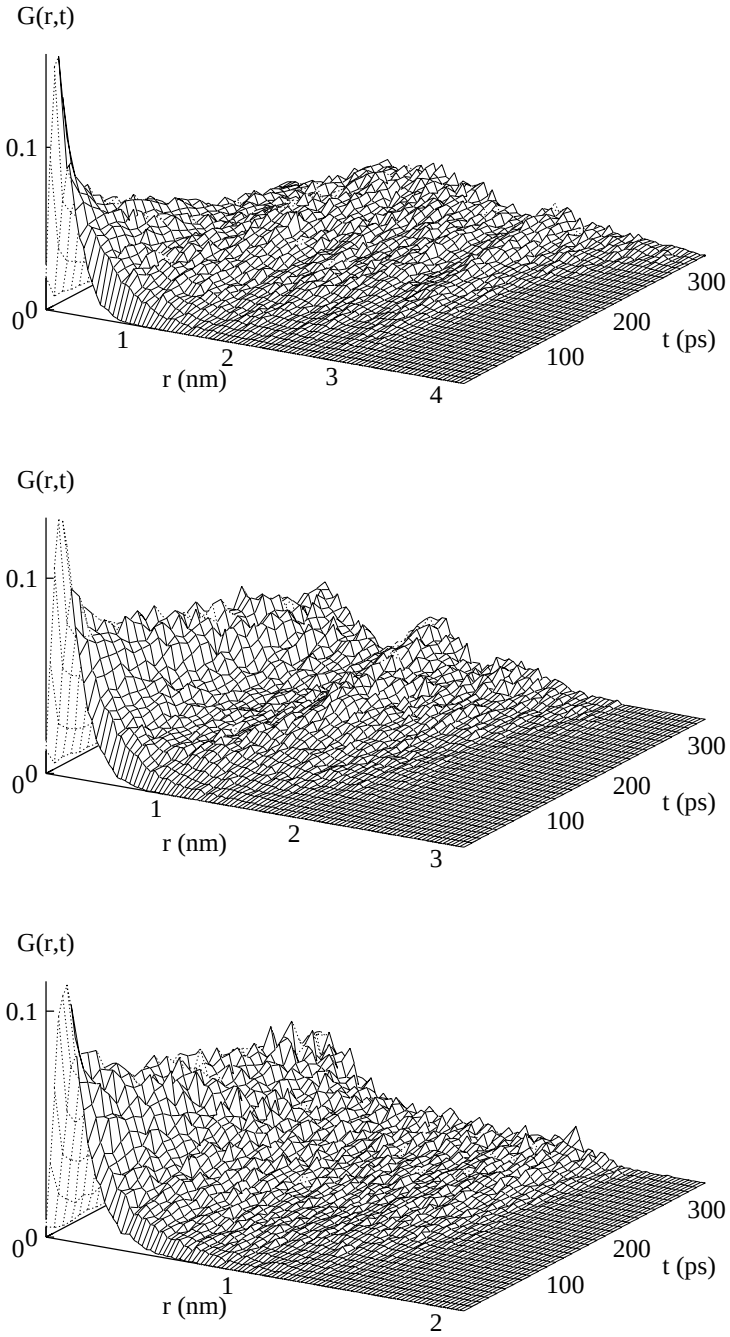

Figure 5.5: Scalar van Hove self correlation functions $G_s(r,t)$ for the penetrants of size σ = 0.350 nm (top), σ = 0.400 nm (middle) σ = 0.450 nm (bottom). Note the difference in length scale. ($G_s(r,0)$ is not shown.)

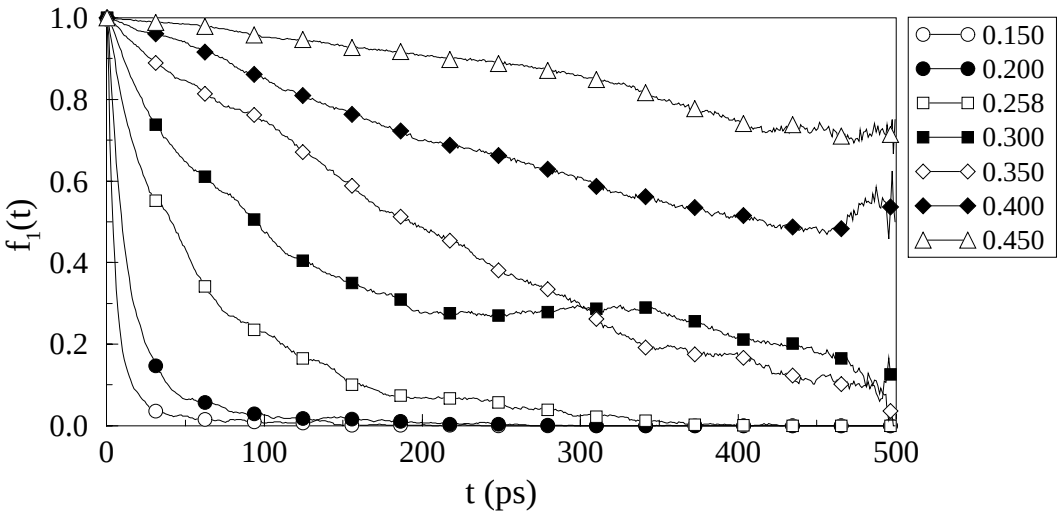

Figure 5.6: Average fraction of penetrants $f_1(t)$ within 1 nm of its origin at time $t_0 + t$. The symbols are shown for identification only. (Real data points are every 2 ps.)

This correlation function is the probability that a penetrant at time t is at distance r from it's position at time $t = 0$. The results also show the above mentioned behavior; for the smallest penetrant the delta function at time zero quickly smears out without any definite structure. The appearance of jump diffusion as is seen in the trajectories for σ = 0.258 nm cannot be seen in the van Hove correlation plot yet. This is because there is a broad range of jump lengths *between* holes, comparable in scale to the range of motion *within* the holes. For larger penetrants the time it spends in one hole increases and for σ = 0.350 nm one sees the appearance of more structure in the van Hove correlation function. Penetrants with σ = 0.400 nm show the most structure in $G_s(r,t)$ and one can see three distinct maxima, a clear signature of the hopping mechanism. For the largest penetrant σ = 0.450 nm there are very little jumps within the simulation time and no second maximum is present yet.

In figure 5.6 I have plotted the function $f_1(t)$ (eq. 5.11) denoting the fraction of penetrants which are within 1 nm of its original position at time t, where I have have taken a distance of 1 nm as a rough measure for an average hole. It is clear that the actual hole size depends on the penetrant size, but this effect is not taken into account. The value of $t_{0.50}$ has been estimated by fitting the functions $f_1(t)$ to a stretched exponential ($\exp(at^b)$ and taking the time at $f_1(t) = 0.5$. This measure for a "residence" time, $t_{0.50}$ is shown for the various penetrants in figure 5.7, where the corresponding values for the position restrained simulations are shown as well.

These residence times also reflect the gradual crossover from liquid-like diffusion to

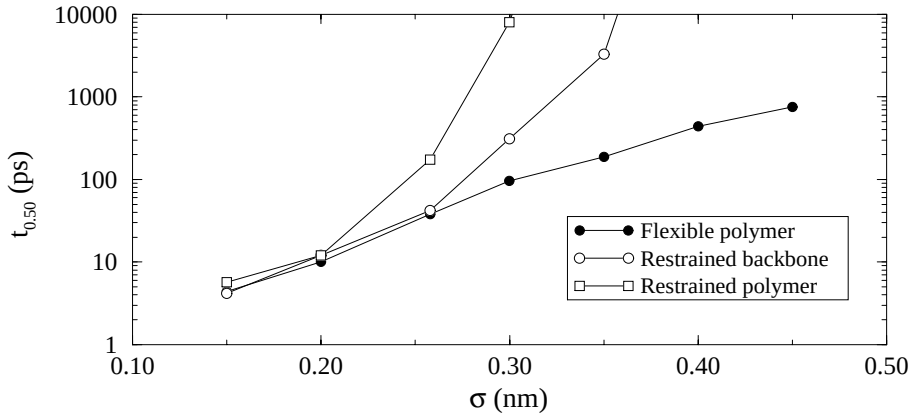

Figure 5.7: Residence times $t_{0.50}$ for the various penetrants, for the normal MD simulation (flexible polymer) and the position restrained simulations (restrained backbone and restrained polymer).

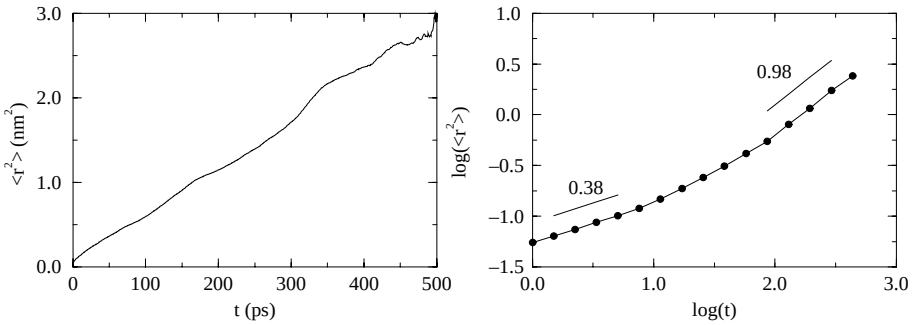

Figure 5.8: Mean squared displacement of penetrants with σ = 0.350 nm (left) and the same curve on a double logarithmic scale (right). Also indicated in this graph is the slope at two different regions.

jump-diffusion. For σ = 0.150 nm, $t_{0.50}$ is only $\approx$ 4 ps but this increases exponentially with increasing σ. For the largest penetrant a value of $\approx$ 750 ps was found. So after 750 ps approximately 50 % of these penetrants will have moved to another hole. This gives a nice indication of how long a simulation would have to be to accurately sample the diffusion process for these penetrants! For the position restrained simulations the residence times for the two smallest penetrants is roughly equal to that of the normal simulation, but diverges rapidly for larger penetrants.

It is interesting to note that the values of $t_{0.50}$ for the normal simulations are exponentialy dependent on penetrant size for the complete range investigated ($t_{0.50} = 0.35 \exp(17.7\ \sigma)$), while for the restrained simulations this is clearly not the case.

From the trajectories as shown in figure 5.3 the mean squared displacement, $\left\langle r^2(t) \right\rangle$,

can be calculated and using equation 4.5 the diffusion coefficient D. But, as is shown on page 25, one can only *correctly* calculate D from the slope of the MSD curve if the exponent n,

$$\left\langle r^2(t) \right\rangle \propto t^n, \tag{5.14}$$

equals unity. This exponent can be calculated from the slope of $\log(\left\langle r^2(t) \right\rangle)$ vs. $\log(t)$. Figure 5.8 shows an example of this calculation for one set of penetrants. The mean squared displacement curve seems to be reasonably straight, but if we look at the same curve on a double logarithmic scale it is clear that for $t < 10$ ps, where $n = 0.38$, that there is clear anomalous diffusion. Only after $t \approx 100$ ps the slope of the curve $n = 0.98$ and approaches unity. Thus the diffusion constant for the penetrants of size σ = 0.350 nm can only be calculated from the slope of the MSD curve after 100 ps. In figure 5.9 the mean squared displacement curves for all the penetrant sizes are given together with the value of the exponent n at that position (the local slope of the log-log curve).

It must be noted that the mean squared displacement is calculated by using all possible time origins so that the statistical error increases with time. As the accuracy of the MSD-curve decreases with time, so does the accuracy of n.

In some cases (σ = 0.400 nm and 0.450 nm) n never reaches a value close to 1 and thus it can be concluded that it is not possible to calculate a real diffusion coefficient for these penetrants. In these simulations one can only *estimate* the diffusion coefficient and this was done by using the slope of the mean squared displacement between 200 and 400 ps, although this is an arbitrary choice. This estimate serves as an upper bound to the diffusion constant.

Figure 5.10 graphically displays the diffusion coefficients as function of penetrant size on a double logarithmic scale. In the accompanying table these data are also given numerically for completeness. The results for the two different series of position restrained simulations are also show in the same figure. For these data the same rules hold as were discussed above. Some penetrants have not shown real diffusive motion yet and these are represented by open symbols in the figure and in parentheses in the table.

The trend is obvious, smaller penetrants have a higher diffusion coefficient than large pentrants, for the normal MD simulation as well as for the two position restrained simulations, as is to be expected. If we look at the curve for the normal MD simulations we see that, except for the smallest penetrant, the data points are linear on this double logarithmic scale. This means that the diffusion constant scales as:

$$D \propto \sigma^n \tag{5.15}$$

where n is found to be -6.2 ($\pm$ 0.1). Alternatively the diffusion coefficient scales with

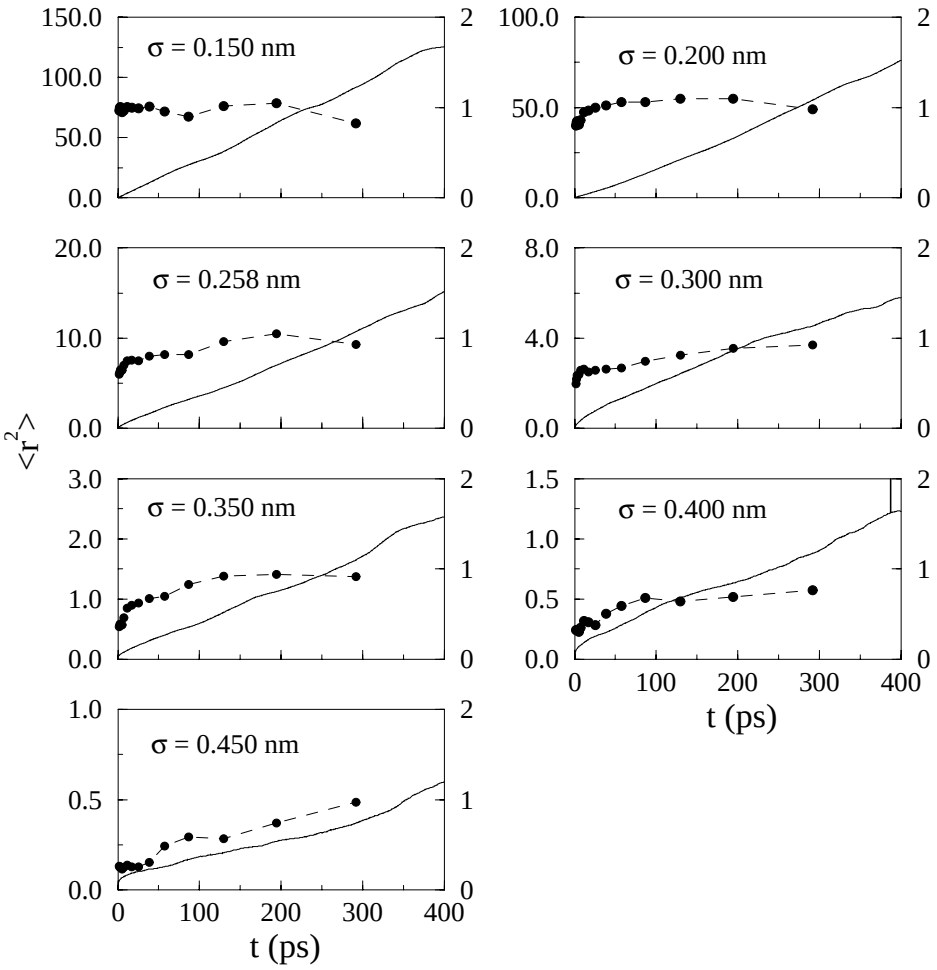

Figure 5.9: The mean squared displacements of the penetrants during the simulations are shown by the solid line (left axis). The dots show the value of n, the slope of $log(\langle r^2(t)\rangle) vs. log(t)$ (right axis). The dashed line is only shown for clarity.

molecular volume with an exponent of -2.1.

The penetrants diffuse roughly a factor of 4 faster in a completely flexible polymer than in a completely frozen polymer. In the intermediate system (restrained backbone) only the CH_3 groups are able to move, but the thermal motion of the side chain groups enhances the diffusion of the penetrants by roughly a factor of 2 compared to the completely restrained system. This means that not only the chain motion of the polymer, but also the transfer of kinetic energy of the polymer to the penetrant plays a vital role in the diffusion process. The power law dependence of D on penetrant size is clear for all three sets of simulations. Although it looks like D decreases more rapidly for larger penetrants in the position restrained simulations, but due to the large errors in D this is

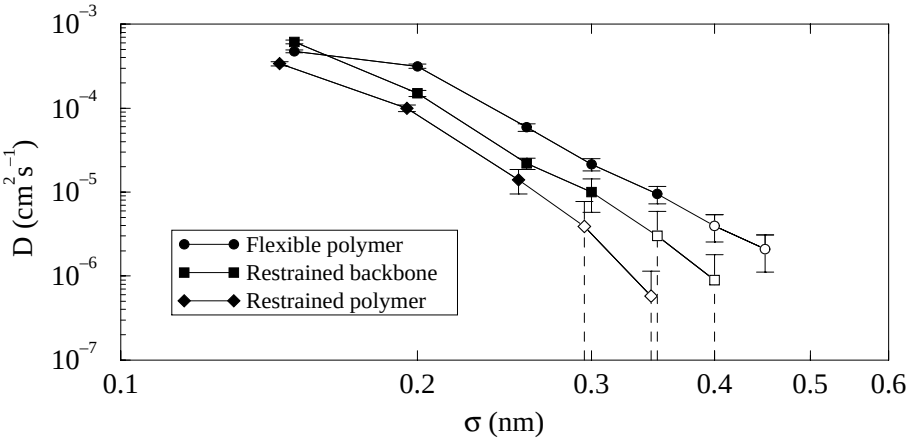

Penetrant size	Diffusion constant D ($cm^2 s^{-1}$)		
σ (nm)	Flexible Polymer	Restrained backbone	Restrained polymer
0.150	$4.8\,[0.2]\cdot 10^{-4}$	$6.1[0.3]\cdot 10^{-4}$	$3.4[0.2]\cdot 10^{-4}$
0.200	$3.2\,[0.2]\cdot 10^{-4}$	$1.5[0.1]\cdot 10^{-4}$	$1.0[0.1]\cdot 10^{-4}$
0.258 (He)	$5.9\,[0.6]\cdot 10^{-5}$	$2.2[0.3]\cdot 10^{-5}$	$1.4[0.5]\cdot 10^{-5}$
0.300	$2.1\,[0.4]\cdot 10^{-5}$	$1.0[0.4]\cdot 10^{-5}$	$(< 7\cdot 10^{-6})$
0.350	$1.0\,[0.2]\cdot 10^{-5}$	$(< 6\cdot 10^{-6})$	$(< 1\cdot 10^{-6})$
0.400	$(4\,[1]\cdot 10^{-6})$	$(< 2\cdot 10^{-6})$	-
0.450	$(2\,[1]\cdot 10^{-6})$	-	-

Figure 5.10: Diffusion constants versus penetrants size σ on a double logarithmic scale. The open symbols are estimates for the diffusion coefficients, see text. The error bars are calculated using the formula in appendix B. The curve for the restrained polymer is shifted slightly to the left to show the error bars more clearly. In the accompanying table the same data is given numerically as well where the estimated values are given in parentheses and errors are given in square brackets. In some cases the error in the diffusion coefficient is so large that only an upper limit can be given.

uncertain. Longer simulations need to be done to be conclusive.

The exponent by which the diffusion coefficient scales with penetrant size for the position restrained simulations is approximately the same as for the normal simulation. Although it must be noted that these data points are less linear and there is a hint for a faster decay than a simple power law behavior. But the errors in the data points make this assumption hard to prove.

The only penetrant that deviates from the power law dependence in the normal simulation is the smallest penetrant (σ = 0.150 nm). A possible explanation for this will be presented in chapter 7 in combination with the results obtained from the analysis of the free volume (chapter 6).

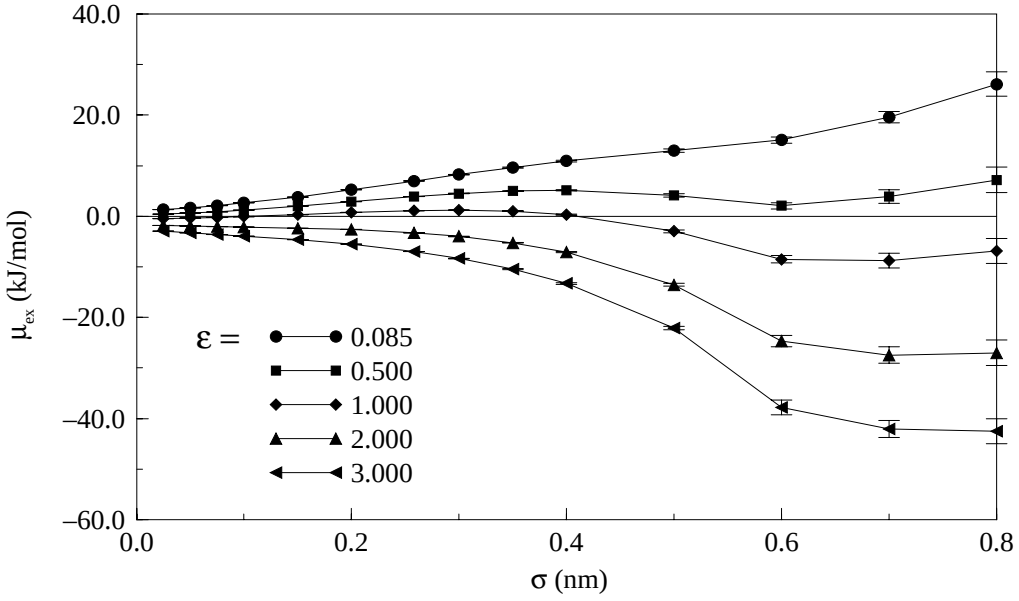

Figure 5.11: Chemical potential (μ_{ex}) as function of penetrant size σ and Lennard-Jones interaction parameter ε(in kJ mol^{-1}). The errors are indicated with error bars. For all data points shown the condition for sufficient sampling (equation 5.4) is fullfilled.

5.5.3 Solubility / Chemical potential

The solubility is calculated by use of the chemical potential. As the calculation of this chemical potential by means of the particle insertion method is computationally more efficient than the diffusion calculations[8], a wider range of parameters has been used than in the diffusion calculations. The chemical potential μ_{ex} is calculated for a series of penetrants with a range of sigma and epsilon data (σ = 0.025 - 0.8 nm, ε = 0.085 - 3.0 kJ mol^{-1})[9] using the particle insertion method (section 4.5). The calculations were carried out using a trajectory of 500 ps MD simulation of PDMS without any penetrant (same simulation as was described in the chapter 4). At every 0.5 ps 80,000 insertions were performed (total 40 milion insertions) for every set of σ and ε.

The chemical potential calculated in this way is shown in figure 5.11. For the complete region shown the chemical potential is lower for larger interaction parameter ε. For the smallest value of ε (0.085 kJ mol^{-1}), μ_{ex} increases continuously with penetrant size.

[8] In practice the chemical potential can be calculated for several penetrants at the same time with negligable extra cost of time, while for the diffusion calculations a complete simulation has to be performed for every set of parameters.

[9] Except for the smallest σ, this range of σ and ε parameters is in the physical relevant region. For example: helium σ = 0.258 nm, ε = 0.085 kJ mol^{-1}; xenon σ = 0.406 nm, ε = 1.9 kJ mol^{-1}; CCl_4, σ = 0.588 nm, ε = 2.7 kJ mol^{-1} [61]

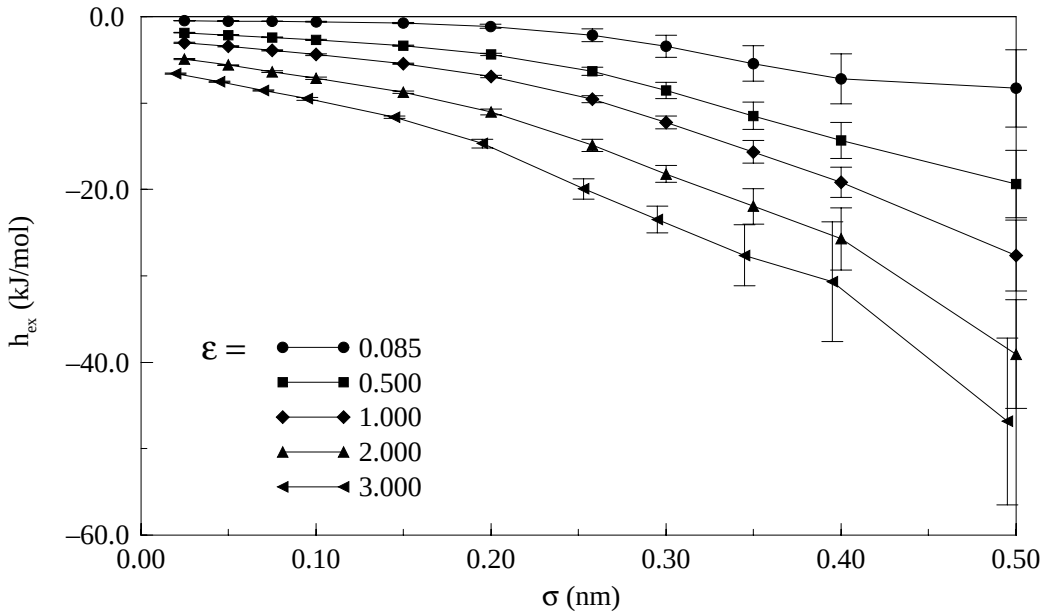

Figure 5.12: The excess molar enthalpy h_{ex} as a function of penetrant size σ and Lennard-Jones interaction parameter ε (in kJ mol^{-1}). The errors are indicated with error bars and the lowest curve is displaced slightly to show the error bars more clearly.

With ε = 0.50 kJ mol^{-1} a maximum in the chemical potential appears at σ = 0.4 nm, after which the chemical potential drops. This is also visible for ε = 1.0 kJ mol^{-1} , but the maximum is shifted to 0.3 nm. For even larger values of ε (2.0 and 3.0 kJ mol^{-1}) the maximum has disappeared completely and the chemical potential starts out as a decreasing function. Note that an decreasing chemical potential means an increase in solublity, thus for the larger values of ε larger penetrants would dissolve easier in the membrane than smaller ones for this range of σ!

With further increasing penetrant size the chemical potential reaches a minimum and starts to increase again.

The chemical potential (or excess molar free energy) is made up of two contributions: the enthalpy and entropy ($\mu_{ex} = h_{ex} - Ts_{ex}$).

The excess molar enthalpy can be calculated by use of equation 5.5. From this the entropy can be evaluated as well and the results are shown in figures 5.12 and 5.13. If we look at the excess molar enthalpy h_{ex} (fig. 5.12) the first thing we see is that the statistical errors in the data points are larger than in the chemical potential and increase with increasing penetrant size and interaction parameter. The reason for this is the slow convergence of the second and third term in equation 5.5. Both of these terms are large and almost equal so the difference is very inaccurate. Moreover the last term is an ensemble average over one data point only for each time frame while the other values are averaged over several thousand samples for each frame. For this reason the enthalpy

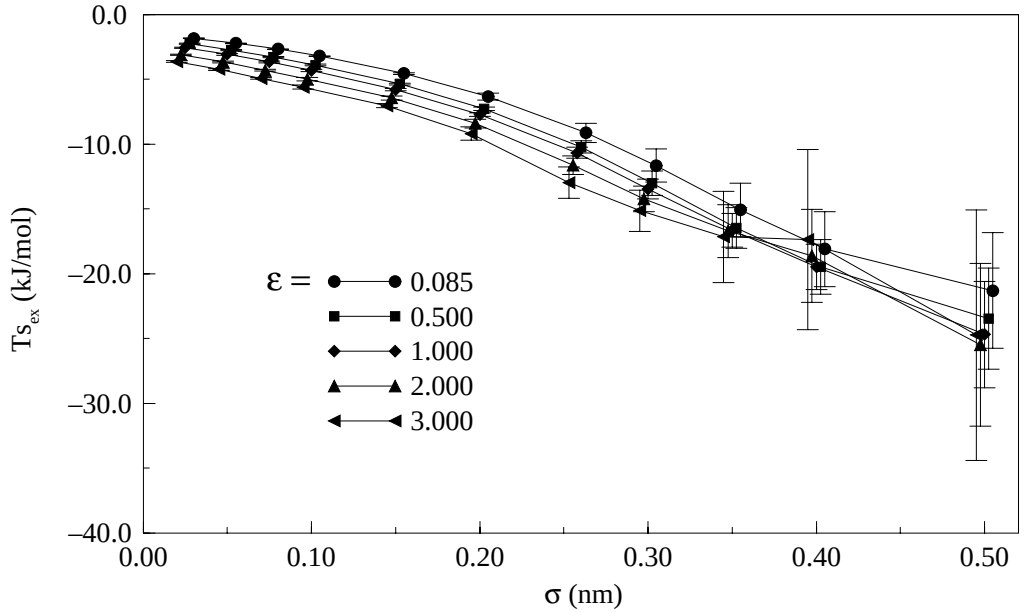

Figure 5.13: The excess molar entropy times temperature Ts_{ex} as a function of penetrant size σ and Lennard-Jones interaction parameter ε (in kJ mol^{-1}). The errors are indicated with error bars and the different curves are displaced slightly with respect to each other for reasons of clearity.

is not shown for $\sigma > 0.5$ nm.

For $\sigma < 0.5$ nm the enthalpy is more favorable (=more negative) for a larger value of ε, which is what you would expect. The trend for all values of ε is similar. The energetic interaction becomes more favorable with increasing penetrant size.

The enthalpy of a penetrant in the polymer host can be thought to be made up of two separate contribution, first the number of neighbors with a favorable interaction, and second the surface tension of the hole the penetrant is situated in. The data seem to show that for σ up to 0.5 nm the competition between these two contributions is dominated by the favorable interaction energy.

The other contribution to the chemical potential is the entropy and this reflects the probability that a penetrant can find a hole in which it can "dissolve".

The difference in entropy (fig. 5.13) for all values of ε is very small. Below 0.2 nm the differences are statistically significant (Note that the displacement of the curves in figure 5.13 to show the different error bars properly shifts the curves away from each other). The entropy is lower (= more unfavorable) for larger ε, which can be understood in the following way: a smaller ε means a wider energy well which in turn means an increase in possible favorable positions. Remember that the *real energy contribution* is included in the enthalpy.

The entropy decreases with increasing penetrants size, which says nothing more than that the probability of occurrence of a suitable hole decreases with penetrant size. This is logical if one sees that a penetrant can fit in a hole that is exactly its size *or larger*. So for any distribution of hole sizes, the entropy should decrease with penetrant size.

In table 5.3 the results for ε = 0.085 kJ mol^{-1} (which were given in graphical format previously) are brought together.

σ(nm)	μ_{ex} (kJ mol^{-1})		S		h_{ex} (kJ mol^{-1})		Ts_{ex} (kJ mol^{-1})	
0.025	1.3405	[0.0006]	0.5842	[0.0002]	-0.48	[0.03]	-1.82	[0.03]
0.050	1.6938	[0.0008]	0.5070	[0.0002]	-0.52	[0.03]	-2.21	[0.03]
0.075	2.120	[0.001]	0.4273	[0.0002]	-0.55	[0.04]	-2.67	[0.04]
0.100	2.619	[0.001]	0.3499	[0.0002]	-0.59	[0.04]	-3.20	[0.04]
0.150	3.810	[0.004]	0.2170	[0.0003]	-0.73	[0.05]	-4.54	[0.06]
0.200	5.20	[0.01]	0.1243	[0.0006]	-1.1	[0.2]	-6.3	[0.3]
0.258	6.94	[0.03]	0.0618	[0.0008]	-2.1	[0.7]	-9.1	[0.7]
0.300	8.20	[0.06]	0.037	[0.001]	-3.4	[0.9]	-11.6	[1.0]
0.350	9.6	[0.1]	0.021	[0.001]	-5.0	[2.0]	-15.0	[2.0]
0.400	10.9	[0.2]	0.012	[0.001]	-7.0	[3.0]	-18.0	[3.0]
0.500	12.9	[0.4]	0.0054	[0.0008]	-8.0	[4.0]	-21.0	[5.0]
0.600	15.0	[1.0]	0.0023	[0.0006]	-		-	
0.700	20.0	[1.0]	0.0004	[0.0002]	-		-	
0.800	26.0	[3.0]	0.00003	[0.0003]	-		-	

Table 5.3: Chemical potential μ_{ex}, solubility S, enthalpy h_{ex} and entropy s_{ex} (times temperature) for ε = 0.085 kJ mol^{-1} (the value of ε for which diffusion coefficients are calculated as well). The error is given in square brackets. For a graphical presentation of these data see figures 5.11, 5.12 and 5.13

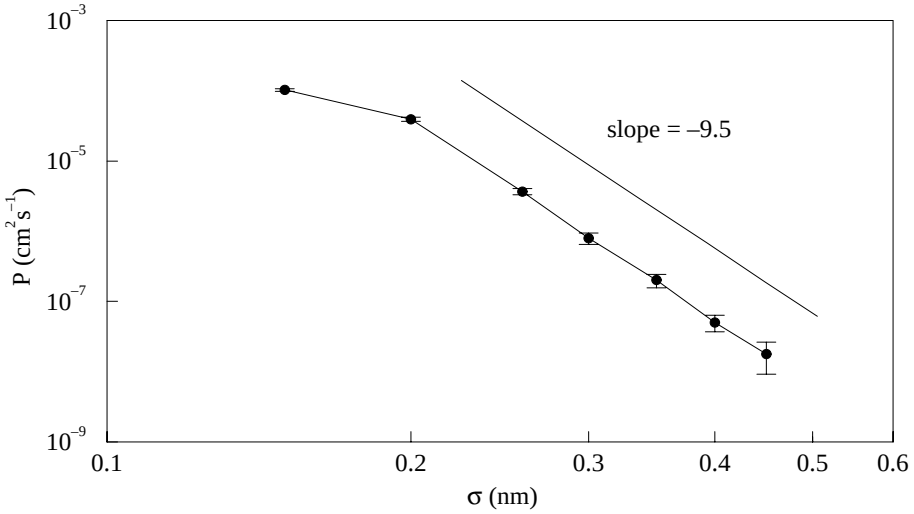

Figure 5.14: Permeability coefficient P as function of penetrant size for $\varepsilon = 0.085$ kJ mol^{-1} .

5.5.4 Permeability

The permeability coefficient P as defined in the solubility-diffusion mechanism can be calculated from the diffusion coefficient D and solubility coefficient S by use of equation 2.2 ($P = DS$). Table 5.4 shows the values of P for the various penetrants and in figure 5.14 these permeability coefficients are represented in a graphical format as well.

It follows from this figure that for ε = 0.085 kJ mol^{-1}, the permeability coefficient P decreases with penetrant size in the range σ = 0.15 nm to 0.45 nm. Except for the smallest σ it shows a power law behavior:

$$P \propto \sigma^{-9.4}. \tag{5.16}$$

Knowing that the diffusion constant scales with approximately σ^6, we can deduce that the solubility roughly scales with the penetrant volume $v \sim \sigma^3$. It must be stressed however that this is only the case for the range for which the diffusion constants have been calculated as can be seen in figure 5.15 where the solubility for ε = 0.085 kJ mol^{-1} is shown as function of penetrant size on a double logarithmic plot. For this reason it is only coincidence that the permeability approximately scales according to a power law. Over a larger range, or a different range of σ, this would not have been the case.

For other values of ε we have not calculated diffusion coefficients, but one can argue that the trend of D vs. σ will be approximately the same, that is $D \propto \sigma^n$. But as the chemical potential for higher interaction parameters is not so “uneventfull” as for ε = 0.085 kJ mol^{-1} , the solubility will play a more important role. Depending on the interplay of D

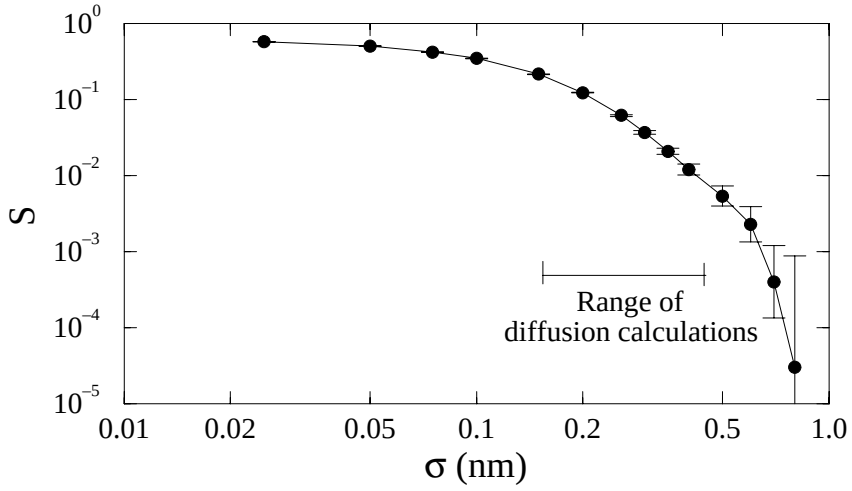

Figure 5.15: Solubilities for penetrants with ε = 0.085 kJ mol^{-1} on a double logarithmic scale.

and S, the permeability can, in a certain range of penetrant size, increase with σ. Thus a larger penetrant will permeate faster through a membrane than its smaller counterpart. The permeability will then reach a maximum and decrease again with increasing σ.

σ (nm)	D (cm^{2}s^{-1})		S		P (cm^{2}s^{-1})	
0.150	4.8	$[0.2]\cdot10^{-4}$	0.2170	[0.003]	1.03	$[0.05]\cdot10^{-4}$
0.200	3.2	$[0.2]\cdot10^{-4}$	0.1243	[0.006]	3.9	$[0.3]\cdot10^{-5}$
0.258	5.9	$[0.6]\cdot10^{-5}$	0.0618	[0.008]	3.6	$[0.4]\cdot10^{-6}$
0.300	2.1	$[0.4]\cdot10^{-5}$	0.037	[0.01]	8.0	$[1.0]\cdot10^{-7}$
0.350	1.0	$[0.2]\cdot10^{-5}$	0.021	[0.01]	2.0	$[0.4]\cdot10^{-8}$
0.400	4.0	$[1.0]\cdot10^{-6}$	0.012	[0.01]	5.0	$[1.0]\cdot10^{-8}$
0.450	2.0	$[1.0]\cdot10^{-6}$	0.0085	[0.009]	1.8	$[0.8]\cdot10^{-8}$

Table 5.4: Permeability coefficient P as function of penetrant size σ for ε = 0.085 kJ mol^{-1}.

5.6 Discussion

Let me first note that there is no significant effect of the penetrants on any of the properties of the polymer. The diffusion coefficient of the polymer chains, as well as the structure factor and interchain radial distribution functions are all effectively the same as presented in the previous chapter. So the effect that the large penetrants exert a higher local force in the hole they are situated in is not significantly for the calculated polymer properties.

The diffusional process

The picture of the diffusional process as presented by the simulations is clear. For the smaller penetrants the diffusion is almost liquid-like. The penetrant is not confined to a limited region of space. As the penetrant size increases the penetrant finds it more and more difficult to leave the hole it is situated in and *jump diffusion* starts to appear. Penetrants are stuck in a hole for some time (residence time) and it picks up momentum from "kicks" by the polymer chain, where the radial distribution functions show that this kicking is mainly done by the methyl side chains. When there is an opening in the direction of the momentum, the penetrant moves to another hole. In a video representation of the penetrant motion one could clearly see this "pin-ball" like behavior of the penetrants.

The residence times of the penetrants seem to be exponentially dependent on the penetrants size (at least within the range investigated).

Effect of polymer mobility

The effect of position restraining is comparable to the lowering of the temperature below the glass transition temperature T_g of the polymer. There are of course several differences. The temperature of the polymer is not simply lowered to a temperature below T_g, but lowered to a temperature T=0, while the penetrants still have a "temperature" of 300K. The partly restrained simulation where the side chain groups were allowed to move are more comparable to a glassy polymer. The large movements of the total chain are frozen, but the side chains still show thermal motion. This thermal motion of the side chains results in an increase of the diffusion coefficient with a factor of two compared to the completely fixed polymer.

Unfortunately there are no experimental data to which I can compare the diffusion data of the restrained simulations, but the trend shown is clear: the polymer mobility is an important factor, not only the overall motion of the chain, but also the thermal motion of the direct environment of the penetrant. This thermal motion provides the necessary "kick" needed to jump to the next hole.

The fact that the difference in D between the normal MD simulation and the position restrained simulations is more or less the same over the whole range of penetrant size, seems to contradict the difference in residence times. While there is little difference in residence time for the smaller penetrants, the diffusion coefficients differ by a factor of ≈ 2 and ≈ 4 (restrained backbone and completely restrained polymer respectively). For the larger penetrants the residence times are very different, which means that the penetrants are in principle restrained to their hole, but the difference in D is about the same. But if we look at table 5.5 we see that there is no real contradiction. The diffusion constant can be visualized as a function of the average distance between jumps L and the average time between jumps (for which I use the residence time $t_{0.50}$):

$$D = \frac{1}{6} L^2 / t_{0.50}. \tag{5.17}$$

If I calculate these average jump distances for all the simulations for which normal diffusion is seen (or sufficiently close), one sees that for all simulations this L is approximately the same ≈ 1.1 nm. They should be approximately equal as the average properties of the polymer matrix is the same for all simulations.

Chemical potential, enthalpy and entropy

The interplay of enthalpy and entropy results in an interesting behavior of the chemical potential as function of the penetrant size σ and its interaction parameter ε. Both the entropy and enthalpy are descending functions (up to σ = 0.5 nm), but the rate of descent in the enthalpy depends strongly on ε while the rate of descent in the entropy is nearly independent of ε.

For small ε the enthalpy does not match the entropy and as a result the chemical potential is dominated by the increasingly unfavorable entropy, *i.e.* μ_{ex} increases with σ. In other

Flexible polymer				Restrained backbone			Restrained polymer		
σ (nm)	D (cm^2s^{-1})	$t_{0.50}$ (ps)	L (nm)	D (cm^2s^{-1})	$t_{0.50}$ (ps)	L (nm)	D (cm^2s^{-1})	$t_{0.50}$ (ps)	L (nm)
0.150	$4.8 \cdot 10^{-4}$	4.4	1.1	$6.1 \cdot 10^{-4}$	4.2	1.2	$3.4 \cdot 10^{-4}$	5.7	1.1
0.200	$3.2 \cdot 10^{-4}$	10	1.4	$1.5 \cdot 10^{-4}$	12	1.0	$1.0 \cdot 10^{-4}$	12	0.8
0.258	$5.9 \cdot 10^{-5}$	38	1.2	$2.2 \cdot 10^{-5}$	42	0.7	$1.4 \cdot 10^{-5}$	175	1.2
0.300	$2.1 \cdot 10^{-5}$	96	1.1	$1.0 \cdot 10^{-5}$	310	1.4	-	-	-
0.350	$1.0 \cdot 10^{-5}$	188	1.0	-	-	-	-	-	-
0.400	-	-	-	-	-	-	-	-	-
0.450	-	-	-	-	-	-	-	-	-

Table 5.5: Average jump distances L calculated from the residence times $t_{0.50}$ and the diffusion constants D, by use of equation 5.17.

words, the larger number of favorable interactions a larger penetrant has is not enough to match the smaller amount of available space that commes with the increase in size.

As the interaction parameter increases the effect of the enthalpy grows as well. For ε = 1.0 kJ mol^{-1} the entropy and enthalpy are almost equal up to σ = 0.4 nm, which means that there is almost no size effect on the solubility of the penetrants. If ε increases even further the enthalpy becomes dominant and larger penetrants dissolve more easily in the membrane than smaller ones. This effect does not seem to extend to even large penetrants, as we can see chemical potential levels off again, and probably rises steeply for $\sigma > 0.8$ nm.

The enthalpy of penetrants in the polymer system is dominated by the number of neighbors of the penetrant up to $\sigma \approx 0.5$ nm. This is also seen in the total effective interation $W_{total}(r)$ calculated from the the radial distribution function. Here the total interaction energy also becomes more favorable with growing penetrant size. Most of these favorable interaction come from the interactions with the "core" atoms Si and O.

A note or the error in the calculated values has to be made. For increasing σ the statistical errors in the all the calculated values increase. The statistical errors in the enthalpies for $\sigma > 0.5$ nm become very large. In this range the resulting entropy *rises* with penetrant size (not shown). As this is not consistent with chemical intuition it is concluded that the systematic error in the enthalpy values is substantial and the calculated values can not be used.

Comparison of small and large system

If we compare the simulations of the small and large system we have to keep in mind that the simulations with the small system were performed at constant pressure and the simulations with the large system at constant volume[10]. The diffusion coefficient of helium in the small system was $18 \cdot 10^{-5}$ cm^{2}s^{-1} . This is roughly a factor of 3 larger than the corresponding number from the simulation of the large system ($5.9 \cdot 10^{-5}$ cm^{2}s^{-1}). There are a number of reasons for this discrepancy. First, the density in the larger system is slightly higher than in the small system, this results in less available volume for the penetrants. This difference in density is a direct consequence of the difference in chain length. Because of the longer chains, the end-group concentration in the large system is smaller. Because end-groups need more volume, the density of the long-chain system is larger. This smaller end-group concentration results in a second effect. As was shown in figure 4.13 the end groups are more mobile that the inner monomers. As the diffusion of penetrants is believed to be influenced by monomer motion it can be argued that

[10] At that moment the simulation package GROMACS was not able to perform constant pressure simulations, although the large system was equilibrated using constant pressure using GROMOS. The reason why the simulations were performed with GROMACS is that this package could be executed on the very fast 32-i860 processor machine

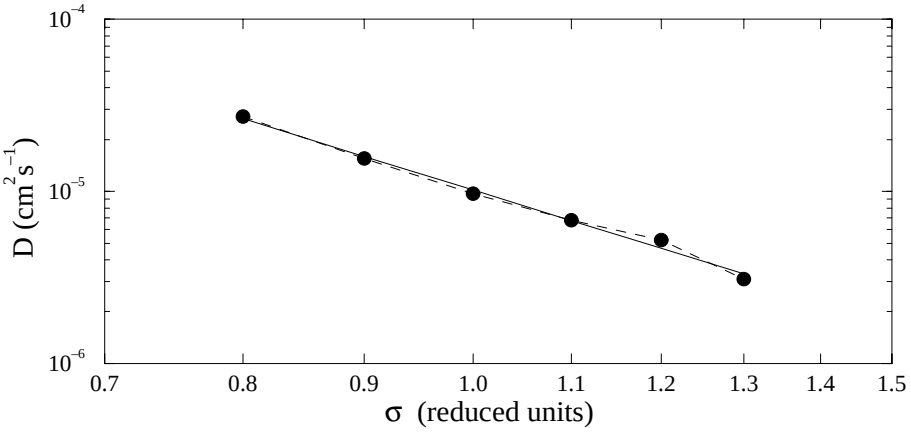

Figure 5.16: Diffusion coefficients as function of penetrant size. Reproduced from [40]. The slope of the regression line is -4.3.

a smaller end-group concentration will result in a smaller diffusion coefficient. This argument is hard to quantify in the present study and should be investigated further. A third consideration is that the diffusion coefficient in the small system was calculated from the trajectory of only one penetrant. If we calculate the diffusion coefficients of the eight separate penetrants in the larger system we see that they range from $1.0 \cdot 10^{-5}$ to $12 \cdot 10^{-5}$ $cm^2 s^{-1}$. So there is a considerable spread in the one-particle values. All these effects can give rise to a difference in D.

The difference in chemical potential for He in both simulations (small system μ_{ex} = +3.8 kJ mol^{-1}, large system μ_{ex} = +6.9 kJ mol^{-1}) is also a result of the difference in density of the two systems. A higher density means less volume with negative (=favorable) interaction energies. Thus a high density will give rise to a higher chemical potential, and hence a lower solubility.

Comparison to experimental values and other simulations

The relation between polymer size and diffusion coefficient can only *directly* be compared to an early simulation by Sonnenburg [40]. In this work they simulated a highly idealized polymer network and one penetrant, interacting with each other only by a repulsive interaction. They used penetrants of different sizes and calculated their diffusion coefficients, which are reproduced in figure 5.16. This data clearly shows the power law dependence of D on penetrant size as was seen in our simulations. The slope of the line is -4.3 which is different from our -6.0. The origin of this difference is obvious, the two models for the polymer samples differ substantially. But the trend is clearly the same.

If we compare the penetrant size dependence to experimental data we have to take into account a number of differences. First of all, the modeled penetrants are completely spherical while this is only true (to a certain extent) for a limited number of “real”

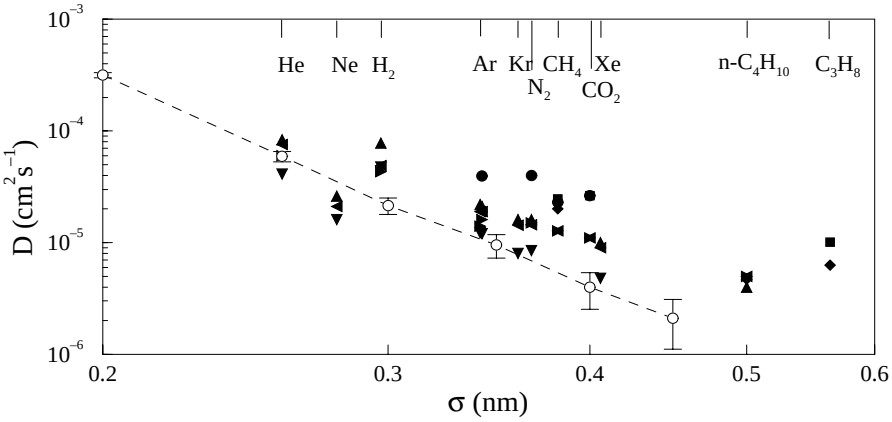

Figure 5.17: The calculated diffusion coefficients (open circles) versus penetrant size σ compared to experimental data [59, 60, 62–64]. The sizes of the atoms are taken from [61]. Note that the experimental diffusion coefficients were obtained only under approximately the same conditions!

penetrants. Second, the interaction parameters of the penetrants are different. Although the effect of interaction parameter is probably smaller than the effect of penetrant size, it can not be disregarded. Third, also the mass of the penetrants is different. Figure 5.17 shows some experimental diffusion coefficients together with the results from our simulations.

The spread in these data is rather large, this is a result of the different measuring conditions, different sources of polymer etc. The calculated data (indicated by the open circles and dashed line) fall clearly in the correct area, although the calculated D seems to be rather low for larger penetrants. But we must be aware of the fact that for larger penetrants the spherical approximation generally is a worse approximation than for the smaller penetrants. A large asphericity of the penetrant will result in a smaller effective size and thus give rise to a larger diffusion coefficient. We should also take into account the fact that the simulations were performed at constant volume and this is clearly not equal to the experimental conditions. Especially for the larger penetrants this can result in diffusion coefficients that are too low.

polyethyl methacrylate	-18.0
polyethylene (ρ = 0.964 g cm^{-3})	-8.7
polyethylene (ρ = 0.914 g cm^{-3})	-7.8
hydrogenated polybutadiene(hydropol)	-7.5
natural rubber	-7.8
polydimethyl siloxane (PDMS)(10 % filler)	-3.3

Table 5.6: Exponent n for various polymers ordered with respect to resistence to penetrant diffusion, when fitted to a power law behavior $(D \sim \sigma^n)$. Data from [65].

The diffusion constants as determined from simulation clearly exhibit a power law dependence on penetrant size: $D \sim \sigma^n$, with n = -6.2. The power law dependence that has been found can be seen in the experimental data as well, although the scatter is rather large. The best fit through these data points would result in an exponent of roughly -3. Table 5.6 shows the calculated values for several other polymers. The polymers in the table are ordered with respect to resistence to penetrant diffusion.

The value for the exponent (slope) of these scaling laws decreases with increasing resistence to diffusion. PDMS is the polymer with the highest penetrant diffusion constants (which was the main reason to use PDMS for this study) and it has the smallest exponent. Especially clear is the difference in slope for the two polyethylene samples at different densities. A higher density leads to a larger resistance to diffusion and thus to a larger exponent. The only glassy polymer in the table (polyethyl metacrylate) has by far the largest diffusion resistance and thus the largest value for the exponent.

The only penetrant simulated in the large system that can be directly compared to experimental data is the penetrant modeling helium, with parameters: σ = 0.258 nm and ε = 0.085 kJ mol^{-1}. The experimental values for the diffusion coefficient of helium however, have to be estimated from data of penetrant diffusion in *filled* PDMS [60]. In this case an inorganic filler is added to the membrane to increase the stability. The estimated value of D_{He} for pure PDMS is roughly 10 $\cdot 10^{-5}$ cm^{2}s^{-1} , which is in good agreement with the calculated values. The value of D for the small system is too *large* by a factor of almost 2, and D in the large system is too *small* by a factor of almost 2. The chemical potential μ_{ex} is in both simulations too small compared to the experimental value of 7.4 kJ mol^{-1}. The value obtained in the simulation of the small system is too low by almost 4 kJ mol^{-1}. This results in a solubility coefficient which is far too large and as a result the permeability coefficient P is way off as well. For the large simulation, the chemical potential is only moderately too small (0.5 kJ mol^{-1}) and this is reflected in a permeability coefficient which is in very good agreement with the experimental value. (All this data is gathered in table 5.7.)

In case of the chemical potentials the simulations can be compared to more experimental values. In addition to helium I have also calculated the chemical potentials for methane, oxygen and nitrogen (table 5.8). We see that except for helium all other values are too low by roughly 3 kJ mol^{-1} . It seemes as if the error increases with ε. The trend and relative differences are reasonably good. As a possible reason for the discreapancy could

	D (cm^{2}s^{-1})	μ_{ex} (kJ mol^{-1})	S	P (cm^{2}s^{-1})
experimental	10 $\cdot 10^{-5}$	7.4	0.051	0.5 $\cdot 10^{-5}$
small system	18 $\cdot 10^{-5}$	3.8	0.22	4.9 $\cdot 10^{-5}$
large system	5.9 $\cdot 10^{-5}$	6.9	0.063	0.38 $\cdot 10^{-5}$

Table 5.7: Comparison of experimental values and simulation results for **helium** *in PDMS.*

be the united atom description, or insufficient reliability of the σ and ε parameters for the penetrants. These parameters are determined from the second virial coefficients in an environment which is clearly different from inside a polymer membrane.

	σ	ε	μ_{ex} (kJ mol^{-1})	
	(nm)	(kJ mol^{-1})	this work	experimental
CH_4	0.373	1.247	-1.09	1.9
O_2	0.343	0.940	1.47	4.3
N_2	0.368	0.761	2.72	6.1
He	0.258	0.085	6.94	7.4

Table 5.8: Comparison of experimental values and simulation results of the chemical potential for several penetrants

Chapter 6

Free volume

Chapter 6 deals with the empty space between the polymer chains, the so called "free volume". In this chapter the basic concepts of percolation theory will be given and related to the free volume within the polymer matrix. Computer experiments to evaluate the statistical properties of this volume will be described and results will be given.

6.1 Introduction

The term "free volume" usually refers to the empty space between the molecules, the volume not occupied by the polymer, although a number of other definitions are in use. In this thesis I will use the definition that the volume that is accessible to a penetrant modeled by its hard sphere diameter is (appropriately) called the "accessible volume". And I will use the term "free volume" for the volume accessible to a penetrant of size zero, and in general descriptions. By this definition, a polymer has one specific free volume, and for each penetrant an accessible volume that depends on both this free volume and the penetrant's size.

The accessible volume is an important quantity in the description of both diffusion and solubility. The accessible volume is, for example, a simplified measure of the excess entropy of insertion. If the molecular system would consist of hard spheres only, the solubility would be given completely by the accessible volume. Once the penetrant has entered the polymer matrix it can only diffuse through its available volume, the volume accessible to that penetrant. You can imagine that not only the total accessible volume is important, but also the distribution and the dynamics of this volume. For a penetrant to move through the polymer it has to find a path of connected accessible volume throughout the complete polymer matrix.

All of this indicates that a good statistical description of this accessible volume and its

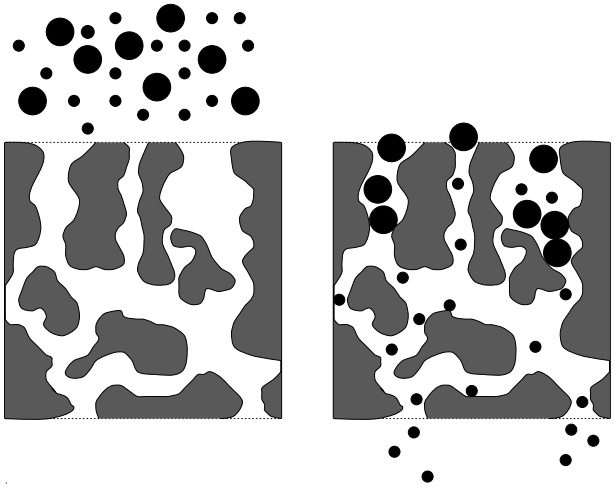

Figure 6.1: A static description of the diffusion process where the membrane acts as a sieve. The smaller particles have more accessible volume and thus will permeate faster.

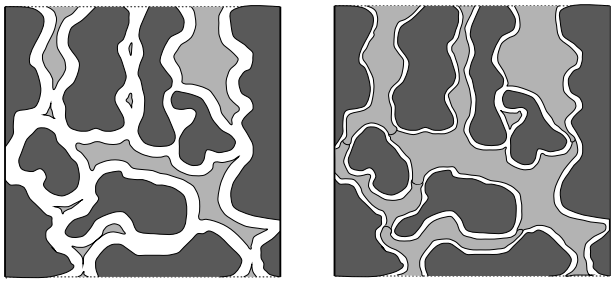

Figure 6.2: The same membrane as the previous picture, but now is the volume accessible to both the large (left) and the small (right) penetrant particle is indicated.

distribution could be of great importance for a thorough understanding of the permeation process.

The selective effect of the accessible volume distribution on diffusion can be visualized in the following way. Assume that there is at each instant a distribution of holes in the polymer due to thermal fluctuations. Although the detailed structure of the polymer is constantly changing the distribution of holes in the macroscopic matrix is constant.

Each penetrant in the polymer matrix can, through an activated process, move to an adjecent accessible volume hole. At each diffusion step the smallest penetrant will find a larger number of holes to jump to than a larger penetrant. Thus it will have a higher possibility for a diffusive jump and therefore will have the highest diffusion rate. In a simplified way the polymer acts as a sieve, as is indicated in figures 6.1 and 6.2. In this schematic mechanism the polymer dynamics are not explicitly taken into account. For large penetrants these dynamics can however have a large effect on the diffusion.

Molecular dynamics simulations provide all the information to study the hole-size dis-

tribution directly, albeit on a very small scale. From our MD simulations of the PDMS model i can calculate the free volume distribution in this polymer and analyze its distribution on a time scale of 500 ps and a sample size of ≈ 80 nm^3.

The distribution of hole sizes (in very simple systems) is thoroughly studied in *percolation theory*. In this chapter I will try to link the statistical properties of accessible volume holes in PDMS to the results found in percolation theory. But the step from the simple percolation system to a polymer is a large step. So I also investigated a system of intermediate complexity, *i.e.* a system of randomly placed overlapping spheres, where the size of the spheres is comparable to the size of the basic units in the polymer system *i.e.* the atoms.

The next section will first briefly discuss the general foundations of percolation theory. Then the different models studied will be described after which the results for these models will be given and discussed.

6.2 Percolation theory

6.2.1 General

Percolation theory in its simplest form deals with the statistics of an idealized disordered system. The term "percolation" was coined by Broadbent and Hamersley [66] as opposed to the term "diffusion" : *If diffusive processes involve a random walk of a particle in a regular medium, then percolation processes involve a regular motion (e.g. fluid or electrical current flow) through a random medium.* The percolation model has been used to characterize many disordered systems, such as porous media, fragmentation and fractures, gelation, random-resistor systems, forest fires and epidemics. (For a good introduction to percolation theory see [67]). There are a number of basic percolation models[1], but for simplicity I shall only describe site percolation on a square (or cubic) lattice.

6.2.2 Percolation threshold

Consider a square lattice where each site is occupied with probability p and empty with probability $(1 - p)$, (figure 6.3). A group of occupied sites which are directly

[1]There are for example a number of lattices on which the percolation properties can be evaluated: triangular, honeycomb or hexagonal, diamond, BCC, FCC etc., and there is a difference between bond percolation and site percolation. In site-percolation a site can either be occupied or not, and only directly neighboring sites are connected. In its counterpart, the bond percolation, all sites are occupied and lines are drawn between neighboring sites. Then each line can be open with probability p, or closed with probability (1 - p)

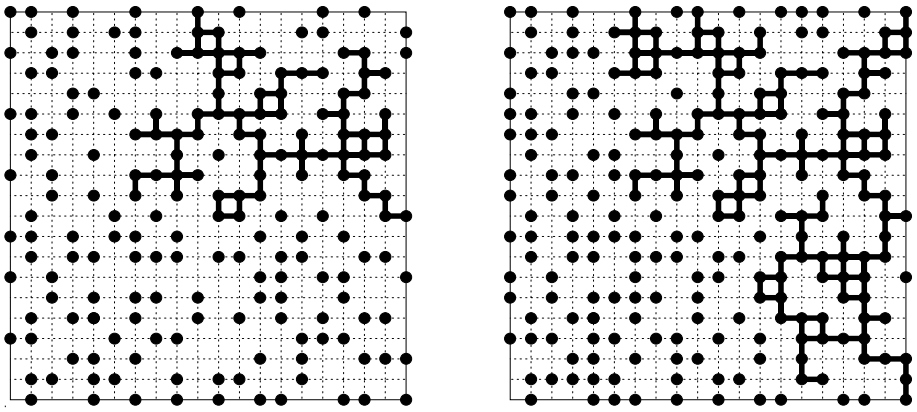

Figure 6.3: Example of two dimensional percolation on a 20×20 *square lattice at p* ≈ 0.45 *(left) and p* ≈ 0.60 *(right). The occupied sites are indicated with a* $\bullet$ *and the empty sites appropriately without. The largest cluster is indicated with the thick line. Note that at p* ≈ 0.60 *the largest cluster percolates*

connected form a cluster. For example, let us assume that the occupied sites are electrical conductors and the empty sites are insulators and that electrical current can only flow between nearest neighbors. At low conductor concentration (low p) there will be many small and isolated clusters and thus no net current can flow. At large p there will be mainly large clusters spanning the complete lattice and an electrical current can flow from one side of the lattice to the other. Thus at a certain threshold concentration p_c there will be one cluster spanning the complete lattice and current can flow for the first time. This critical concentration p_c is called the *percolation threshold*.

6.2.3 Fractal dimension

The fractal nature of these clusters is described by the fractal dimension d_f. This fractal dimension describes the dependence of density on the length scale or how, on average, the size or mass of a cluster M within a sphere of radius r scales with r,

$$M(r) \propto r^{d_f}. \tag{6.1}$$

For example the 2-d percolating cluster given in the example above would have (for an sufficiently large sample size) a fractal dimension of 1.9. Its 3-d counterpart is found to have a fractal dimension of 2.5.

6.2.4 Correlation length

Below and above p_c the behavior of the *finite* clusters is governed by a correlation length ξ. This ξ can be interpreted as a typical length up to which the clusters are self-similar and can be regarded as fractal. For length scales larger that ξ the structure is not self similar and can be regarded as homogeneous. In other words,

$$M(r) \propto \begin{cases} r^{d_f} & r \ll \xi \\ r^d & r \gg \xi \end{cases} \tag{6.2}$$

where d is the space dimension. So on length scales beyond ξ the system is homogenous. At the percolation threshold p_c, ξ diverges to infinity and holes occur at all length scales.

6.2.5 Universal constants and power laws

The percolation transition is a simple case of a phase transition. It is a geometrical phase transition where the critical concentration separates a phase of finite clusters ($p < p_c$) from a phase where an infinite cluster is present ($p > p_c$). The probability P_∞ is the probability that a site in the lattice belongs to the infinite cluster. Below p_c, P_∞= 0 and above p_c, P_∞ increases with p as

$$P_\infty \propto (p - p_c)^\beta \tag{6.3}$$

Many other relevant quantities are described by power laws and critical exponents, for example the aforementioned correlation length ξ, scales as

$$\xi \propto (p - p_c)^{-\nu}. \tag{6.4}$$

These scaling exponents are all related to each other, for example the fractal dimension d_f and the euclidian dimension d are related to β and ν as:

$$d_f = d - \beta/\nu \tag{6.5}$$

With values of β = 0.41, ν = 0.88, d_f results in 2.53, for d = 3. Another often mentioned exponent is the exponent γ, by which the mean cluster size S is scaled

$$S \propto \mid p - p_c \mid^\gamma \tag{6.6}$$

The exponents β, ν and γ are universal and depend only on the (space) dimension, but *not* on the lattice structure or on the type of percolation[67]. This is an important principle, because if this is true for a system like the polymer matrix then a number of relations found in percolation theory could also be applied to polymer physics. The number of these universal exponents is still growing, but most of them are not needed within the scope of this thesis.

6.2.6 Cluster size distribution

The most important critical exponent for our purposes is τ, which describes the cluster size distribution n_v. That is the probability to find a hole of a size (or volume) v or alternatively the probability that a site belongs to a cluster of size v. In the one dimensional case (a linear chain of sites) n_v is simply the product of the probability p^v that v sites are connected and the probability $(1-p)^2$ that the two perimeter sites are empty $n_v = p^v\,(1-p)^2$.

In general, the probability of finding a cluster of v sites having t perimeter sites is $p^v(1-p)^t$. There is however more than one realization possible for a cluster of v sites. Clusters with the same v may have different t. On our square lattice for example a cluster of 3 sites can have either 7 or 8 perimeter sites and a cluster of 4 sites can have 8, 9 or 10 perimeter sites

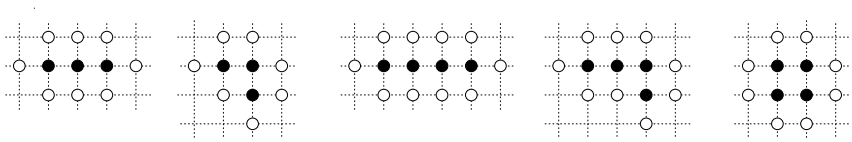

v=3, t=8 v=3, t=7 v=4, t=10 v=4, t=9 v=4, t=8

We can now define a quantity $g(v,t)$, which gives the number of conformations for a cluster of v sites and t perimeter sites. The *general* expression for n_v then becomes

$$n_v = \sum\, g(v,t)\, p^v(1-p)^t. \tag{6.7}$$

There is however no analytic relation for this $g(v,t)$.[2] Thus one has to resort to assumptions.

For small probabilities p where the clusters are independent one can argue that n_v decays exponentially with v:

[2] Except for the one-dimensional or the infinite dimensional (the Cayley tree or Bethe lattice [68, 69]) case.

$$n_v \propto \exp(-cv) \tag{6.8}$$

This nice exponential is however not applicable at higher probabilities. Based on results from computer experiments and combinatorial approaches the assumption is made that at p_c the cluster size distribution has a power-law decay:

$$n_v \propto v^{-\tau}. \tag{6.9}$$

It is postulated that in general one has a combination of an exponential and a power law behavior:

$$n_v \propto \ v^{-\tau} \ \exp(-cv) \tag{6.10}$$

where $c = \mid p - p_c \mid^{1/\sigma}$, σ being another critical exponent. Based on this relation, one can find relations between the exponent τ and the other critical exponents σ, β and γ:

$$\beta = \frac{\tau - 2}{\sigma}, \qquad\qquad \gamma = \frac{3 - \tau}{\sigma}, \tag{6.11}$$

and knowing that both β and γ are positive one finds that

$$2 < \tau < 3. \tag{6.12}$$

The value reported in the literature, $\tau = 2.18$ [67], fulfils this inequality.

But there is more, or as Stauffer says “Not everything in life is connected with critical phenomena near p_c” [67]. The relations 6.9 and 6.10 are valid near p_c. For $p > p_c$ and $p < p_c$ different relations hold:

$$n_v(p < p_c) \propto \ v^{-\theta} \ \exp(-c'v), \tag{6.13}$$

and

$$n_v(p > p_c) \propto \ v^{-\theta'} \ \exp(-c''v^{1-1/d}), \tag{6.14}$$

where θ and θ' have reported values of 3/2 and -1/9 respectively [67]. These relations hold for $v > v_\xi$, so for clusters of a size exceeding the correlation length ξ.

6.3 Percolation principles in real systems

The transfer of concepts of percolation on a random grid to accessible volume in a polymer system is fairly straightforward. Where in simple percolation the gridpoint is occupied in a random fashion, now a gridpoint is occupied when a penetrant, with its center at that location, can fit into the polymer without overlapping with the polymer atoms. The probability p is now varied by varying the size of the penetrant.

A cluster is still defined in the same manner, but a cluster now is an accessible volume hole. If the system percolates, then a penetrant situated in the percolating hole can move through the complete polymer sample.

The cluster size distribution, or in diffusion language hole size distribution, is widely used in free volume diffusion theories. One has to take care not to overestimate the importance of the hole size distribution. It is tempting to try to use it in the way that is common to a number of free volume diffusion theories: If we know *the* hole size distribution then we can calculate the accessible volume as function of penetrant size.

For this one then has to assume that **one** cluster **size** distribution **fits all**, so one distribution provides sufficient information to calculate the accessible volumina for any penetrant. There is however no *one* hole size distribution. As we have seen in the previous section, the exact form of the distributions depends on where we are with respect to p_c. But also on an intuitive level we can see why this approach will fail. Imagine a system with many aspherical holes. If we calculate the accessible volume distribution for a penetrant of size zero, we will find a certain percentage of holes with size v. But if we try to put *spherical* penetrants with volume v into these holes they will not fit in these holes because the shape of the hole is not spherical. In the results section, we will see that most holes are very irregular.

So, using the terminology introduced in the beginning of this chapter, there is one size distribution of *free* volume, which in molecular systems mainly consists of one hole of a size approximately equal to the free volume. But there are many (different) *accessible* hole size distributions.

6.4 Computer experiments

With this theory in hand we can start to explore the differences and equalities of the model system and "real" systems. In order to link percolation theory to the diffusion properties in polymers I have studied three different systems: the random grid, a system consisting of randomly placed spheres[3] and the polymer.

[3] In this thesis only the results of overlapping spheres are presented. But I have studied other systems as well: Randomly placed nonoverlapping spheres and a system of Lennard Jones particles generated

6.4.1 Percolation models

- **Random grid** (standard percolation system): As the standard percolation grid has been thoroughly studied, this is our starting point. Every gridpoint of a cubic *periodic* grid is filled with equal probability p, independent of the other gridpoints. The system size is indicated with the symbol L, which means that the lattice is $L \times L \times L$. The filled points are shown as black dots in the accompanying picture, which is a 2D representation of the 3D system.

Random grid

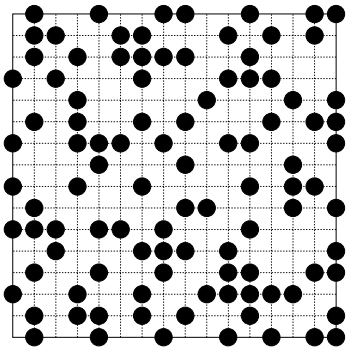

- **Random overlapping spheres**: A next step is to incorporate the size and shape of simple atoms. We do this by studying a system of overlapping spheres. At random positions on the grid spheres with radius R are placed and all gridpoints within these sphere are taken to be occupied. At the limiting value $R = 1$ gridpoint this system reduces to the simple random grid. (In the experiments we have taken R=5, which with the system size L=100, is comparable to the radius of an average atom in the polymer system mapped onto a grid of $L = 100$.

Overlapping circles

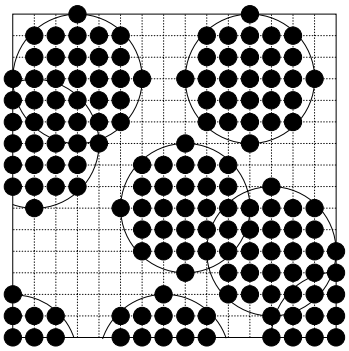

- **Polymer (PDMS)**. The target system of this study is of course the polymer sample. Now the underlying matrix is our simulated PDMS polymer, where we analyzed the simulation without penetrants as described in chapter 4.

Polymer

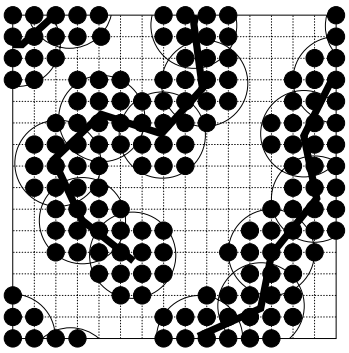

All percolation experiments have been performed using a simple cubic lattice; only direct neighbors can be connected (no diagonal connections) and the standard size for the grid is $100 \times 100 \times 100$.

with a molecular dynamics simulation. All results for these systems are for the purpose of this thesis equivalent and will not be mentioned here.

In case of the polymer system, for which the box dimensions are not equal in all three directions, the polymer is mapped onto the lattice in the following way: First the maximum box dimension is calculated, this is then mapped on 100 grid points. Using the same mapping factor the two other grid dimensions are calculated (which will be less than 100 gridpoints). Note that it is essential that the polymer atom coordinates are *not* discretized, but the gridpoints are simply used to check whether or not this point in space is free. The accessible volume for a penetrant of size σ_{pen} is calculated by use of the relation $\sigma = (\sigma_{pen} + \sigma_{pol})/2$. Every gridpoint that falls within σ of any of the polymer atoms is said to be occupied.

For the system of spheres and the polymer we can look at the percolation statistics of the "occupied" space as well as the "unoccupied" space. In the standard percolation system, the random grid, they are equivalent. But in the other two systems they describe different systems. From the diffusion point of view the statistics of the space between the spheres/molecules, the unoccupied space, is most important. In the polymer system we only looked at the percolation of voids or unoccupied space, because the percolation properties of the occupied space are completely irrelevant for diffusion studies. In the system with spheres we looked at both, and the two complementary systems will be described by "spheres" for the occupied space and "voids" for the unoccupied space.

6.4.2 Extended percolation descriptions for PDMS

The final model in the previous section is the polymer sample. There are however, still some difficulties if we want to link the percolation statistics of this model to diffusion data. First of all, the dynamics of the polymer is only incorporated into this model by using different samples along the molecular dynamics trajectory to calculate the average properties. Also the complex interaction of a penetrant and the polymer is not taken into account, but it is modeled by a hard sphere repulsive potential only.

Energy percolation

A logical step would be to change the hard sphere interaction into a Lennard-Jones-like description of the atoms. However, if we do that then there is no clear distinction between *accessible* and *non-accessible* volume, just areas of high or low, positive or negative interaction energy. The areas of negative (=favorable) energy are connected to each other by energy barriers, saddle points, and if a penetrant has enough energy, it can move over that barrier as if the two areas were connected. In this case these two regions should be treated as *one* accessible hole. For each penetrant size there will be an energy at which there is for the first time one percolating cluster. In this way we have defined a *percolation energy*.

I have simplified this approach a little to increase computational speed. To calculate

the *effective* size of a penetrant with potential energy E, one solves the Lennard-Jones equation $V = 4\varepsilon((\sigma/r)^{12} - (\sigma/r)^6)$ with $V = E$ and $r = \sigma_E$, which gives.

$$\sigma_E \;=\; \sigma \;\left(\; \frac{1}{2} \;\left(1 + \sqrt{1 + (E/\varepsilon)}\;\right)\right)^{-1/6} \tag{6.15}$$

For every pair interaction with the polymer (every set of σ and ε) the effective σ's are calulated and used for the accessible volume determination. By using these effective size parameters for different values of E per penetrant we can calculate the percolation energy, *i.e.* the energy needed to create a spanning cluster.

With these effective penetrant size we can also calculate the accessible volume of a penetrant at a certain energy, for example, 1 kT. In the results I have used a value of 0.085 kJ mol^{-1} for ε. These percolation energies will be given in units of kT, where T= 300 K.

One can also define the property *percolation free energy*, where the energies are averaged with their Boltzmann weight. But as the physical background for both is not quite clear, and the results do not differ qualitatively, this property is not further mentioned.

6.4.3 Analysis of the results

Percolation threshold

How does one identify p_c from calculations on a finite sample? This p_c will be different from the percolation threshold in an infinite sample. In a finite sample p_c will always be lower than the real p_c, because the spanning cluster only needs to be of the size of the sample itself and not infinite. Let us call the probability of finding a percolating cluster on a grid of size L at a probability p, $\Pi(p, L)$. In an *infinite* sample we expect $\Pi(p, L)$ to be 0 anywhere below p_c and 1 anywhere above p_c. So $\Pi(p, L)$ is a step function for an infinite sample. In a finite sample $\Pi(p, L)$ is not a step function, but a continuous function. There are a number of ways to define an effective percolation threshold p_{eff} for this system. Possible definitions are, that probability p at which $\Pi(p, L) = 0.5$, or $1/e$, or p where $\Pi(p, L)$ has its inflection point. Another definition of p_{eff} [67] is that p at which the second moment of the hole or cluster size distribution $m_2(p)$ (eq. 6.16) is at its maximum.

$$m_2(p) = \sum_{v=1}^{\infty} v^2 n_v \tag{6.16}$$

In this equation the sums are over all clusters except the infinite cluster (if it exists). The correlation length ξ is the critical length scale in the system. Far below p_c, ξ is small

and only small clusters exist. This means that $m_2(p)$ is small. When p approaches p_c, ξ diverges (eq. 6.4). Thus there are cluster on all length scales, giving rise to a large $m_s(p)$. Above p_c there can only be small clusters again (except for the infinite cluster) which means that the second moment decreases again.

All these definitions converge to p_c for large L, but the proportionality factor is different. So in principle all definitions are equal for infinite sample size. In this work I have used the computationally simplest definition: p_{eff} is that probability at which $\Pi(p, L) = 0.5$. In the results p_{eff} will be called p_c for simplicity, but we have to remember that this is simply the percolation system of the finite system on hand and is dependent on system size.

For the cluster size distributions, *at* p_c, this definition is not used. The theoretical cluster size distribution in the standard percolation system around p_c is given by $n_v \propto v^{-\tau}\ \exp(cv)$ and c scales with $|p - p_c|$ (see equation 6.10, section 6.2.6). As there is a spread in the percolation threshold, the cluster size distribution samples evaluated at the *average* percolation threshold, will contain this spread as well. But as we have seen the effect of sampling above and below p_c is the same for the cluster size distribution: the introduction of an exponential behavior. Therefore for the calculation of the cluster size distribution, the percolation threshold is evaluated for each sample (time frame) seperately. This is done by use of a simple iterative scheme. When we are sufficiently close to p_c (error in p_c less than 1%), the cluster size distributions are evaluated. These are then averaged to obtain the final distribution.

Cluster / Hole size distribution

For the cluster size distributions all the (occupied or unoccupied) grid points should be checked, and assigned to a hole. These are evaluated by use of a recursive algorithm. In short the procedure is as follows: After identification of free grid points one chooses one of these grids points (arbitrary) as a starting point. Then its neighboring gridpoints in all directions are checked to see if they are free as well. If one of the gridpoints is free, then this gridpoint is chosen as a new starting point. This procedure is repeated until no more connected free gridpoints are found (in practice the gridpoints that are already found are set to "occupied" so no gridpoint is examined twice). The number of gridpoints found in this cluster is the size of this cluster. We then move on to the next free grid point as the start of a next cluster and the same procedure is started again, and so on until the complete grid is checked.

The distribution of all volume sizes calculated on a grid of for example $100\times100\times100$ can range from 1 gridpoint to 10^6 gridpoints. We have to present this flood of data in an efficient way and do this by use of bins based on powers of 2. So the first bin would contain the number of clusters of size 1, the second clusters of size 2 and 3, the third of 4 to 7, then 8-15, 16-31, 32-63 in general 2^n to $2^{n+1} - 1$. Thus the data are equidistant

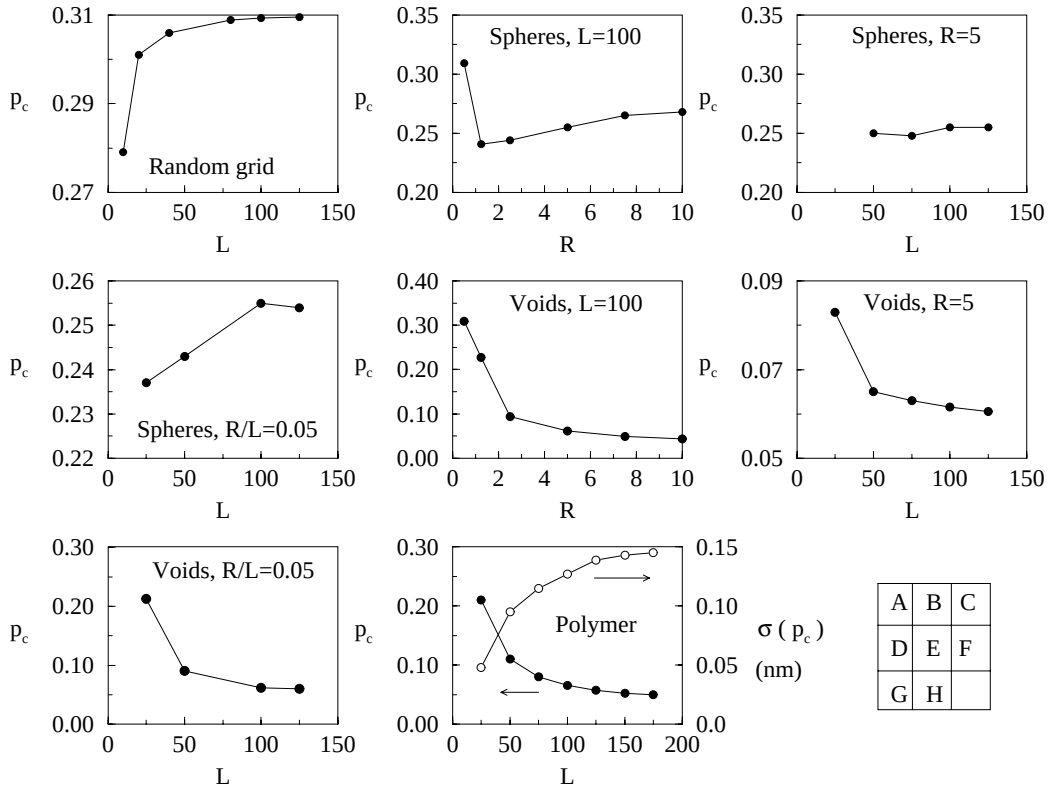

Figure 6.4: Effective percolation thresholds for the various systems as function of system parameters L (grid size) and R (radius of sphere). Note that in graphs D and G the sphere radius is not constant, but R/L is. In graph H (polymer system) also the size of the penetrant at p_c is plotted. The error in all values is typically 2 percent.

on a logarithmic scale.

6.5 Results

6.5.1 Percolation thresholds

It is important to see how the examined properties depend on the size of the system. For this reason the effective percolation thresholds for the random grid have been calculated for a series of grid sizes ranging from L=10 to 125 (grid = $L\times L\times L$) and the results are shown in figure 6.4 A. We see that there is a substantial finite-size effect. For the smallest grid the percolation threshold is $\approx$ 0.18, but it converges to a value of $\approx$ 0.31 (the value for p_c at L=125 is 0.3095). This is very close to the best known estimate, obtained by Monte-Carlo simulations, of 0.31161 [70].

For a system of randomly placed spheres another variable enters the scene: the radius R. As mentioned before there are in fact two complementary systems: the system of spheres and the system of voids. For both systems the percolation thresholds have been calculated for varying R with L=100, and for varying L with R=5 gridpoints. (Figure 6.4, graphs B,C,E and F.)

At R=0.5 there is no difference between the system of spheres, the system of voids or the random grid, and thus p_c is the same as well. For larger R they diverge, and the percolation thresholds for the two systems drop below the value of the random grid, due to the imposed correlations between neighboring gridpoints by the introduction of spheres.

In graph B (system of spheres, constant L, varying R) we see a drop in the percolation threshold after which it increases to a value of ≈ 0.27. This behavior is probably a result of the combined effect of an increase of the correlation between neighboring gridpoints and finite size effects.

If the size of the grid is varied (graph C) with R = 5, we see that the value for p_c fairly rapidly converges to a value of 0.255. Thus the finite size effects are fairly small in the case of spheres.

The percolation threshold for the voids is much lower than for the spheres. If we attribute the drop in p_c to the imposed correlations than we can conclude that this effect is larger for the voids than for the spheres. If we look at graphs E and F we see that with constant L, p_c drops to $\approx$ 0.04 at R = 10, and with constant R the percolation threshold reaches 0.06 at L = 125. This indicates that the finite size effects for voids are bigger than for spheres.

This striking difference in p_c between the voids and the spheres is a direct consequence of the difference in shape of these clusters as shown in figure 6.5. The fractal dimensions of both of these percolating clusters is about the same, $d_f \approx 2.1$, which is calculated by direct evaluation of equation 6.1 [4]. But the total size of the percolating cluster is roughly 4 times as large for the system of spheres as compared to the system of voids, so the percolating cluster is much more dense.

In the polymer system there is another intrinsic length scale that comes into play: the size of the molecular system (which will be called L_{sys}). So far the system size was equal to the grid size. The polymer system size however can not be varied as easily as L and R in the previous two systems. Also the typical size of the spheres (or atoms in this case) are fixed. In the ideal case one would like to work in the limit $R/L_{sys} \rightarrow 0, L \rightarrow \infty$. But within this work both R and L_{sys} are fixed, so the only parameter that can be varied is the size of the grid L on which the system is mapped, going to the continuum limit.

To see this effect in the system of random spheres I have investigated this system for different values of L while changing R so that R/L constant (R/L = 0.05, which is

[4]The fractal dimension d_f of our random grid system is calculated to be $\approx$ 2.45, literature value 2.52.

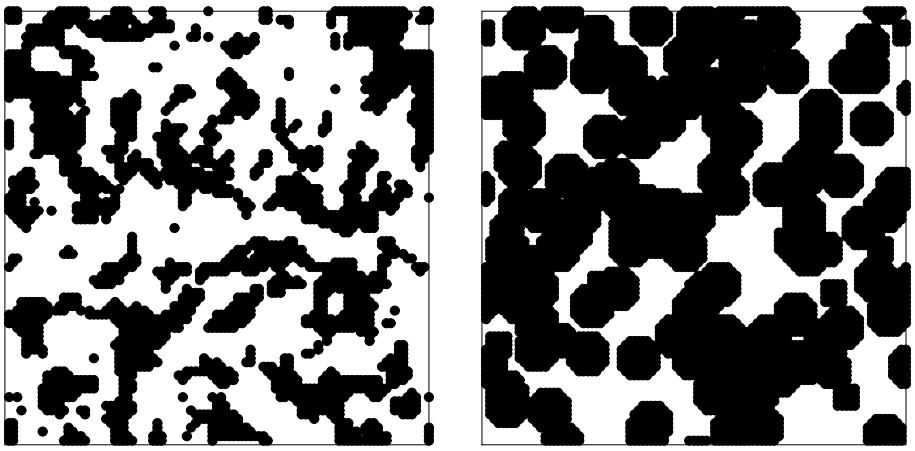

Figure 6.5: Difference in cluster shape (shown in black) in the random overlapping spheres system. The left picture shows clusters of voids and the right picture clusters of spheres. Both systems are close to their respective percolation thresholds. Shown is a 2d projection of a (10 grid units thick) slab of a 3d system of $100 \times 100 \times 100$.

roughly the same order of magnitude as for the polymer system). The results are shown in the same figure (6.4, D (spheres) and G (voids)).

We see that even for constant R/L the percolation thresholds are not constant, the better description of the spheres has a substantial effect on the percolation thresholds. The best estimates for p_c are 0.255 (spheres) and 0.0598 (voids).

We can compare the percolation thresholds to the values reported in the literature for the continuum limit.

For the voids the reported values[71–73] range from 0.032 to 0.034. Our value of $\approx$ 0.06 is still considerably larger. Thus it can be concluded that the finite size effects are still large.

The reported values for the percolation threshold in the system of spheres in the continuum limit show a considerable spread. Chiew [74] reportes a range for the variable η of 0.388 to 0.293, while most are in the region of η= 0.35. This η is related to our p_c as

$$p_c = 1 - \exp(-\eta) \tag{6.17}$$

After some tedious mathematics we find η for our system (at L=125) to be 0.294, which is within the reported range. Most of the reported values however are close to η = 0.35, which indicates that also here the finite size effects are still large.

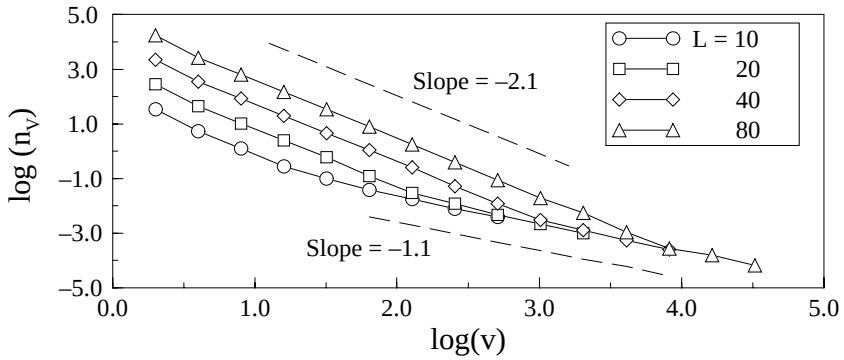

Figure 6.6: Cluster size distributions at the percolation threshold in the random grid system as function of grid size L. (Grid = $L \times L \times L$.)

In the polymer system (shown in graph H) L ranges[5] from 25 to 175. The percolation threshold decreases to a value of 0.050 at L = 175. For a grid of this size the size of the penetrant at p_c is 0.145 nm, while for a grid of L = 100, p_c = 0.066 and $\sigma(p_c)$ = 0.127.

If we assume that the continuum limit in the system of spheres is valid for the polymer model as well then we can estimate the penetrant size at p_c in the continuum limit. The relation between p_c and $\sigma(p_c)$ is approximately found to be:

$$\sigma(p_c) = 0.2 - 1.25(p_c) + 2.5(p_c)^2, \tag{6.18}$$

by fitting the results for several grid sizes to a quadratic function. This results in σ = 0.160 nm at p_c in the continuum limit. This means that for the smallest penetrant in the diffusion simulations presented in the previous chapter, the accessible volume percolates.

6.5.2 Cluster / Hole size - distribution at p_c

Random grid

The same finite size effects that influence the percolation thresholds are of great importance in the interpretation of the cluster size distributions. For several values of L the cluster size distributions in the random grid system at their respective percolation thresholds are shown in figure 6.6 on a double logarithmic scale.

The curve for each L consists of two regions, one with a slope of $\approx$ -2.2 and one with

[5] A grid of 175 $\times$ 175 $\times$ 175 is the largest possible grid within the memory capacity of the computer used

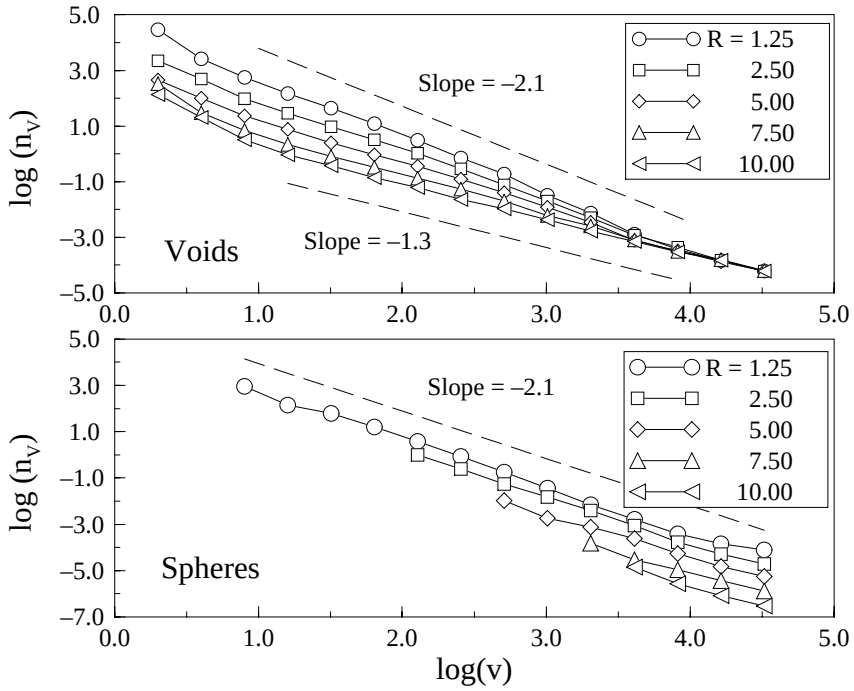

Figure 6.7: Cluster size distributions for the system of spheres and voids as function of sphere radius R with $L = 100$. All distributions have been evaluated at their respective percolation thresholds. In the bottom graph (spheres) the curves have been shifted down with respect to each other for reasons of clarity. All curves were originally on top of each other.

slope $\approx$ -1.1. But the crossover point shifts to larger clusters with grid size L. It seems as if the finite size effects introduce a correlation length before which normal behavior is observed, but after which the slope of the distribution decreases to roughly half of its original value. The slope of the curve until the crossover point is -2.2, which is very close to the literature value of τ of -2.18.

Random spheres

In figure 6.7 the cluster size distributions are shown for the systems of spheres and voids. In these calculations the grid size was taken to be constant (L=100) and R varied from 1.25 to 10.0 gridpoints. If we compare the distributions for the system of spheres and the voids we see a clear difference. First of all, the curves for the spheres all have the same slope and lie on top of each other (in the figure they are slightly displaced with respect to each other). The slopes in the system of voids vary with sphere radius. For the smallest radius the slope is $\approx$ -2.1, and for R = 10, the slope increases to a value of -1.3.

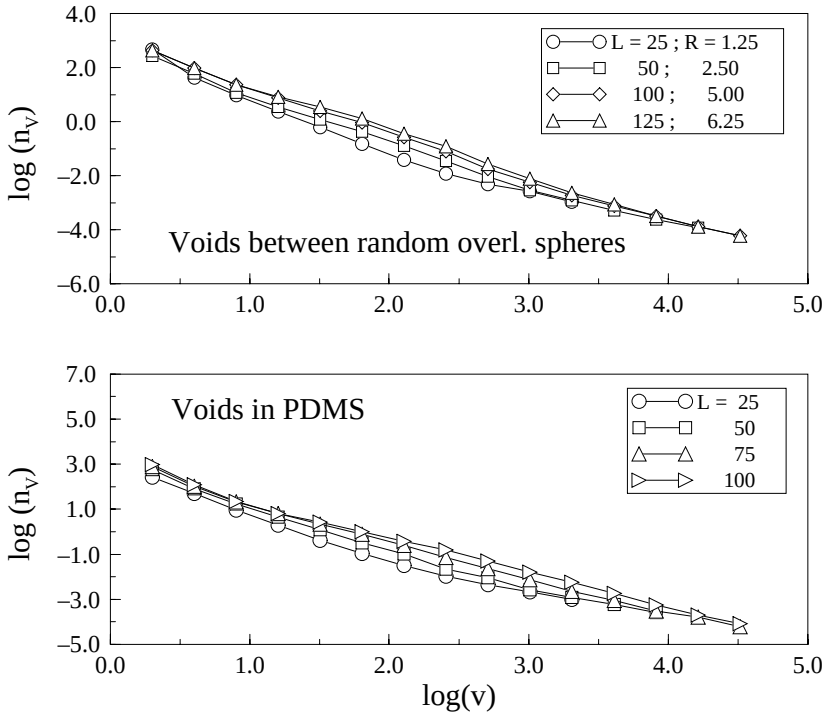

Figure 6.8: Hole size distributions in the polymer system as function of grid size L. All distributions have been evaluated at their respective percolation thresholds.

Second, the curves for the system of voids all start at the same cluster size, while for the spheres the smallest cluster increases with sphere radius. This is easily explained: the smallest cluster in the system of spheres is a sphere of volume $\approx 4/3\pi R^3$, so this increases with R, while the smallest possible *void* is one gridpoint in all cases.

A third point that should be noted is that in the distributions of the voids the first part (first two gridpoints) is clearly steeper for all curves. This is probably a result of the coarseness of the grid. These small spheres can not be described well enough on this grid. This effect is not seen for the spheres because the smallest clusters in the system are larger, as was already noted.

So the effect of introducing spheres is a lowering of the slope of the cluster size distribution curve in the system of voids. In the case of spheres this effect cannot be seen, only the starting point of the distribution changes.

Polymer system

In figure 6.8 two graphs are displayed. The top graph shows the cluster size distributions for the voids in the system of random overlapping spheres where R and L are varied,

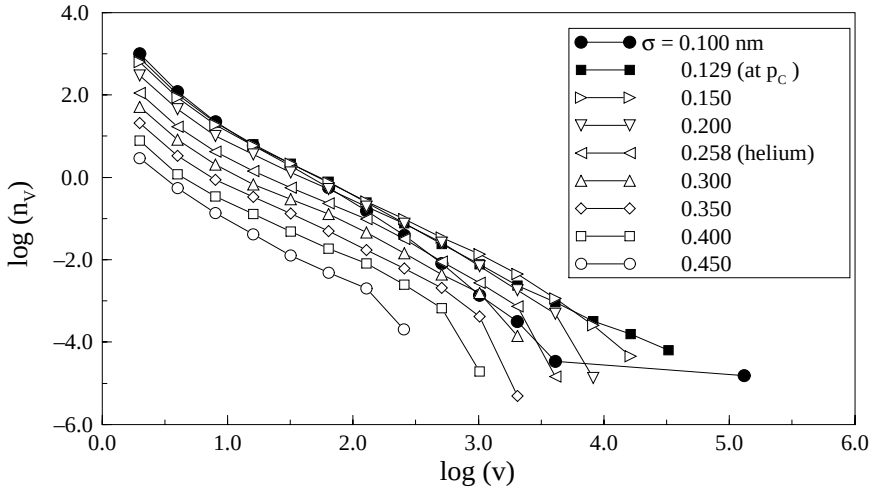

Figure 6.9: Hole size distributions in the polymer system for various penetrant sizes.

so that R/L is constant at 0.05. In the bottom graph the distributions of voids in the polymer system as function of grid size L are shown. In this system the ratio R/L_{system} is also fixed (and approximately 0.05) so both graphs can be compared. Both systems indeed show similar behavior.

For the smallest grid the distribution consists of two regions where the slope of the first part of the curve is $\approx$ -2.3 and of the second part -1.2. If we enlarge the grid a third region appears for both systems.

In the polymer system, for L = 175, the distribution has a slope (on the double logarithmic plot) of -2.5 for volumes up to roughly 10 gridpoints, which again is a result of the coarseness of the grid. The second region ranging from volumes of 10 to $\approx$ 300 gridpoints ($\log(v) = 2.5$), has a slope of -1.3 and the last part, up to volumes of 30.000 gridpoints has a slope of -1.5.

We furthermore see that (except for L=25) the values of the distribution for the first three and the last two data points are approximately equal for all grid sizes. Only for intermediate cluster sizes the number of clusters increases. Note that all distributions are not normalized with respect to the total number of clusters.

If we compare both systems we do not see any effect of the interatomic correlation that is present in the polymer system. Both systems are effectively the same.

In none of these curves we see the same effect that we saw in the random grid case (figure 6.6); a larger grid does not introduce a similar crossover point in the distribution curve which shifts to larger cluster sizes with L.

6.5.3 Cluster / Hole size - distribution in the polymer system away from p_c

All the results given so far were concerned with the behavior at p_c. Let us now focus our attention on the hole size distributions in the polymer system away from p_c, which is, from a diffusion point of view, the most interesting region. Most realistic penetrants fall within this region. In figure 6.9 I have plotted the hole size distribution (with L=100)[6] as function of penetrant size. The first thing that can be noted is that for all curves the same grid coarseness effect can be seen for the first two points.

The curves with the open symbols are all below p_c (*i.e.* the accessible volume does not percolate). For all of these curves we find an exponential behavior next to the power law behavior. This exponential behavior is most visible for the largest holes, which is exactly what is predicted by percolation theory, which states that for $p < p_c$ one finds $n_v \propto v^{-\theta} \exp(-c'v)$ (eq. 6.13), where c is a function of $\mid p - p_c \mid$ and thus of σ. And with increasing penetrant size (going further away from p_c) the crossover from power law to exponential behavior indeed shifts to smaller hole sizes (*i.e.* an increase in c).

The slope of the linear part of the curves is approximately the same for all penetrants (below p_c): roughly -1.5 which is consistent with percolation theory that predicts θ = 1.5.

According to this theory, at (and close to) the percolation threshold one should find $n_v \propto v^{-\tau} \exp(cv)$, with τ = 2.18. The results however show an exponent of $\approx$ -1.5 even at p_c. Surprisingly, above p_c, for a penetrant of 0.100 nm, we see that this exponent drops to a value of -2.0. It is as if, although the accessible volume already percolates, the real percolation behavior for the hole size distribution is only found well above p_c. This is not consistent however with the fact that the effective percolation threshold occurs at a value for σ smaller than σ at the real p_c, *i.e.* infinite system. The latter is estimated to be σ = 0.160 nm.

6.5.4 Free / Accessible volume in the polymer system

One would like to be able to predict the accessible volume for a given penetrant, knowing its molecular volume, from the hole size distribution curve. In principle the accessible volume V_{acc} is given by:

$$V_{acc}(v^*) \propto \int_{v^*}^{\infty} v\ n_v dv \tag{6.19}$$

or if we use the general form for $n_v \propto v^{-1.5} \exp(bv)$, as we found for the polymer system, this becomes

[6] Although we have seen that finite size effects are still appreciable for a grid of this size, this grid has been used for reasons of limited computer power and time.

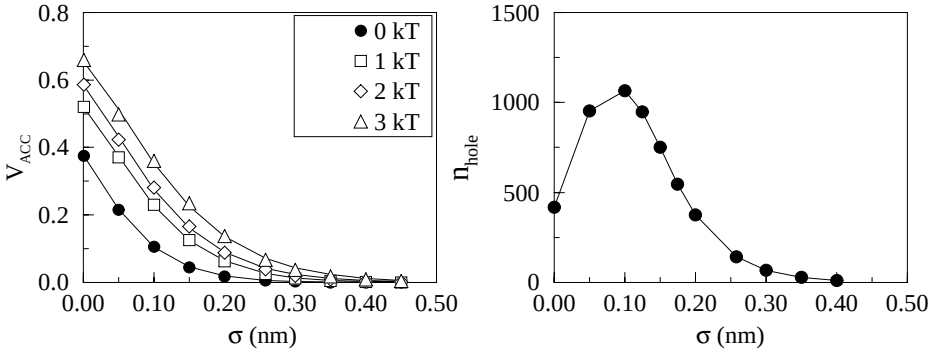

Figure 6.10: **Left:** *Accessible volumina for penetrants with diameter σ in the PDMS system. The lines through the data point are fits to a stretched exponential.* **Right:** *Number of holes in the polymer sample as function of σ (0 kT only).*

$$V_{acc}(v^*) \propto \int_{v^*}^{\infty} v\ v^{-1.5}\ \exp(bv)dv, \tag{6.20}$$

where b is in principle a function of the penetrant volume v^*. This integral however cannot be evaluated analytically and without the exponential part the integral diverges, unless the exponent is more negative than -2, in agreement with the inequality 6.11.

However the integral can be evaluated numerically, which means nothing else than directly calculate the accessible volume for each penetrant. The results are shown in figure 6.10. The total free volume, that is the accessible volume of a penetrant of size zero, averaged over the 500 ps simulation is calculated to be 37.5 %. This free volume and the accessible volumes of the penetrants of size $\sigma < 0.5$ nm are displayed in figure 6.10. For a penetrant with the size of a helium atom (σ = 0.258 nm) the accessible volume would be roughly 0.6 % and for a penetrant like methane (σ = 0.373 nm) this would drop to approximately 0.06 %.

The accessible volume is in principle the volume accessible to a hard sphere penetrant at 0 kT. In the same figure I have also displayed the accessible volumina for the same penetrants using their effective size at a certain energy (see section 6.4.2). As the functional form of the curves is not know from theory all that can be said is that the data points fit to a stretched exponential $V_{acc} = a\exp(b\sigma^c)$ with a constant value for c (=1.3), while a and b increase with the energy at which the accessible volumina are calculated.

The number of holes that are accessible to a penetrant is of importance to the diffusion process. The number of holes that is found in the polymer sample for each penetrant (with L=100) is displayed in figure 6.10. For a penetrant with size zero there are roughly 400 holes, but this quickly rises to a maximum of $\approx$ 1000 at the percolation threshold. After the percolation threshold the number of holes drops rapidly.

It is further found that below the percolation threshold this n_{hole} scales perfectly with the accessible volume as $n_{hole} \propto V_{acc}^{0.85}$ (not shown). In chapter 7 these data will be related to the diffusion data.

6.5.5 Extended percolation models

For every energy level (in figure 6.10) there will be a separate σ for which the percolation threshold is found. Or alternatively for every σ, there will be an energy at which its accessible volume percolates. For the calculation of the percolation energy the effective penetrant size at a certain energy is calculated as indicated in section 6.4.2. The percolation energy is that energy for which the effective size of a penetrant is small enough for its accessible volume to percolate. So the percolation energy is a measure of how much energy a penetrant needs to be able to cross the energy barriers in the polymer sample such that it has one percolating path through the sample.

As we can see from the figure the percolation energy vs. σ displays a power law behavior. It scales with penetrant diameter as $E_p \propto \sigma^{5.8}$, or roughly the square of the molecular volume. The percolation energy for a particle with the size of helium (σ = 0.258 nm) is 6.6 kT. For a penetrant the size of methane (σ = 0.373 nm) E_p is already $\approx$ 55 kT.

Alternatively one could talk about a percolation temperature. If we define the percolation temperature for a penetrant as that temperature at which the percolation energy equals 1 kT, we find a percolation temperature for helium of 1980 K and for methane of 16,500 K! It is not directly clear how the previously mentioned extrapolation to the continuum limit would lower these values. Still the percolation temperature for helium would be well above 1000 K. It that has to be taken into account that this temperature only applies to the penetrant. The effect of increased temperature on the polymer, which is very important, is not taken into consideration. The concept of percolation temperature is used merely for illustration.

6.5.6 Diffusion of accessible volume holes

To study the dynamics of the accessible volume I calculated the diffusion coefficient of the holes. For this the center of geometry of each hole was calculated at every time frame. The problem with the calculation of the diffusion constant is the identification of the holes at different times. Holes can be created, holes can vanish, one hole can split up in a number of holes and *vice versa*. No hole carries a label to identify it. To follow the hole i with geometric center $x_i(t)$ at time t, I first calculated the nearest center at time $t + \Delta t$ to be $x_i(t + \Delta t)$ and then decided using a distance criterion whether this center can be identified as the same hole. The choice of distance for this criterion is of course not well defined, but I found it not to be too critical. The distance used for this was 0.25 nm. Using this strategy only a few continuous trajectories of reasonable length could

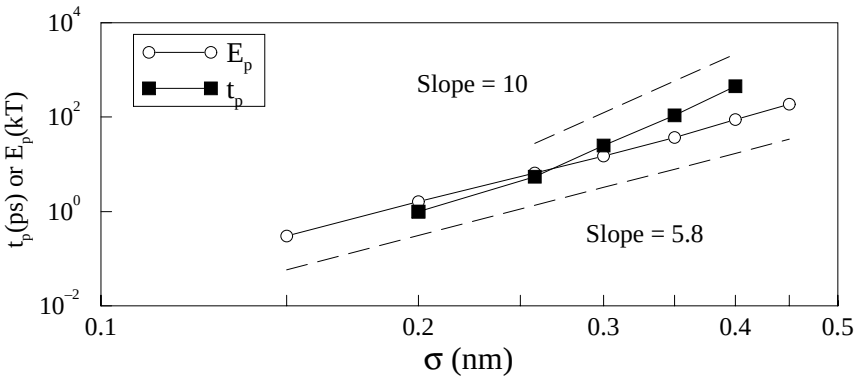

Figure 6.11: Percolation energy E_p as function of penetrant size σ on a double logarithmic scale.

be produced and the diffusion coefficient for these holes was found to be in the order of 10^{-7} cm^{2}s^{-1} . A more accurate result could not be obtained with this procedure.

6.6 Discussion

What have we learned from comparing the polymer system to the two test systems? We have seen that the difference in percolation threshold of the random grid and the polymer system is a result of the shape of the basic units: the atoms. The correlation between the atoms, *i.e.* the interatomic bond, the vanderWaals repulsive interactions etc. do not seem to be significant qualitatively. The system of randomly placed overlapping spheres shows the same percolation behavior as the polymer system.

Spheres vs. voids

With the introduction of spheres two complementary systems appear; the system made up of spheres or atoms and that made up of voids, the space between the atoms. Both of these systems show completely different percolation behavior. The percolation threshold in the system of spheres is much higher than in the system of voids. This is a direct result of the shape of the clusters. The percolation threshold of the voids for the finest grid (with a sphere radius of 5 gridpoints) is approximately 6 %. This 6 % is comparable to the percolation threshold found in a system of polyethylene evaluated with a comparable grid size and method[75]. Considering the fact that this is still higher than the value of $\approx$ 3.4% which is found for continuum percolation [71] we can conclude that the finite size effects are still appreciable.

These finite size effects are a result of two terms: the grid coarseness and the limited system size. An interesting difference between the system of spheres and the system of

voids is that for the voids both contributions have a similar effect. But for the spheres, the trends are opposite.

The fact that the percolation threshold decreases with L (in the system of voids) seems to contradict the inituitive picture. In normal percolation one can argue that if a given cluster percolates in an the infinite system than it will certainly percolate in a finite system. A possible explanation is that the clusters in the case of voids are much more sparse, as is shown in figure 6.5. To understand this we have to introduce the ideas of the *backbone* of the percolating cluster and the *dangling ends* of the cluster. The backbone consists of the cluster sites that are necessary for the percolating cluster. If one site in the backbone changes from 1 to 0 (or *vice versa*) then the cluster is not percolating anymore. A dangling end in not necessary. If part of a dangling end breaks than simply the total mass of the cluster decreases, but it is still percolating.

One could now say that because of the specific nature of the clusters in the system of voids, the relative density of dangling ends increases. With this the probability of finding a percolating cluster increases with L, and the percolation threshold decreases.

Polymer system

The assumption that the continuum limit for the system of voids is applicable to the polymer system as well is based on the fact that no significant qualitative differences are found between both systems. Although it is found that the percolation threshold generally decreases with increasing cluster anisotropy [76], it is not clear that the introduction of interatomic interactions does in fact increase the anisotropy of the voids between atoms. (See also [77] where the authors show that, in a system of spheres, interactions between the spheres can either lower of raise the percolation threshold.)

Applying the assumption mentioned above, the percolation threshold in the polymer is reached for penetrants of σ = 0.160 nm. This is not within the range of realistic penetrants. Helium, for example, has a σ-value of 0.258 nm.

Cluster/ Hole size distributions

We have also seen that the cluster size distribution is a property of a very complex nature and one should take care in interpreting it. The finite size effects are still appreciable for the grid sizes and system sizes used in this study. All the limits should be investigated thoroughly before concluding whether or not the cluster size distribution is indeed described by the equations given in percolation theory and thus are independent of the underlying system that generates the distribution. This would mean that the statistical properties of this distribution would not depend on the type of polymer!

For all realistic penetrants the hole size distribution of the accessible volume in the poly-

mer system is found to be a combination of a power law and an exponential contribution. The exponent of the power law is roughly -1.5, while the exponential contribution increases for larger penetrants.

To conclude one could say :

- the system of spheres and the resulting voids show different percolation behavior.
- the voids in the system of random overlapping spheres show the same behavior as the voids in the polymer system.
- the percolation threshold in the polymer system is reached for penetrants with σ = 0.160 nm. For realistic penetrants the percolation threshold is not reached.
- the percolation threshold can however be reached at higher energies (or temperatures).

Chapter 7

Permeation and free volume

This final chapter aims to combine all the previously presented results. It is found that the entropy of insertion is consistent with the accessible volume data. The diffusion data does not fit the free volume theories of Fujita and of Vrentas & Duda. It does, however, seem to fit a model based on percolation theory.

7.1 Introduction

In the two preceding chapters I have presented the results of the simulations to study the permeation process through PDMS (chapter 5) and the detailed analysis of the free and accessible volume in this polymer (chapter 6). As mentioned before, there is a strong correlation between these two, and in this chapter I shall try to elucidate this correlation. The structure of this chapter will be less strict than the previous chapters. Theory shall be mixed freely with results and discussion. First I shall focus on the relation between solubility and free volume. Then I shall look at the difference between normal diffusion and fractal diffusion. In the third section I shall compare the diffusion data to some well known free volume theories of diffusion. Next I shall discuss the relationship between the extended percolation models, as they were presented in the previous chapter, and diffusion. The final section of this chapter will present a current view on permeation, diffusion and solubility of small penetrants in PDMS.

7.2 Solubility and accessible volume

The solubility or chemical potential is considered to consist of two contributions: entropy and enthalpy. Thus the relation between solubility and accessible volume is made up of

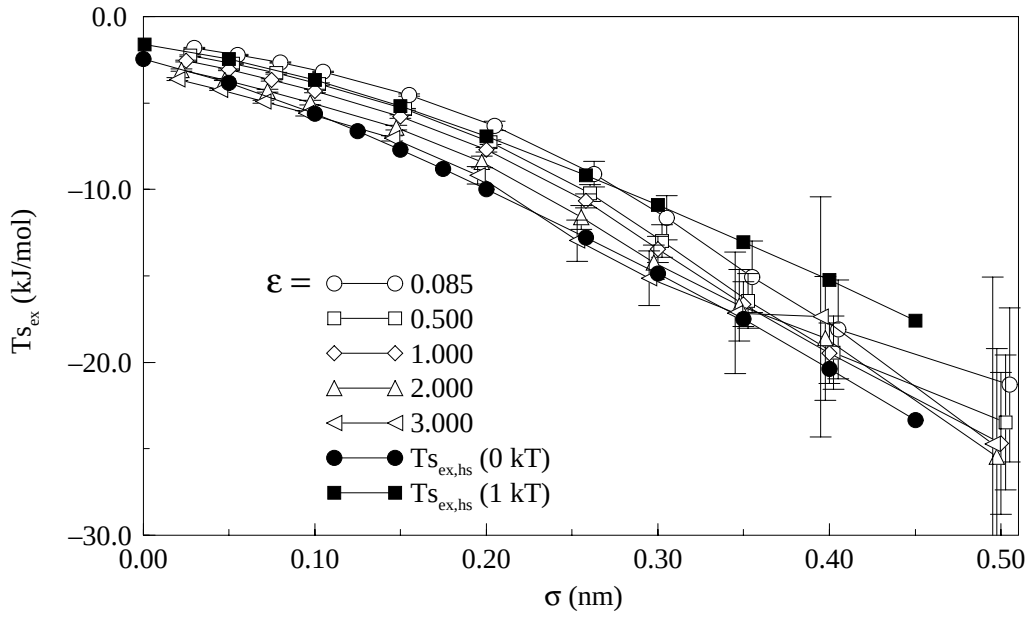

Figure 7.1: Excess entropy s_{ex} (times temperature) as calculated inderectly by the particle insertion method versus the natural logarithm of the accessible volume.

two contributions also.

Entropy

In chapter 5 the excess chemical potential μ_{ex} and the excess enthalpy h_{ex} have been calculated. From these two the excess entropy of insertion s_{ex} is calculated. In figure 7.1, this excess entropy contribution is shown again.

If the system would not have consisted of Lennard-Jones spheres, but of hard spheres then the excess entropy would be directly related to the probability of successfully inserting a hard sphere in the polymer. This probability is equal to the (fractional) accessible volume V_{acc} that was calculated in chapter 6. By use of

$$T s_{ex,hs}(\sigma) = RT \ \ln(V_{acc}(\sigma)) \tag{7.1}$$

the hard sphere entropy of insertion $s_{ex,hs}$ can be calculated.

It is also possible to calculate the effective hard sphere entropy at 1 kT. This is done by using the accessible volume of a penetrant using its effective penetrant size at 1 kT with (presented in figure 6.10). Both of these entropies are also shown in figure 7.1. There is a good agreement between the entropy calculated from the chemical potential

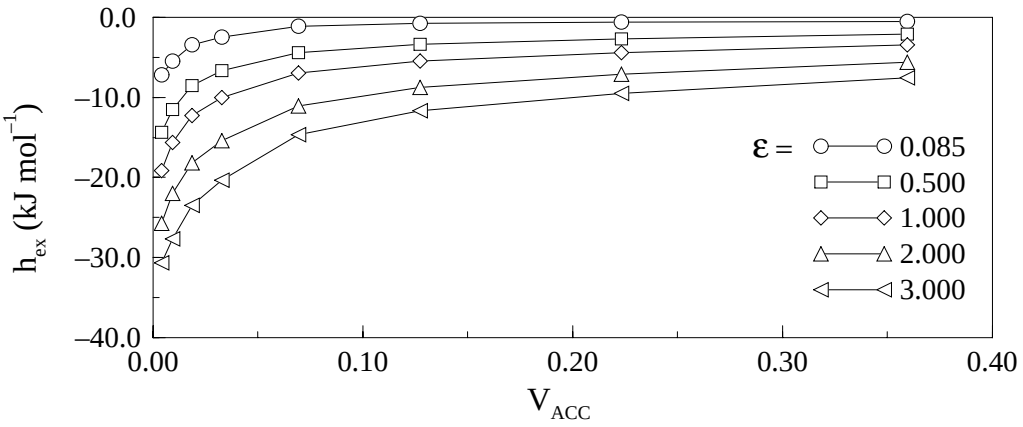

Figure 7.2: Enthalpy as function of penetrant diameter σ.

and enthalpy and from the accessible volumina. Thus the details of the Lennard-Jones interactions are not important for the entropy contribution.

The hard sphere entropy at 0 kT is closest to the entropy with ε = 3.0 kJ mol^{-1} . This is reasonable as the Lennard Jones potential with a large ε value is closest to the hard sphere potential. The accessible volume for a Lennard Jones penetrant with ε = 3.0 kJ mol^{-1} is less than with, for example ε = 0.085 kJ mol^{-1} . The energetic more favorable interaction with a larger ε is reflected in the enthalpy rather than the entropy.

The hard sphere entropy calculated with the effective size at 1 kT is less negative than at 0 kT. Penetrants with a higher energy have the possibility to visit a larger fraction of the conformational space; the accessible volume is larger. The fact that this hard sphere entropy at 1 kT is close to the entropy with ε = 0.085 kJ mol^{-1} is not strange if we remember that the effective size of the hard sphere penetrant is calculated using ε = 0.085 kJ mol^{-1} .

Enthalpy

The relation of the enthalpy and accessible volume is not directly clear. For the entropy it does not matter exactly how large the hole is. For the enthalpy this is more critical. The insertion with the most favorable interaction would be in a hole in which the penetrant exactly fits. In this case the number of neighbors with a favorable interaction is largest. Another factor in the enthalpy is the surface tension of the hole. The total effect is shown in figure 7.2, where the excess molar enthalpy of insertion is plotted as function of penetrant diameter.

7.3 Diffusion in a static percolation system

The diffusion of a particle in a static percolation system is a problem that has found a great deal of attention in the percolation literature [67, 78, 79] and may give some insight in the special features of penetrant diffusion in polymers.

In general the motion of a particle can be described by

$$\left\langle r^2(t) \right\rangle \propto t^{2/d_w} \tag{7.2}$$

where this exponent d_w is called the diffusion exponent or the fractal dimension of the path. In normal diffusion d_w is equal to 2. If the particle does not move in a regular medium, but on some kind of fractal medium (either on a grid or in a continuum description) the motion of that particle is restricted and d_w can be larger than 2. In that case the diffusion has a fractal nature and strictly speaking is no real diffusion any more.

First let us see how we can describe the motion of a particle that is located in a finite cluster. The particle can only move within this cluster and therefore it is restricted to finite distance, thus $\left\langle r^2(t) \right\rangle$ reaches a constant value. This immediately shows that if we want net diffusion in a static system we always have to be above the percolation threshold p_c. If not, only finite clusters exist and all the particles are restricted to their cluster and no net transfer of mass can occur.

What happens at $p > p_c$? Now there are two different cases to consider. First the diffusion on the infinite cluster alone and second the diffusion on the total percolation system. Net diffusion is only possible if the diffusant is situated on the percolating cluster, but if the diffusants are placed randomly in the sample, the total system is to be considered.

Diffusion on the infinite cluster

Let us define the diffusion constant of particles on the infinite clusters as D'. This is related to the overall diffusion constant D by $D = D'P_\infty$ (P_∞ is the fraction of cluster sites belonging to the infinite cluster).

Remember that the only length scale in a random percolation system is ξ. On times smaller than the average time t_ξ needed to visit a region of size ξ the particle sees the fractal nature of the cluster. At times larger than this t_ξ the particle effectively sees an Euclidian lattice with a lattice size ξ (see figure 7.3). Each cell of size ξ acts as a “trap” with a release time t_ξ. Thus

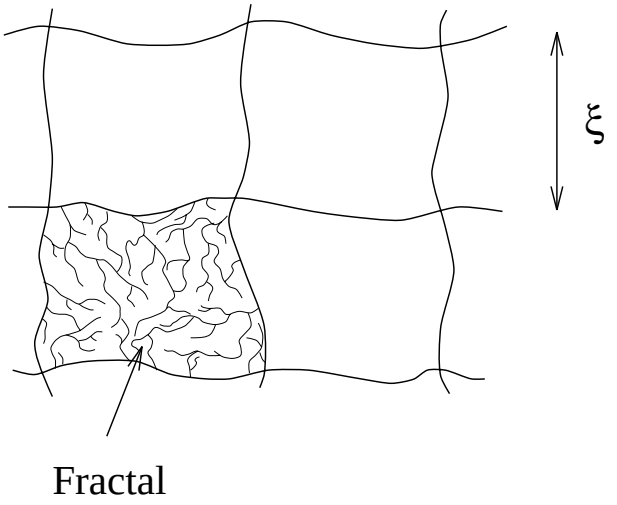

Figure 7.3: Schematic representation of the fractal nature if the medium. On length scales smaller than ξ a diffusing particle feels the fractal nature of the medium, beyond that it feels an Euclidian lattice with lattice size ξ.

$$\left\langle r^2(t) \right\rangle \propto \begin{cases} t^{2/d'_w} & t \ll t_\xi \\ t & t \gg t_\xi \end{cases} \tag{7.3}$$

where the notation d'_w is used for the diffusion exponent on the percolating cluster. We have to note that at $p = p_c$, $t_\xi = \infty$ as ξ diverges. So it will never reach "nonfractal" diffusion. Scaling relations give an expression for this diffusion exponent in the known critical exponents :

$$d'_w = 2 + \frac{\mu - \beta}{\nu}. \tag{7.4}$$

where μ, β and ν are the critical exponents which were given in chapter 6.

Diffusion on the total cluster

This approach can be extended to the diffusion of a particle on the total percolation lattice. We now have to average over all possible starting points, including those on finite clusters. And we end up with a similar formulation as equation 7.3 :

$$\left\langle r^2(t) \right\rangle \propto \begin{cases} t^{2/d_w} & t \ll t_\xi \\ t & t \gg t_\xi \end{cases} \tag{7.5}$$

where

$$d_w = \frac{d'_w}{1 - \beta/2\nu}. \tag{7.6}$$

Note that $d_w > d'_w$ since the finite clusters slow down the motion of the particle. The best known values for d'_w and d_w are [79] d'_w = 3.8, d_w = 5.0.

7.3.1 The polymer as a percolating system

If we try to extend these ideas to penetrant diffusion in polymers then we have to be aware of a couple of differences. First of all, the polymer is dynamic while the simple percolation system is not. This is a very important difference, especially when we are considering larger penetrants. For larger penetrants the accessible volume is far below its percolation threshold, and no (long time) diffusion could occur if the matrix would be rigid. All the penetrants would be trapped in their local environment. But as we know, even large steroid-like penetrants can diffuse through a PDMS membrane [21].

Also we have not taken into account the interaction of the penetrant and the polymer. One can imagine that in certain situations penetrants can, through their thermal energy, push a polymer chain away, or generate a conformational change (*e.g.* dihedral flip).

Another thing that complicates the interpretation of the fractal nature of diffusion is the fact that the length scale ξ on which fractal behavior is observed, is highly dependent on the size of the penetrant. For a penetrant *at* the percolation limit this ξ is infinite and fractal diffusion is observed at all length scales. Away from p_c this ξ drops rapidly and fractal behavior is limited to small length scales. The typical time spent on this length scale, t_ξ however increases with penetrant size and the resulting behavior depends on the balance between these two effects.

As we can see in chapter 5, figure 5.9 the value of t_ξ can not easily be extracted with high accuracy. For the largest penetrants this t_ξ is in the order of the simulation time of 500 ps.

As in the polymer system a number of effects are superimposed, the diffusion exponents d_w vary roughly anywhere from 2 to 6, depending on the region and the penetrant. The value of 2 of course denotes nonfractal diffusion. But there is no clearcut crossover from one region of fractal nature to a nonfractal diffusion region.

7.4 Diffusion models

To describe the diffusion of small molecules in rubbery polymers a number of theories have been developed. Most of these theories can be classified as either molecular models or free-volume models. The molecular models are based on the specific motions

of penetrant molecules and polymer chains, and the interaction parameters. The most important molecular model was proposed by Pace and Datyner [80] in 1979. Their diffusion theory is based on two separated molecular diffusion theories: that of DiBenedetto and Paul[81, 82] and that of Brandt [83]. They assume that the penetrant has two modes of motion in the polymer: i) along the axis of a "tube" formed by four adjacent paralel chains and ii) perpendicular to this axis. These two modes are believed to occur effectively in series. The first mode of motion is assumed to have no activation energy and occurs much faster than the second process. This second process requires an activation energy which is equal to the energy necessary to separate two polymer chains and is the rate limiting step. The model of Pace and Datyner succeeds in calculating the activation energies of diffusion, considering the molecular structure.

The free volume models do not offer a detailed, microscopic description of the penetrant-polymer system, but attempt to relate the diffusion coefficient to the free volume available in the system, usually from statistical considerations. This thesis mainly addresses the connection between free volume and diffusion so I will concentrate on the free volume models.

7.4.1 Free volume models

Free volume models are based on the idea that a penetrant can only move through the "free volume" in the polymer and that thus the diffusion can be described using a statistical description of this free volume. A widely used free volume model was developed by Fujita [46, 84]. Fujita's model is based on an earlier theory of self-diffusion in a hypothetical liquid of hard-sphere molecules proposed by Cohen and Turnbull [85]. According to these investigators, hard-spheres in a liquid are confined most of the time in cages bounded by their immediate neighbors. Occasional fluctuations in density may enlarge a cage enough to permit considerable displacement of the sphere. In this picture diffusion occurs not as a consequence of an activation process but rather as a redistribution of free volume within the liquid.

Fujita applied the Cohen and Turnbull formulation to the diffusion of small molecules in amorphous polymers above T_g by reinterpreting the meaning of some of its terms. This yields the following expression for the diffusion coefficient

$$D = RTA_d \exp(-B_d v^*/v_f) \tag{7.7}$$

where A_d and B_d are characteristic parameters, v^* is the critical cavity size for diffusion and v_f is the fractional free volume per unit volume of the polymer-penetrant system.The dependence of D on the size of the penetrant comes from the assumption that the critical cavity size v^* is proportional to the molar volume of the penetrant v [86]: $v^* = c\ v$ On substituting this relation into equation 7.7, we obtain the expression

$$\ln(D) = a - b\ v. \tag{7.8}$$

Another free-volume based model is that of Vrentas and Duda [87, 88]. In this model the diffusion constant is given as

$$D = D_0 \exp\left[\frac{-\gamma(w_1 v_1^* + w_2 v_2^* \xi)}{v_{hf}}\right] \tag{7.9}$$

where w_i is the mass fraction of component i, v_i^* the specific hole-free volume of component i required for a jump, v_{hf} the average hole free volume and γ an overlap factor of the different holes. The size of the penetrant comes in via the parameter ξ which is defined as *the ratio of the critical molar volumes of the two jumping units: penetrant/polymer.* This ξ should be proportional to the molecular volume $\frac{1}{6}\pi\sigma^3$. This concept however should not be applied to strictly. It was found by fitting this model to experimental data of penetrant diffusion in polyvinylidene chloride (PVDC) [89, 90] that ξ is related to σ as :

$$\xi = 0.63\,\sigma^{1.24}. \tag{7.10}$$

Thus the penetrant size dependency of the diffusion coefficient is given as:

$$\ln(D) = a - b\ v^{0.413} \tag{7.11}$$

It is assumed that the exponent in equation 7.10 is universal and that different polymers can be described by different prefactors [89].

7.4.2 Fit of the calculated data to free volume models

In figure 7.4 MD-data are shown together with best fits to both the Fujita and the Vrentas & Duda models. (Also a fit to a percolation model, which is discussed in the next section, is shown.) Both free volume models seem to predict rougly the correct trend, although the model of Vrentas & Duda seems to be closer to the computed data. Both models predict, for the smallest penetrants, a slower decay of D with v (or σ), and, for the larger penetrants, a faster decay. It must be noted however that the error in the diffusion coefficient for the largest penetrants is considerable as we have seen in chapter 5.

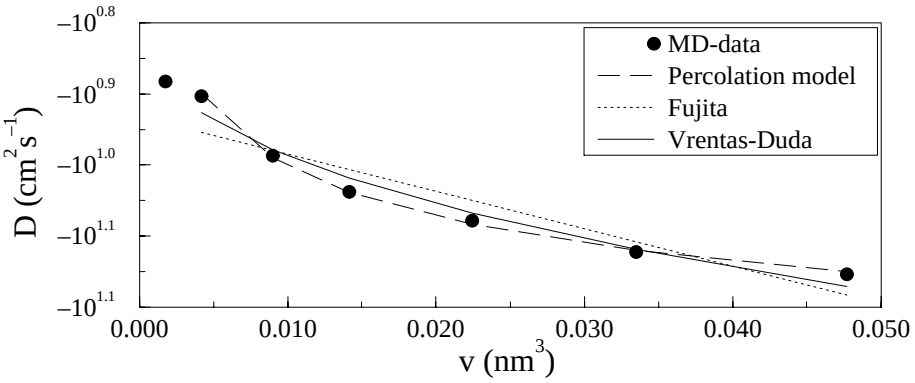

Figure 7.4: Size dependence of diffusion data. Shown are the data calculated in the MD simulations and fits to three different free volume based models. The first data point is excluded from the fits.

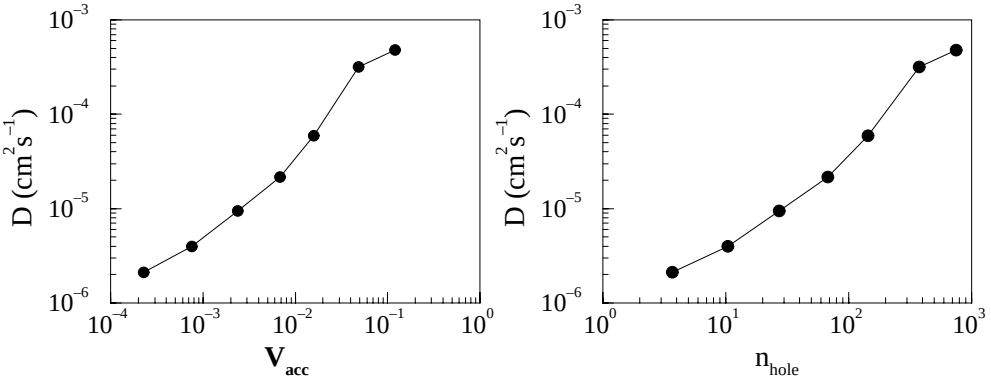

Figure 7.5: **Left:** *Diffusion constant as function of accessible volume.* **Right:** *Diffusion constant as function of the number of accessible volume holes.*

7.5 Diffusion, accessible volume and hole size distributions

Takeuchi [75] defined the quantity $\alpha(v)$ as the fraction of hole volume available to a penetrant with volume v:

$$\alpha(v) = \frac{\int_v^\infty v'\ n(v')dv'}{\int_0^\infty v'\ n(v')dv'} = \frac{1}{V_0}\ \int_v^\infty v'\ n(v')dv' \qquad (7.12)$$

where V_0 is the free volume, *i.e.* the accessible volume of a penetrant of size zero. If we use the form of $n_v \propto v^{-1.5}$, which we approximately found in our PDMS sample, then the integral diverges. In practice, however, the integral is evaluated numerically and $\alpha(v)$ is simply the accessible volume (scaled by the free volume).

If we use the theoretical value found in percolation theory at p_c: $n_v \propto v^{-2.18}$, then we end up with a relation of

$$\alpha(v) \propto v^{-0.18}. \tag{7.13}$$

In figure 7.4 this relation is also plotted (percolation model). We see that this relation fits perfectly to the calculated diffusion coefficients and is a better description of the calculated values than free volume models of Fujita and Vrentas & Duda.

So where we previously found D to scale according to approximately minus the square of the molecular volume, $D \propto v^{-2}$, we now find the relation:

$$D \propto \exp(av^{-0.18}) \tag{7.14}$$

It can thus be concluded that D scales according to the theoretical behavior of the accessible volume at the percolation threshold (as described in percolation theory), eventhough for none of these penetrants the accessible volume percolates. Furthermore the actual cluster size distribution for none of the penetrants corresponds to the theoretical distribution. It is obvious that the penetrants have to diffuse on an effectively percolating cluster to be able to diffuse.

Thus the behavior is governed by the ideal cluster size distribution that scales according to $n_v \propto v^{-2.18}$ and not by the actual distribution that is found at p_c in the polymer. This seems to indicate that these distributions are a result of finite size effects. Whether it is the grid coarseness or the limited system size that is the trouble is not clear, although it must be noted that the diffusion relations have been found at this limited system size.

This variable $\alpha(v)$ is in principle an accessible volume calculated from the properties at the percolation threshold. The theoretical behavior of the hole size distribution away from p_c is not taken into acount. In chapter 6 I have calculated the actual accessible volumina per penetrant and these are related to D in figure 7.5. We can see, that although a good correlation between D and V_{acc} is found, the relation is not a clear powerlaw behavior as with α.

Takeuchi [75] found that for a given penetrant in different polymer models[1] the diffusion constant scaled with the number of holes found at the percolation threshold $n_{c,hole}$ in the polymer matrix as:

[1]The, infinite chain, models varied in bond angle and bond angle force constant.

$$D \propto \exp(-b\ n_{c,hole}) \tag{7.15}$$

It might thus be interesting to see how the number of holes relates to the penetrant size within one polymer. Note that this is a completely different quantity than what Takeuchi investigated. Figure 7.5 shows also this relation. As we have found that the accessible volume scales with the number of holes as $n_{hole} \propto V_{acc}^{0.85}$ the functional form of the relation of D with n_{hole} is the same as with accessible volume.

7.6 Diffusion and percolation energy

How does the diffusion coefficient relate to percolation energy as defined in the previous chapter? Figure 7.6 shows the relation between this percolation energy E_p and D.

If the percolation energy could be visualized as an activation energy we would expect D to scale exponentially with E_p.

$$D \propto \exp(-E_p/RT), \tag{7.16}$$

the Boltzmann weight of the percolation energy. But as we have seen the percolation energy scales as $\sigma^{5.8}$, whereas the diffusion constant scales as $\sigma^{-6.2}$ so it should not come as a surprise that we see an almost inverse proportionality (if we again leave out the smallest penetrant).

$$D \propto E_p^{-1.05}. \tag{7.17}$$

We have seen that the diffusion data fits both to a power as to a stretched exponential. Figure 6.11 also shows the fit to a stretched exponential and we find a relation:

$$D \propto \exp\left(-1.5\ E_p^{0.8}\right). \tag{7.18}$$

Both relations fit equally well.

As the physical background of these relations is unclear it is uncertain whether the power-law or the stretched exponential is a better description of the relations. It is also unclear if these relations are applicable to other polymer systems as well, so further experiments over a range of polymers and possibly over a wider range of penetrant sizes should be performed.

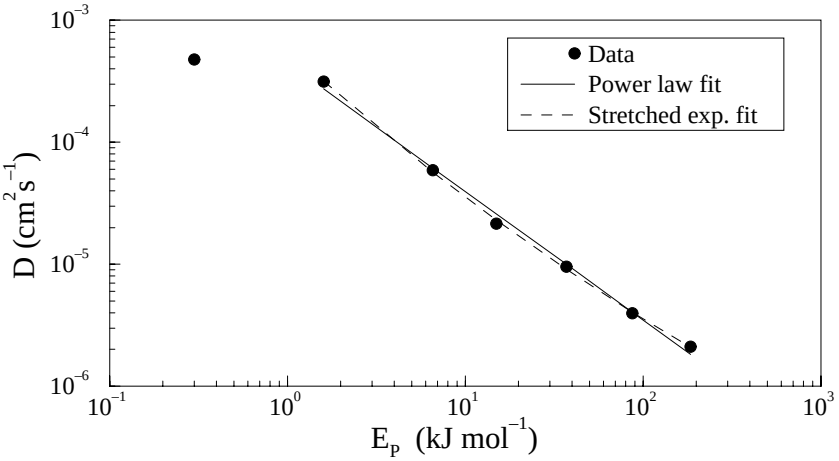

Figure 7.6: Diffusion coefficient D versus percolation energy E_P, with power law fit and streched exponential fit.

7.7 Permeation, Diffusion and Solubility ; Current views

It is clear that computer simulations can give a detailed insight in the processes governing the permeation of small penetrants across a polymer membrane. Based on the results presented in this thesis a number of conclusions can be drawn:

- The diffusion constant for small atoms (< 0.4 nm) in PDMS can be evaluated with sufficient accuracy. For larger penetrants, or more dense polymers, longer simulations are needed. Great care has to be taken to make sure the diffusion can be regarded as real diffusion and not as fractal diffusion.

- Also the chemical potential can be derived accurately enough for these small penetrants to predict permeability coefficients. If one would like to evaluated the chemical potential for larger penetrants or in more dense polymers then one would probably have to resort to other methods. The particle insertion method of Widom becomes ineffective for these systems. A good option might be a combination of the particle insertion method and the thermodynamic integration method [1, 2]. First the chemical potential is calculated for a small penetrant with the particle insertion method, and then this penetrant is enlarged to the final penetrant size (and/or shape) with the thermodynamic integration method.

- The solution diffusion mechanism provides a good description for the permeation of small penetrants through a polymer membrane.

- It is advisable to perform simulations with different system sizes, in order to get a thorough understanding of the finite size effects. Probably the system size used in this study is sufficiently large to correctly describe the trends, but with the increasing computer power it should be possible to make sure of the assumption that it is also

sufficient to get quantitatively correct results.

- Within the diffusion simulations three different regimes can be identified. In the penetrant size range used in this study mainly one diffusion regime (below p_c; hop diffusion) is probed, but we also touched on the two other regimes:

Above percolation limit The first regime is the diffusion of the smallest penetrants. These penetrants have an accessible volume that is above the percolation limit. Within our (normal; completely flexible polymer) MD simulation the only penetrant above the percolation limit was σ = 0.150 nm. (The percolation limit was estimated at σ = 0.160 nm.)

For these penetrants the size dependence is much smaller than below p_c. This is the reason that the value of D does not follow the same power law behavior that was shown by the other penetrants.

This limit is normally not reached in the PDMS system at this temperature, but as we have seen the effective accessible volume increases at higher temperatures. The percolation temperature as I have introduced for helium is still well above 1000 K, but we have to remember that the polymer will also expand at increased temperatures. So the effective percolation limit may be reached for helium at much lower temperatures. For these small penetrants the classical approximation is probably no longer valid and quantum effects are bound to occur.

In the restrained simulations the deviation from the powerlaw behavior for the smallest penetrant was not found. The reason for this is that for the specific polymer conformation that was chosen for these simulations, the percolation limit was not reached yet for the smallest penetrant. In the completely flexible simulation there is a substantial spread in instantaneous percolation limit.

Below percolation limit, hop diffusion Most of the penetrants used in this simulations diffuse according to this mechanism.

As the accessible volume for the penetrant drops below the percolation limit the penetrant has to cross energy barriers to move to the next hole. The penetrant picks up momentum from the polymer (*pin-ball motion*) and if the (random) *kick* is in the correct direction the penetrant can move to the next hole, which is an activated process. The average time it spends in such a hole seems to be exponentially dependent on the size of the penetrant.

The accessible volume properties of the polymer are of great importance to the diffusion process. We have seen that the penetrant size dependence in this diffusion regime can be described by a free volume model based on the theoretical cluster size distribution at the percolation threshold.

Below percolation limit, continuous diffusion As was presented in the previous chapter the diffusion coefficient of the holes in the polymer was estimated to be in the order of 10^{-7} cm^2s^{-1} . For all the penetrants this process of hole diffusion is part of the complete diffusive process, but only for the larger penetrants it becomes an important process. For σ = 0.450 nm, the total diffusion coefficient is roughly only one order of magnitude larger than the diffusion coefficient of the holes.

For penetrants this large (and larger) the probability to reach the next hole becomes so small that the major mechanism of diffusion will be the reorientation and diffusion of the accessible volume holes themself. The mechanism will be similar to Brownian diffusion through a viscous fluid.

In this regime there will (in principle) be a different size dependence than in the previous two regimes. This size dependence will probably be less than in the "hop diffusion" region. Figure 7.7 shows a schematic representation of these three regimes.

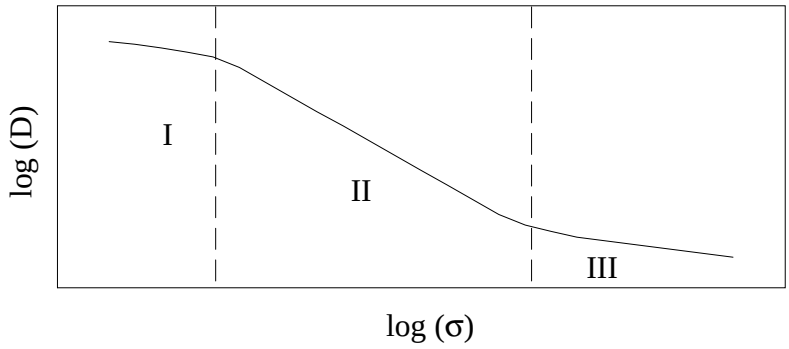

Figure 7.7: Schematic representation of the three diffusion regimes. I: above percolation limit. II: below percolation limit, hop diffusion. III: below percolation limit, continuous diffusion.

• These three diffusion regimes might also be important in a another application: diffusion in swollen polymers. It is know that under certain conditions a swelling agent is able to dissolve into the polymer in such large concentrations that the polymer system swells considerably. Penetrants, other than the swelling agent, are able to diffuse through the polymer by diffusion through the swelling agent. The penetrant accessible volume is filled with this swelling agent. This accessible volume may now be percolating, so that, depending on the size of the penetrant, the first diffusion regime is also reachable.

Although the mechanics of diffusion are probably different, the three regimes model is still applicable.

• In the regime of hop diffusion, the diffusion seems to be governed by either a power law behavior, for which the physical background is unclear, or by a stretched exponential. The exponential behavior is consistent with the statistical properties of

the accessible volume at the percolation limit. For net diffusion to occur, the penetrant accessible volume needs to be effectively percolating. So it is the statistical behavior at this effective percolation limit that govern the diffusion process (in the hop diffusion regime).

In the third regime it is not clear how the diffusion depends on the size of the penetrant, but it is probably less dependent on the properties of the accessible volume at the percolation limit.

Appendix A

Reprint

Molecular dynamics simulation of the transport of small molecules across a polymer membrane

R.M. Sok, H.J.C. Berendsen
and
W.F. van Gunsteren

Reprinter from *J. Chem. Phys.* **96**, 4699 (1992).

Appendix B

The error in the diffusion coefficient

Let $\boldsymbol{r}(t)$ be the displacement of a diffusing particle and $r = |\boldsymbol{r}|$. The probability distribution of $\boldsymbol{r}$ is gaussian, and the probability distribution of $r^2 = x^2 + y^2 + z^2$ is given by a χ^2 distribution for 3 degrees of freedom. If we write $s = r^2$, we have

$$f(s)ds = \frac{\sqrt{s}}{4\sqrt{\pi}\,(Dt)^{3/2}}\ \exp(-s/4Dt)\ ds \tag{B.1}$$

where D is the diffusion constant and t the time.

$$\begin{aligned} \langle s \rangle &= \int_0^\infty s\ f(s)\ ds \\ &= \frac{1}{4\sqrt{\pi}\,(Dt)^{3/2}}\ \int_0^\infty\ s^{3/2}\ \exp(-s/4Dt)\ ds \end{aligned} \tag{B.2}$$

on substituting $u = s/(4Dt)$, we find

$$= \frac{(4Dt)^{5/2}}{4\sqrt{\pi}}\ \int_0^\infty\ u^{3/2}\ \exp(-u)\ du \tag{B.3}$$

The integral is the error function $\Gamma(\frac{5}{2})$ and is equal to $\frac{3}{4}\sqrt{\pi}$ so:

$$\langle s \rangle = \frac{4^{5/2}Dt}{4\sqrt{\pi}(Dt)^{3/2}}\ \frac{3}{4}\sqrt{\pi} \tag{B.4}$$

If we work this out we obtain the well known relation:

$$\langle s \rangle = 6Dt. \tag{B.5}$$

Let us now concentrate on the error in s, again we use

$$\left\langle (s - \langle s \rangle)^2 \right\rangle = \int_0^\infty (s - \langle s \rangle)^2 \, f(s) ds \tag{B.6}$$

and using equation B.1 we find:

$$\left\langle (s - \langle s \rangle)^2 \right\rangle = \frac{1}{4\sqrt{\pi}(Dt)^{3/2}} \int_0^\infty (s - 6Dt)^2 \, s^{1/2} \, \exp(-s/4Dt) ds \tag{B.7}$$

Again take $u = s/(4Dt)$

$$\left\langle (s - \langle s \rangle)^2 \right\rangle = \frac{4(Dt)^2 \, (4Dt)^{3/2}}{4\sqrt{\pi} \, (Dt)^{3/2}} \int_0^\infty (4u^2 - 12u + 9) \, u^{1/2} \, \exp(-u) du \tag{B.8}$$

the integral is a combination of error functions and has a value of $3\sqrt{\pi}$, so

$$\begin{aligned} \left\langle (s - \langle s \rangle)^2 \right\rangle &= 8(Dt)^2 \, 3\sqrt{\pi} \\ &= \frac{2}{3}\sqrt{\pi}(6Dt)^2 \end{aligned} \tag{B.9}$$

Thus the average value of s with its standard error is :

$$\langle s \rangle \pm \frac{\sqrt{\left\langle s - \langle s \rangle^2 \right\rangle}}{\sqrt{n}}, \tag{B.10}$$

so,

$$\langle s \rangle = 6Dt \left(1 \pm \frac{\sqrt{\frac{2}{3}\sqrt{\pi}}}{\sqrt{n}} \right), \tag{B.11}$$

where n is the number of independent samples. The choice for n in a real system is not so obvious. In this thesis i have taken the total simulation time divided by the residence time $t_{0.50}$ (page 40). This residence time is approximately the time a penetrant resides in a certain hole.

Appendix C

Deriviation of enthalpy expression

The excess enthalpy of insertion h_{ex} can be evaluated by use of an enhanced version of Widom's particle insertion method. The deriviation of the expression used for this is given in this appendix. Let us denote the inserted particle with subscript 0 and the system particles with subscript i, so

particle 0 : inserted particle
particle i = 1...N : system particles

The energy of interaction between the inserted particle and the system particles is given by:

$$E_{0i} = \sum_{i}^{N} V_{0i}(r_{0i}) \tag{C.1}$$

and the internal system energy is:

$$E_{ij} = \sum_{i<j}^{N} V_{ij}(r_{ij}) \tag{C.2}$$

where $V_{ab}(r)$ is the interatomic interaction potential of particles a and b at distance r. The expression for the excess chemical potential of the inserted particle μ_{ex} in Widom's method is given as :

$$\mu_{ex} = -kT \ln \langle \exp(-\beta E_{0i}) \rangle \,, \tag{C.3}$$

where

$$\langle \exp(-\beta E_{0i}) \rangle = \frac{\frac{1}{V} \int d\boldsymbol{r} \ \exp(-\beta E_{0i}) \ \exp(-\beta E_{ij})}{\int d\boldsymbol{r} \exp(-\beta E_{ij})}. \tag{C.4}$$

Where we used the shorthand notation $d\boldsymbol{r} = d\boldsymbol{r}_1 \ldots d\boldsymbol{r}_N$. The excess partial molar enthalpy h_{ex} associated with the process of solvation can also be calculated in a way similar to that of the chemical potential. It can be derived using :

$$h_{ex} = \frac{\partial \left(\frac{\mu}{T} \right)}{\partial (1/T)} \tag{C.5}$$

and using $\frac{\partial}{\partial \beta} = k \ \frac{\partial}{\partial (1/T)}$ we find

$$h_{ex} = -\frac{\partial \ln \langle \exp(-\beta E_{0i}) \rangle}{\partial \beta}. \tag{C.6}$$

This evaluates to:

$$h_{ex} = -\frac{1}{\langle \exp(-\beta E_{0i}) \rangle} \ \frac{\partial}{\partial \beta} \langle \exp(-\beta E_{0i}) \rangle \tag{C.7}$$

Let us first concentrate on the derivative:

$$-\frac{\partial}{\partial \beta} \langle \exp(-\beta E_{0i}) \rangle$$

$$= -\frac{\partial}{\partial \beta} \ \frac{\frac{1}{V} \int d\boldsymbol{r} \exp(-\beta E_{0i}) \ \exp(-\beta E_{ij})}{\int d\boldsymbol{r} \exp(-\beta E_{ij})} \tag{C.8}$$

$$= \frac{\frac{1}{V} \left(\int d\boldsymbol{r} \exp(-\beta E_{0i}) \ \exp(-\beta E_{ij}) \right) \left(\int d\boldsymbol{r} (-E_{ij}) \ \exp(-\beta E_{ij}) \right)}{\left(\int d\boldsymbol{r} \exp(-\beta E_{ij}) \right)^2} -$$

$$\frac{\frac{1}{V}\left(\int d\boldsymbol{r}\exp(-\beta E_{ij})\right)\ \left(\int d\boldsymbol{r}(-E_{0i}-E_{ij})\ \exp(-\beta E_{0i})\exp(-\beta E_{ij})\right)}{\left(\int d\boldsymbol{r}\exp(-\beta E_{ij})\right)^2}. \qquad \text{(C.9)}$$

We can also write this using the $<>$ notation as:

$$= -\langle E_{ij}\rangle\langle\exp(-\beta E_{0i})\rangle + \langle E_{0i}\exp(-\beta E_{0i})\rangle + \langle E_{ij}\exp(-\beta E_{0i})\rangle \qquad \text{(C.10)}$$

So the final expression for the excess enthalpy of the inserted particle is:

$$h_{ex} = \frac{\langle E_{0i}\ \exp(-\beta E_{0i})\rangle}{\langle\exp(-\beta E_{0i})\rangle} + \frac{\langle E_{ij}\ \exp(-\beta E_{0i})\rangle}{\langle\exp(-\beta E_{0i})\rangle} - \langle E_{ij}\rangle\,. \qquad \text{(C.11)}$$

The first term in this expression simply is the energy of the inserted particle weighed with its Boltzmann weight (and normalized). The second and third term can be thought of as being a correction term to the first. They will cancel each other if there is no correlation between the system energy and the energy of the inserted penetrant. In practice the correction term will show poor convergence. A similar expression for the patial enthalpy in the constant-NPT ensemble is given in [91].

References

[1] T.P. Straatsma, "Free Energy Evaluation By Molecular Dynamics Simulation", Thesis University of Groningen, (1987).

[2] T.P. Straatsma, H.J.C. Berendsen and J.P.M. Postma, *J. Chem. Phys.*, **85**, 6720 (1986).

[3] B. Widom, J. Chem. Phys. **39**, 2802 (1963).

[4] W.J. Ward III, W.R. Browall and R.M. Salemme, *J. Membr. Sci.*, **1**, 99 (1976).

[5] J.M.S. Henis and M.K. Tripodi, *Separation. Sci. Technol.*, **15**, 1059 (1980).

[6] T.C. Dahl, *Pharm. Res.*, **9**, 398 (1992).

[7] Y. Sun, *et.al., J. Controlled Release*, **5**, 69 (1987).

[8] S.A. Stern and S. Trohalaki, in “Barrier Polymers and Structures”, W.J. Koros (ed.), *ACS symp. ser.*, American Chemical Society, Washington DC, pp 22-59 (1990)

[9] T. Graham, *Philos. Mag.*, **32**, 401, (1866).

[10] H.A. Daynes, *Proc. Roy. Soc. Lond.*, Ser. A **97**, 286 (1920).

[11] R.M. Barrer, *Trans. Farad. Soc.*, **35**, 628 (1939).

[12] N. C. Wyeth, In “High Performance Polymers; Their Origin and Development”, (R. B. Seymour and G. S. Kirshenbaum ed.), Elsevier, New York, 425. (1986).

[13] W. J. Koros in , “Barrier Polymers and Structures”, W.J. Koros (ed.) *ACS symp. ser.*, American Chemical Society, Washington DC., pp 1-21 (1990)

[14] T.M. Aminabhavi, U.S. Aithal and S. S. Shukla, *J. Macromol. Sci.- Rev. Macromol. Chem. Phys.*, **C28(3&4)**, 421-474 (1988).

[15] H. Nishide, *at.al., Macromolecules*, **19**, 494 (1985).

[16] E. Tsuchida, H. Nishide and M. Ohyanagi, *J. Macromol. Sci. -Chem.*, **A25**(10&11), 1327 (1988).

[17] T.M. Aminabhavi, U.S. Aithal, *J. Macromol. Sci.- Rev. Macromol. Chem. Phys.*, **C31(2&3)**, 117, (1991).

[18] M.L. Dunham, D.L. Bailey and R.Y. Mixer, *Ind. Eng. Chem.*, **49**, 1373 (1957).

[19] K. Kawai, T. Nohmi and K. Kamide, *Polym. Prepr., Am. Chem. Soc., Div. Polym. Chem.*, **20**, 309 (1979).

[20] J. Folkman, D.M. Long and R. Rosenbaum, *Science*, **154**, 148 (1966).

[21] T.J. Roseman, *J. Pharm Sci.*, **61**, 46 (1972).

[22] M.P. Allen and D.J. Tildesley, *Computer Simulation of Liquids*, Claredon, Oxford (1987).

[23] L. Verlet, *Phys. Rev.*, **159**, 98, (1967).

[24] L. Verlet, *Phys. Rev.*, **165**, 201, (1968).

[25] R.W. Hockney and J.W. Eastwood, *Computer Simulation Using Particles* (McGraw-Hill, New-York, 1981).

[26] H.J.C. Berendsen and W.F. van Gunsteren, *GROMOS Reference Manual* (University of Groningen, Groningen, 1987).

[27] J-P. Ryckaert, G. Ciccotti and H.J.C. Berendsen, J. Comp. Phys. **23**, 327 (1977).

[28] H.J.C. Berendsen, J. P. M. Postma, W. F. van Gunsteren and A. DiNola, J. Chem. Phys. **81**, 3684 (1984).

[29] H.J.C. Berendsen, in "Molecular Dynamics and Protein Structure", J. Hermans (ed.), Polycrystal Book Service, Western Springs, IL., pp 18-22 (1985).

[30] K. Kremer, G. Grest and I. Carmesin, *Phys. Rev. Lett*, **61**, 566 (1988).

[31] D. Rigby and R.J. Roe, *J. Chem. Phys*, **87**, 7285 (1987)

[32] D. Rigby and R.J. Roe, *J. Chem. Phys*, **89**, 5280 (1988)

[33] D. Rigby and R.J. Roe, *Macromolecules*, **22**, 2259 (1989)

[34] P.V. Pant, J. Han, G.D. Smith abd R.H. Boyd, *J. Chem. Phys*, **99**, 597 (1993)

[35] *Polymer Handbook*, edited by J. Brandrup and E.H. Immergut (Willey InterScience, New York, 1975).

[36] A.C. Lasaga and G.V. Gibbs, *Phys. Chem. Minirals*, **14**, 107 (1987).

[37] J.H.R. Clarke and D.Brown, Molec. Sim. **3**, 27 (1989).

[38] P.G. de Gennes, *La Recherge*, **7**, 919 (1979).

[39] S. Trohalaki, D. Rigby, A. Kloczkowski, J,E, Mark and R.J. Roe, *Polym. Prepr., Am. Chem. Soc., Div. Polym. Chem.*, **30**, 23 (1989).

[40] J. Sonnenburg, J. Gao and J.W. Wiener, *Macromolecules*, **23**, 4653 (1990).

[41] H.Takeuchi and K.Okazaki, J. Chem. Phys. **92**, 5643 (1990).

[42] H. Takeuchi, *J. Chem. Phys.* **93**, 2062 (1990).

[43] H. Takeuchi, *J. Chem. Phys.* **93**, 4490 (1990).

[44] H. Takeuchi, R.J. Roe, J.E. Mark, *J. Chem. Phys.*, **93**, 9042 (1990).

[45] T.A. Weber and E. Helfand, *J. Chem. Phys*, **71**, 4760 (1979).

[46] H. Fujita, *Fortschr. Hochpolym. Forsch.*, **3**, 1 (1961).

[47] F. Müller-Plathe, *J. Chem. Phys.*, **94**, 3192 (1991).

[48] F. Müller-Plathe, *J. Chem. Phys.*, **96**, 3200 (1992).

[49] F. Müller-Plathe, *Macromolecules*, **25**, 6722 (1992).

[50] P.V.K. Pant, R.H. Boyd, *Macromolecules*, **25**, 494 (1992).

[51] R.H. Boyd, P.V. Pant, *Macromolecules*, **24**, 6325 (1991).

[52] P.V.K. Pant, R.H. Boyd, *Macromolecules*, **26**, 679 (1993).

[53] S. Toxvaerd, *J. Chem. Phys.*, **93**, 4290 (1990).

[54] F. Müller-Plathe, S.C. Rogers, W.F. Gunsteren, *Chem. Phys. Lett.*, **199**, 237-43 (1992).

[55] F. Müller-Plathe, S.C. Rogers and W.F. Gunsteren, *J. Chem. Phys.*, **98**, 9895 (1993).

[56] A.A. Gusev and U.W. Suter, 12th Workshop Proceedings, *Speedup Journal*, **6** 29 (1993).

[57] K. S. Shing and K.E. Gubbins,*Mol. Phys.*,**46**(5), 1109, (1982).

[58] D.A. McQuarrie, “Statistical Mechanics” (1976), Harper & Row, New York, Evanston, San Francisco, London.

[59] Y. Ichiraku et.al., *J. Membr. Sci.*, **34** 5 (1987).

[60] *Data for Helium are estimates based on data for filled PDMS membranes. For example from :* R.M. Barrer and H.T. Chio, *J. Polym. Sci. C*, **10**, 111 (1965).

[61] J.O. Hirschfelder, C.F. Curtiss and B. Bird, "Molecular theory of gases and liquids" (1984), Wiley, New York.

[62] W.L. Dobb, *Am. N.Y. Ac. Sci.*, **146**, 119 (1968).

[63] S.A. Stern, *et.al., J. Polym. Sci., Polym. Phys.*, **25** 1263 (1987).

[64] O.J. Sweeting, "The Science and Technology of Polymer Films", vol II, Wiley (1971) New York.

[65] V. Stannett, In "Diffusion in Polymers", J. Crank and G. S. Park (ed.), Academic Press, London and New York, 41-73 (1986).

[66] S.R. Braudbent and J.M. Hammersley, "Percolation processes I. Crystals and mazes," Proc. Cambridge Philos. Soc. **53**, 629 (1957)

[67] D. Stauffer and A. Aharony, *Introduction to Percolation Theory*, Second Edition, Taylor & Francis, London, Washington DC, (1992).

[68] J.W. Essam, *Rep. Prog. Phys.*, **34**, 843 (1980).

[69] S. Havlin, *et.al*, *J. Stat. Phys.*, **47**, 173 (1987).

[70] P.N. Strenski, R.M. Bradley and J.M. Debierre, *Phys.Rev.Lett.*. **66**, 133 (1991).

[71] T. Viscek and J Kertesz, *J. Phys. A.*, **14** (1981).

[72] W.T. Elam, A.R. Kerstein and J.J. Rehr, *Phys. Rev. Lett.*, **52**, 1516 (1984).

[73] J. Kertész, *J. Phys. (Paris), Lett.*, **41**, L393 (1981).

[74] Y.C. Chiew and E.D. Glandt, *J. Phys. A.*, **16**, 2599 (1983)

[75] H. Takeuchi and K. Okazaki, *Makromol. Chem., Macromol. Symp.*, **65**, 81 (1993).

[76] M. Lupowski and P.A. Monson, *J. Chem. Phys.*, **89**, 3300 (1988).

[77] A.L.R. Bug, S.A. Safran, G.S. Crest and I. Webman, *Phys. Rev. Lett.*, **55**, 1896 (1985).

[78] A. Bunde and S. Havlin, in "Fractals and Disordered Systems", A. Bunde and S. Havlin (ed.), Springer Verlag, New York Berlin Heidelberg, pp 51-93 (1991)

[79] A. Bunde and S. Havlin, in “Fractals and Disordered Systems”, A. Bunde and S. Havlin (ed.), Springer Verlag, New York Berlin Heidelberg, pp 97-146 (1991)

[80] R.J. Pace and A. Datyner *J. Polym. Sci. Polym.Phys.Ed.*, **17**, 437 (1979).

[81] A.T. DiBennedetto and D.R. Paul, *J. Polym. Sci*, **A 2**, 1001, (1964).

[82] D.R. Paul and A.T. DiBennedetto, *J. Polym. Sci*, **C 10**, 17, (1965).

[83] W.W. Brandt, *J. Chem. Phys.*, **63**, 1080, (1959).

[84] H. Fujita, In “Diffusion in Polymers” (J. Crank and G. S. Park ed.), Academic Press, London and New York, pp 107-140(1986).

[85] M. H. Cohen and D. Turnbull, *J. Chem. Phys.*, **31**, 1164 (1959).

[86] A.E. Chalykh and V.B. Zlobin, *Russ. Chem. Rev.*, **57**, 504 (1988).

[87] J.S. Vrentas and J.L. Duda *Macromolecules*, **9**, 785, (1976).

[88] J.S. Vrentas and J.L. Duda *J.Polym.Sci. Polym.Phys.Ed.*, **15**, 403, (1977).

[89] J. Bicerano, *et.al.*, in “Barrier Polymers and Structures”,W. J. Koros (ed.), ACS symp. ser., American Chemical Society, Washington, DC 126, pp 126-158 (1990)

[90] J.S. Vrentas, H.T. Liu, J.L. Duda, *J. Appl. Polym. Sci.*, **25**, 1297 (1980)

[91] P. Sindzingre, G. Ciccotti, C. Massobrio and D. Frenkel, *Chem. Phys. Lett.*, **136**, 35 (1987).

Samenvatting

Doorlaatbaarheid van een polymeer membraan voor kleine moleculen:

Een computer simulatie studie

Polymeren worden in de huidige samenleving op grote schaal in uiteenlopende toepassingen gebruikt. Bij vele van deze toepassingen speelt de doorlaatbaarheid of permeabiliteit van het polymeer voor kleine moleculen een grote rol. Denk hier bijvoorbeeld aan het gebruik van verpakkingsmaterialen voor vlees of fruit, waarbij het van groot belang is dat het materiaal zo min mogelijk zuurstof doorlaat, of aan het gebruik van contactlenzen, die juist zo veel mogelijk zuurstof door moeten laten.

Omdat het belang van de permeabiliteit van polymeren zo groot is zijn er, in de loop der jaren, vele theoretische modellen afgeleid. Al deze modellen geven echter tot op heden niet voldoende inzicht in het proces op *microscopisch*, dat wil zeggen atomair, niveau. Computer simulaties en in het bijzonder *moleculaire dynamica simulaties* kunnen hierbij een handje helpen. Zij zijn bij uitstek geschikt om op microscopisch niveau experimenten uit te voeren.

In moleculaire dynamica (MD) simulaties berekent men, met behulp van de klassieke bewegingsvergelijkingen van Newton, de bewegingen van een aantal atomen of moleculen onder invloed van hun onderlinge interacties. Deze onderlinge interacties worden beschreven door een zogenaamd "force-field", een praktisch hanteerbare benadering van de werkelijke interacties. Met behulp van deze MD-methode kunnen we dus de bewegingen van bijvoorbeeld een polymeermatrix simuleren. Hierbij moet wel worden opgemerkt dat men in simulaties beperkt is tot zeer kleine systemen (enkele duizenden atomen) en tot een zeer korte tijd (nanoseconden).

Wat is nu het uiteindelijke doel van deze simulaties, m.a.w. welke informatie willen we uit de berekeningen halen? Hiervoor moeten we eerst het permeatieproces opdelen in deelprocessen.

Theoretisch kunnen we stellen dat de permeatie van kleine moleculen door een membraan bestaat uit twee verschillende processen. Het eerste proces is het binnendringen van het molecuul in het membraan (het oplossen) en het tweede proces is het transport van het molecuul binnen in het membraan (de diffusie).

Het eerste proces, het oplossen van het deeltje vanuit bijvoorbeeld de gasfase tot in de membraanfase, wordt beschreven met een oplosbaarheidsconstante. Deze constante is direct gerelateerd aan het verschil in vrije energie van het deeltje in de beide fasen. Dit verschil in vrije energie kunnen we uit de MD-simulaties met behulp van de “particle insertion” methode berekenen.

Voor het tweede proces, de diffusie, kunnen we direct gebruik maken van de MD-methode. Wanneer we in het polymeer een aantal kleine moleculen plaatsen en hun bewegingen in de loop van de tijd analyseren, kunnen we hieruit direct de diffusieconstante berekenen.

In dit specifieke onderzoek ligt de nadruk op het effect van de grootte van het deeltje op de permeabiliteit van het membraan. In welke mate bepaalt de deeltjesgrootte de doorlaatbaarheid en vooral, kunnen we begrijpen waarom dit zo is?

Het proefschrift bestaat uit zeven hoofdstukken waarvan de eerste vier de theoretische achtergrond en inleidende experimenten beschrijven. In de laatste drie hoofdstukken worden de berekeningen van de diffusie- en oplosbaarheidsconstante uitvoerig besproken.

Het eerste hoofdstuk is een algemene inleiding en hoofdstuk twee geeft de theoretische onderbouwing van het opdelen van de permeatie in de oplosbaarheid en de diffusie. In hoofdstuk drie ga ik in het kort in op de simulatie- en analyse-methodes die gebruikt gaan worden. De werkelijke simulatie van het polymeer zonder de kleine moleculen worden in hoofdstuk vier uitvoerig beschreven en geanalyseerd.
In hoofdstuk vijf worden de simulaties beschreven waarmee de diffusie-constante en de oplosbaarheid van een aantal deeltjes van verschillende grootte in het polymeer berekend worden. Het blijkt dat het diffusie proces niet voor alle deeltjesgroottes gelijk is. Voor de allerkleinste deeltjes lijkt de diffusie sterk op de diffusie van deeltjes in een vloeistof. Wanneer de grootte van het deeltje toeneemt verandert het proces in een soort "hop-diffusie". Hierbij bevindt het deeltje zich een tijd in één bepaald gebied, een holte, waarna het opeens "hopt" naar een andere holte waarin het weer een tijdje verblijft. De tijd dat het deeltje verblijft in een bepaalde holte neemt toe met toenemende deeltjesgrootte. Voor de allergrootste deeltjes is de verblijftijd zo lang dat dan ook de diffusie van de holte zelf van belang is. De diffusie-coefficïent neemt met toenemende deeltjesgrootte af.

Behalve door de grootte wordt het deeltje ook nog beschreven door een interactie-parameter die een maat is voor de sterkte van interactie met alle andere atomen. Voor het diffusiegedrag wordt meestal aangenomen dat deze interactie-parameter van ondergeschikt belang is, maar voor de oplosbaarheid is dit niet het geval.

Het verloop van de oplosbaarheid als functie van deeltjesgrootte hangt namelijk sterk af van interactie-parameter. Bij een zwakke interactie neemt de oplosbaarheid *af* met toenemende deeltjesgrootte, maar bij een sterke interactie neemt de oplosbaarheid *toe*. Hierdoor is dus ook het verloop van de doorlaatbaarheid van een membraan sterk afhankelijk van zowel de deeltjesgrootte als van de sterkte van de interactie met het polymeer.

In hoofdstuk zes wordt de vrije ruimte, oftewel het vrije volume, in het polymeer onderzocht. Dit vrije volume is van groot belang, omdat het de ruimte is waar het deeltje zich door het polymeer beweegt. De statistische eigenschappen van dit volume blijken redelijk goed beschreven te kunnen worden met behulp van de percolatie theorie. Deze theorie is in eerste instantie opgezet vanuit zeer simpele systemen, maar statistisch gezien is er een grote overeenkomst tussen deze simpele systemen en het vrij volume in een polymeer.

In het laatste hoofdstuk koppel ik de eigenschappen van het vrije volume in het polymeer aan de diffusie en oplosbaarheid van de deeltjes in het polymeer. De relatie tussen diffusie en vrij volume volgt vrij eenvoudig uit de percolatie theorie, alhoewel er nog enkele onduidelijkheden blijven bestaan. Tussen de oplosbaarheid en vrij volume bestaat ook een duidelijke relatie, maar de achterliggende theorie is hiervan nog onduidelijk.

De algemene conclusie van het onderzoek is dat computer simulaties het mogelijk maken om op een uiterst flexibele manier op atomair niveau experimenten uit te voeren die zeer veel inzicht kunnen verschaffen in het proces van doorlaatbaarheid van een polymeermembraan voor kleine moleculen.

Dankwoord

Dit deel van het proefschrift wordt meestal gebruikt om te benadrukken dat het proefschrift, ondanks dat er maar één naam op de omslag staat, niet het werk is van de auteur alleen. Alhoewel ik liever een orgineel eind aan mijn werk had willen breien moet ik toegeven dat dat ook met dit proefschrift niet het geval is.

Als eerste (orgineel als altijd) wil ik natuurlijk mijn promotor en begeleider Herman Berendsen bedanken voor de hulp die hij mij geboden heeft gedurende alle jaren die ik in de MD-groep vertoefd heb.

De volgende persoon die ik wil bedanken is de schrijver van het voorwoord van dit proefschrift: Siewert-Jan Marrink. Wanneer ik in plaats van scheikunde psychologie had gestudeerd, had hij het onderwerp van mijn proefschrift kunnen zijn. Naast een goede collega een nog betere vriend.

Verder mag ik niet vergeten te bedanken: Aldert “vanB” van Buuren, René van Schaik, Marjan Ossebaard, Marco Faber, Simone van Erpecum, Alex de Vries en Jos Tissen (voor heel veel goede tijden), Asprilla†, Axz, Garth, Lars Lor†, Oye, Ryokan en Tahamata† (voor veel spannende avonturen), Adrie, Ineke, Rita, Pa & Ma (omdat ze er altijd waren), Petra (voor al die jaren) Arnold, Ole en Mahakala (voor inspiratie).

Als laatste wil ik Sil bedanken, we vinden onze poortloze poort nog wel.

Sumizome no	If these sleeves
waga koromode no	of my black robe
yuta naraba	were only wider
ukiyo no tami wo	I’d shelter all the people
owamashi mono wo	in this up-and-down world

a poem by *Ryokan*